ABSTRACT

A TEMPORAL AND ECOLOGICAL ANALYSIS OF THE HUNTINGTON BEACH WETLANDS THROUGH AN UNMANNED AERIAL SYSTEM REMOTE SENSING PERSPECTIVE

By

Talha Rafiq

August 2015

Wetland monitoring and preservation efforts have the potential to be enhanced with advanced remote sensing acquisition and digital image analysis approaches. Progress in the development and utilization of Unmanned Aerial Systems (UAS) and Unmanned Aerial Vehicles (UAV) as remote sensing platforms has offered significant spatial and temporal advantages over traditional aerial and orbital remote sensing platforms. Photogrammetric approaches to generate high spatial resolution orthophotos of UAV acquired imagery along with the UAV's low-cost and temporally flexible characteristics are explored. A comparative analysis of different spectral based land cover maps derived from imagery captured using UAV, satellite, and airplane platforms provide an assessment of the Huntington Beach Wetlands. This research presents a UAS remote sensing methodology encompassing data collection, image processing, and analysis in constructing spectral based land cover maps to augment the efforts of the Huntington Beach Wetlands Conservancy by assessing ecological and temporal changes at the Huntington Beach Wetlands.

A TEMPORAL AND ECOLOGICAL ANALYSIS OF THE HUNTINGTON BEACH WETLANDS THROUGH AN UNMANNED AERIAL SYSTEM REMOTE SENSING PERSPECTIVE

A THESIS

Presented to the Department of Geography

California State University, Long Beach

In Partial Fulfillment

of the Requirements for the Degree

Master of Arts in Geography

Committee Members:

Christopher T. Lee, Ph.D. (Chair)
Suzanne P. Wechsler, Ph.D.
Christine Whitcraft, Ph.D.

College Designee

Amy Bippus, Ph.D.

By Talha Rafiq

B.A., 2013, University of Illinois, Urbana-Champaign

August 2015

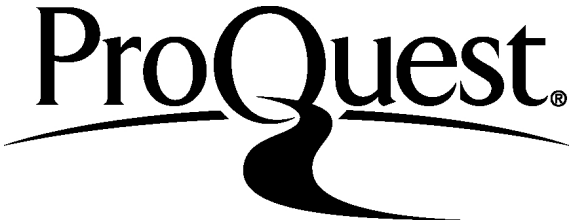

ACKNOWLEDGEMENTS

Bismillah Al-Rahman Al-Rahim. First and foremost all praises are to God, for without him, none of this would be possible. I tremendously appreciate the support, guidance, confidence and most importantly patience offered by my chair and committee Dr. Christopher Lee, Dr. Suzanne Wechsler, and Dr. Christine Whitcraft. Thank you for believing that I had this capability in me. I have learned so much from this experience and I owe it all to you. I want to thank Scott Winslow and Michael Shensky for their assistance and expertise. Additionally, I want to thank Dr. Deborah Thien, Dr. Christine Rodrigue, and Dr. Linna Li for their guidance and support. I want to extend my gratitude to the CSULB Department of Geography for giving me the opportunity to learn and grow both as a graduate student and as a person.

Tyler, Natasha, Adrienne, Anthony, and Heather, from strangers to lifelong friends, I thank you for your love, advice, wisdom, and humor these past two years. To my best friends from Lawler & Terminal Park, Skokie, and Chicago, your love and loyalty are always with me and never forgotten. Mama, Baba, and Hasan, this research is a symbol of your endless love and belief in my abilities to achieve. I would not be here without all your sacrifices. You guys are always in my thoughts and prayers and are my motivation to continue pursuing excellence. I sincerely thank all of you for your love and support and I look forward to the journeys and experiences the future brings.

TABLE OF CONTENTS

CHAPTER Page

Page

LIST OF TABLES

TABLE Page

LIST OF FIGURES

FIGURE Page

FIGURE Page

FIGURE Page

CHAPTER 1

INTRODUCTION

Aerial mapping has a valuable ability to offer a unique perspective of the Earth's surface. This capability has been demonstrated and has exponentially increased for well over a century due to the continued development of platforms in conjunction with the increasing sophistication of cameras, imaging devices, and spectral sensors. The developments in Unmanned Aerial Vehicles (UAV) as remote sensing platforms has transformed the landscape of aerial mapping. While there have been numerous studies demonstrating UAV remote sensing applicability, this study documents their capability in studies involving wetland land cover analysis. This research documents a comprehensive breakdown of the acquisition and analysis strategies needed to utilize UAV aerial imagery for the purposes of assessment of a coastal wetland in Huntington Beach, California. The term Unmanned Aerial Vehicle (UAV) refers to the DJI Phantom Quadcopter which is the actual vehicle that was used to acquire aerial imagery. In this research, the Unmanned Aerial System (UAS) refers to the entire structure relating to UAV aerial image acquisition. This structure includes the software that was used to flight plan, the DJI Phantom Quadcopter, and the acquisition, processing, and analysis of the UAV aerial imagery.

Wetlands are complex ecosystems that produce, protect and preserve life. Their importance stems from the diversity of functions they serve for the environment especially for the countless species of plants and animals that inhabit them. Wetlands are

a type of ecosystem that comprise both land and aquatic systems and make up about 6 percent of the planet's total land surface (Shuyt and Brander 1997; Peterson et al. 2003). They provide environmental, socio-cultural, and economic value. They are home to an abundance of species such as birds, mammals, reptiles, amphibians, and fish (Shuyt and Brander 1997; Toronto and Region Conservation Authority 2011). They also hold high religious, historical, and aesthetical value for communities and provide populations with tremendous economic worth for consumption of goods such as water for drinking, fish for food, trees for fuel, or wood for building material (Shuyt and Brander 1997). There are three main types of wetlands: marine/coastal wetlands, inland wetlands, and man-made wetlands. This research focuses on a marine/coastal wetland system. Often times, coastal wetlands are thought to be one of the last remaining ecosystems to preserve littoral biodiversity and should be monitored and preserved using the most efficient technology available (Coiacetto 1996; Godet and Thomas 2013). The coastal wetland that is the focus of this research is the Huntington Beach Wetlands located in Southern California (Figure 1). The Huntington Beach Wetland is a 57 ha coastal sanctuary located in Orange County. It is situated between the Pacific Coast Highway on one side and oil fields and residential housing on the other (Woodfield and Merkel 2011; Whitcraft, Allen, and Lowe 2013). This research will focus on land cover distribution change at the Huntington Beach Wetlands using UAV acquired imagery and image analysis approaches.

Over the past few decades, anthropogenic effects resulted in an increasingly degraded wetland environment and downsized the once 3000 acre wetland area by 94 percent in 2007 (Huntington Beach Wetland Conservancy 2013). Development of

adjacent oil fields, the construction of the Pacific Coast Highway and nearby roadways, along with land modification of wetland into residential and commercial landscapes produced toxins and pollution that have destroyed habitats and cut off crucial tidal flows in the area. Without these tidal flows, the wetlands slowly dried up and in the process, damaged the vegetation and animals that relied on it for sustenance (Woodfield and Merkel 2011; Whitcraft, Allen, and Lowe 2013). Essentially, these anthropogenic factors reduced vegetation in this area and dramatically reduced wildlife populations. Because the Huntington Beach Wetlands incorporate all the basic characteristics of a traditional wetland ecosystem, it is an important environmental resource and a significant subject for monitoring and preservation analysis.

FIGURE 1. Huntington Beach Wetlands located in Orange County, California.

Founded in 1985, the Huntington Beach Wetlands Conservancy (HBWC) is a non-profit community based organization that owns and manages the Huntington Beach Wetlands (HBWC 2013). They began their construction and restoration of the wetlands in 1993 to revitalize its biological production. Research and analysis of the restoration began in 2007 by Merkel and Associates, Inc. (M&A) in conjunction with HBWC and California State University, Long Beach's (CSULB) Biology department. With an overall focus on restoration and preservation, one major concern of HBWC and CSULB's Biology department is to monitor vegetation dynamics in the area on an annual basis. (Woodfield and Merkel 2011; Whitcraft, Allen, and Lowe 2013). Since 2007, preservation tasks have focused on monitoring land cover changes in annual vegetation abundance through comparison of aerial imagery captured annually. HBWC's physical restoration phase of the wetlands ended in 2009. The work these organizations have done in assessing the preservation of wildlife in Brookhurst Marsh since then, is built upon in this research.

The purpose of this thesis is to assist the preservation task by providing a baseline aerial assessment of Brookhurst Marsh in the Huntington Beach Wetlands. The UAV data collection methods established for this research can be used to ensure repeatability in subsequent surveys for longitudinal assessment. This study provides a step-by-step method for updating the annual vegetation monitoring of the Huntington Beach Wetlands through the capture and spectral land cover analysis of aerial imagery in the hopes that this research and methodology can be utilized by other land managers and agencies to enhance and ease their research and monitoring efforts. By utilizing UAV aerial imagery, this research attempts to build a foundation for rapid temporally dynamic

vegetation community mapping thereby reducing the time and expense needed for conventional aerial photographic acquisition and extensive ground surveys. The goal of this thesis is to provide a viable, efficient, and flexible alternative to current airplane and satellite imagery in the form of UAV acquired aerial imagery using both per pixel spectral mapping and photogrammetric approaches to develop and compare land cover maps, in the hopes of aiding the HBWC in assessing the Huntington Beach Wetlands.

CHAPTER 2

LITERATURE REVIEW

This chapter provides a comprehensive review of approaches utilized in past scholarly research that cover the foundations of remote sensing, land cover mapping, and temporal vegetation analysis. Additionally, it covers the fundamentals of photogrammetry and how they relate to digital model construction. These approaches helped assess the land cover at Huntington Beach Wetlands, both temporally and ecologically. The development of Unmanned Aerial vehicles (UAV), their transition into Unmanned Aerial Systems (UAS) and overview of research conducted using UAV and UAS for data collection are provided. A variety of previous studies have demonstrated the applicability of different remote sensing platforms for the purposes of vegetation analysis. The framework, objective, and significance of this research is discussed in context of the literature reviewed.

Remote Sensing and Photogrammetry

The developments of both remote sensing and photogrammetry go hand-in-hand. The actual practice of remote sensing first embodied in aerial photography was not possible until the development of the photograph and the camera in the nineteenth century (Watts, Ambrosia, and Hinkley 2012; Théau 2012; Wolf, DeWitt, and Wilkinson 2014). In 1859, Gaspard Félix Tournachon, became the first person to take aerial photographs using a hot-air-balloon (Watts, Ambrosia, and Hinkley 2012; Théau 2012; Wolf, DeWitt, and Wilkinson 2014). His development of aerial photography paved the

way for modern day aerial photography and remote sensing. Improvements in cameras and film helped propel the use of photography for mapping. In 1859, Colonel Laussedat experimented using photogrammetry for topographic mapping but limitations with aerial photography restricted his work to using terrestrial photographs (Wolf, DeWitt, and Wilkinson 2014). By 1886, Captain Eduard Deville introduced topographic mapping through photogrammetry to North America and in 1894 he mapped the border between Canada and Alaska (Wolf, DeWitt, and Wilkinson 2014). The invention of the airplane in 1903 by the Wright brothers paved the way for modern-day aerial photography. Ten years later aerial photography was captured using an airplane. This platform offered more sophisticated approaches to both remote sensing and photogrammetry for the purposes of mapping the surface. Eventually further technological advances in both aerial vehicles, cameras and sensors along with computer and software offered extensive aerial photographic capabilities. These capabilities are illustrated in this research through the utilization of aerial photography for the construction of spectral-based land cover maps for wetland monitoring.

Remote Sensing

Modern day remote sensing is defined as collecting or sensing radiation that is naturally emitted or reflected by the earth's surface, from the atmosphere, or by sensing signals transmitted from a device and reflected back to it. Essentially, this is done at a distance to interpret information about the environment and the surface of the earth (Pidwirny 2006; Wolf, DeWitt, and Wilkinson 2014). Aerial remote sensing offers researchers and scientists the capability to observe something on the surface without ever to have come in physical contact with the object in question. Deriving and classifying

spectral information from aerial photography for the purposes of land cover mapping is the remote sensing methodology used in this research.

Objects can be remotely sensed in two forms: actively and passively. Active remote sensing refers to a sensor that provides its own source of electromagnetic radiation to illuminate the object in question and then captures its reflectance (Wolf, DeWitt, and Wilkinson 2014). Passive sensors do not have their own source of electromagnetic radiation, rather they measure the amount of electromagnetic radiation that is reflected or emitted by an object (Wolf, DeWitt, and Wilkinson 2014). Remote sensing platforms enable sensors to reach certain locations to capture a phenomena. The three types of platforms include terrestrial, aerial, and orbital. Terrestrial platforms refer to ground-based platforms which include tripods or a ground-based vehicle such as a truck with a sensor attached to it. Aerial platforms hover and fly across within Earth's atmosphere. These include kites, balloons, and airplanes (Watts, Ambrosia, and Hinkley 2012). Orbital platforms are suspended in orbit around the Earth and they include satellites like the Landsat 8 or something more sophisticated like the International Space Station (ISS) (Peterson et al. 2003). The focus of this study primarily touches upon aerial and orbital platforms, specifically Unmanned Aerial Vehicles (UAV), airplanes, and satellites.

Historically, remote sensing was critical in gathering reconnaissance of enemy troop movement in World War I (Rango et al. 2009; Théau 2012; Wolf, DeWitt, and Wilkinson 2014). These aerial photographs were taken using an airplane as the primary platform. World War II brought with it the induction of color photography, increasing the amount of information that could be gathered about the surface (Rango et al. 2009;

Théau 2012; Wolf, DeWitt, and Wilkinson 2014). Sensors and cameras attached to airplanes gave an unprecedented amount of surface information at the time. The ability to systematically capture aerial photography through the use of an airplane offered greater spatial coverage than was possible with kite or balloon aerial photography.

The next phase in remote sensing took place with the revolution of satellite technology. The first artificial satellite was successfully launched and put into orbit by the Soviet Union in 1957 (Watts, Ambrosia, and Hinkley 2012; Wolf, DeWitt, and Wilkinson 2014). The fervor generated from this carried over to the United States and other countries that wanted to install their own satellites for a wide variety of applications. The development and advancement of satellite technology paved the way for modern-day digital remote sensing (Théau 2012). For this purpose, satellites are a tremendously valuable platform. They can provide fairly high resolution images of nearly any point on Earth. With respect to geography and geospatial science, their most significant characteristic lies in their ability to provide synoptic coverage in a single image (Peterson et al. 2003). This characteristic is very important for researchers dealing with continental to global phenomenon in applications such as climatology or oceanography (Peterson et al. 2003). While there are many types of satellites currently in orbit, this discussion only refers to a handful of those satellites responsible for Earth and environmental monitoring. Famous examples of earth monitoring satellites and sensors that are currently in orbit include Landsat, MODIS, MERIS, and NEMO (Peterson et al. 2003).

Photogrammetry

The concept of photogrammetry contains some relevance to this research as it relates to data collection using UAVs and data processing in the form of constructing digital models using advanced image-based software. "Photogrammetry has been defined by the American Society for Photogrammetry and Remote Sensing [ASPRS] as the art, science, and technology of obtaining reliable information about physical objects and the environment through processes of recording, measuring, and interpreting photographic images and patterns of recorded radiant electromagnetic energy and other phenomena" (Wolf, DeWitt, and Wilkinson 2014, 12). The transition from analog to digital photogrammetry redefined the way in which data is collected (Hassani and Carswell 1992; Taylor and Neely 1994). Digital, as it relates to photogrammetry, refers to the use of storing data in computer memory, which in this case would be pixel information that expresses the exposure on an electronic sensing device (Hassani and Carswell 1992; Wolf, DeWitt, and Wilkinson 2014). This type of photogrammetry relies on digital cameras and sensors that can manipulate and capture images using a computer. This research uses digital photogrammetry for its data collection and data processing through the utilization of Agisoft PhotoScan for digital model and orthophoto construction using sequential aerial images gathered from a UAV.

There are two types of areas within photogrammetry: metric photogrammetry and interpretative photogrammetry (Wolf, DeWitt, and Wilkinson 2014). Metric photogrammetry involves making exact measurements such as size, distance, angles, areas, and shapes from photos to determine the relative location of points (Wolf, DeWitt, and Wilkinson 2014). Metric photogrammetric applications includes the development of

planimetric and topographic maps derived from photographs (Wolf, DeWitt, and Wilkinson 2014). Interpretative photogrammetry deals with recognizing and identifying objects and judging their significance through a systematic analysis and it puts an emphasis on image interpretation and remote sensing (Wolf, DeWitt, and Wilkinson 2014). For the purposes of this research, metric photogrammetric approaches are used in the algorithms of the image based Structure-from-Motion (SfM) software Agisoft PhotoScan to create a digital model of Brookhurst Marsh. This software uses angles, distances, areas, and shapes across sequences of images to construct digital models. Photogrammetry is especially important when it comes to acquiring the UAV aerial imagery. It requires images to be captured at specific angles, overlaps, and intervals to properly create these high quality models (Rango et al. 2009; Eisenbeiss and Sauerbier 2011; Wolf, DeWitt, and Wilkinson 2014). In this study, photogrammetric workflows are used to create two-dimensional orthophotos for the purposes of spectral-based land cover mapping. An in depth look of these photogrammetric workflows used to develop a digital model of Brookhurst Marsh are provided in Phase III of the methodology.

Developments in photogrammetry and remote sensing have shared a similar path to get to where they are presently in the world of physical geography and geospatial science (Wolf, DeWitt, and Wilkinson 2014). Airplanes and satellites have traditionally been the main platforms for remote sensing for over a century. While their capabilities are still valuable, this study centers on an aerial platform that has been making significant advances in the remote sensing world during the past decade. Development in aerospace technologies have expanded the capability of Unmanned Aerial Vehicles (UAV) to function as remote sensing platforms (Rango et al. 2009; Eisenbeiss and Sauerbier 2011;

D'Oleire-Oltmanns et al. 2012; Kelcey and Lucieer 2012; Watts, Ambrosia, and Hinkley 2012).

Unmanned Aerial Vehicles (UAV)

The development of the aircraft coincides with the development of Unmanned Aerial Vehicles (UAV) also known as Unmanned Aerial Systems (UAS) or Remotely Piloted Vehicle (RPV) (Eisenbeiss and Sauerbier 2011; Watts, Ambrosia, and Hinkley 2012). UAV are aerial vehicles that do not have a human pilot onboard. They are aerial platforms that are autonomous or remotely controlled by a ground operator. An Unmanned Aerial System (UAS) encompasses the aircraft component, sensor payloads, and a ground control station.

Beginning in the 1800s, bombs attached to unmanned balloons were dropped in Venice and the American Civil War (Watts, Ambrosia, and Hinkley 2012). The modern UAV/UAS technology most people are familiar with, was introduced in the 1960s. Developed out of the necessity to protect pilots from potential physical harm, engineers began designing systems and architecture to enable control of these aerial platforms without ever having to set foot in them (Rango et al. 2009; Watts, Ambrosia, and Hinkley 2012). Initially, UAVs were strictly a military technology. They were utilized for reconnaissance, patrol and enforcement, and armed countermeasures. The first UAV to take photography for aerial reconnaissance was the Radioplane RP-71 in 1955 in the United States (Rango et al. 2009). Modern UAV capabilities for civilian applications were produced from the advancement of military capabilities during the Vietnam War era (Rango et al. 2009; Watts, Ambrosia, and Hinkley 2012). The most renowned of these is

the Predator drone. Developed in the 1990s, the Predator drone was able to capture 30cm resolution imagery (Rango et al. 2009).

UAVs are categorized into six classes based on their size, flight endurance, and capabilities. These are Micro or Nano Air Vehicles (MAV) (NAV), Vertical Take-Off and Landing (VTOL), Low Altitude-Short Endurance (LASE), Low Altitude-Long Endurance (LALE), Medium Altitude-Long Endurance (MALE), and High Altitude-Long Endurance (HALE) (Watts, Ambrosia, and Hinkley 2012). The MAV or NAV type is utilized for this research. The MAV is designed for short duration missions that operate under an altitude of around 1000 feet and have flight times shorter than 20 minutes (Watts, Ambrosia, and Hinkley 2012). The size limitations of these type of UAVs tend be to be favorable to deploying in the field for efficient field data gathering but have payload constraints (Kelcey and Lucieer 2012; Watts, Ambrosia, and Hinkley 2012). The flight mode is dependent on the type of UAV used. As UAV flight automation increases, the cost of the UAV does as well (Peterson et al. 2003; Rango et al. 2009; Kelcey and Lucieer 2012; Watts, Ambrosia, and Hinkley 2012). For this research, the flight mode utilized is the manual flight mode. This means that all degrees of freedom and motion are controlled by a human operator (Watts, Ambrosia, and Hinkley 2012).

With respect to remote sensing, UAV inclusion is relatively new (D'Oleire-Oltmanns et al. 2012). The spatial characteristic of UAVs makes them more viable for localized research (Peterson et al. 2003; Kelcey and Lucieer 2012). Depending on their payload configurations, UAVs can offer high spatial resolution datasets that are tailored for researchers conducting studies over areas that are difficult to access otherwise

(Peterson et al. 2003; Rango et al. 2009; Eisenbeiss and Sauerbier 2011; D'Oleire-Oltmanns et al. 2012; Kelcey and Lucieer 2012). Repeatability and flexibility is increased using the UAV platform because of their ready-to-deploy capability. The ability of UAVs to provide these valuable datasets comes at a minimal cost with respect to training and risk (Peterson et al. 2003). Additionally, the UAV utilized for this study offers higher spatial resolution capability than airplane or satellites because it operates at altitudes much lower than orbital or standard airplane platforms. Spatial resolution refers to the level of detail in an image which is based on the number of pixels in that image. This characteristic makes the utilization of UAV acquired imagery valuable and advantageous bearing in mind that payloads across all platforms are of consistent quality (Peterson et al. 2003; Rango et al. 2009; Eisenbeiss and Sauerbier 2011; Lin, Hyyppa, and Jaakkola 2011; Kelcey and Lucieer 2012; Chabot, Carignan, and Bird 2014).

There are inconsistencies in aerial data collection using the UAV platform (Mitchell et al. 2012). This accuracy is completely dependent upon the UAS that is utilized. In order to achieve higher accuracy datasets, a UAS has to incorporate more sophisticated navigation systems, precise control mechanisms and higher quality payload configurations (Eisenbeiss and Sauerbier 2011; Watts, Ambrosia, and Hinkley 2012). Unfortunately the cost of the hardware can be prohibitive for independent researchers (Watts, Ambrosia, and Hinkley 2012). Thus traditional UAS applications rely on consumer grade cameras and sensors and their accuracy is dependent on aerial trajectory, global positioning systems, and inertial measurement units. These limits have been circumvented with the utilization of advanced computer visualization and tracking

software that provide a new level of image processing and manipulation even with access to less sophisticated UASs.

A broad spectrum of environmental applications have been enhanced by the utilization of UAVs in conjunction with different image software sets. These UAV remote sensing based applications are illustrated in the following section. For the purposes of this study, the term "UAV" is used to describe the actual vehicle or platform while the term "UAS" refers to the complete end-to-end structure that includes the UAV, any flight planning or navigation software/hardware, the remote sensing payload or sensor, and the processing and analysis of UAV acquired products.

Remote Sensing Applicability

The use of UAV/UAS remote sensing platforms is relatively new. UASs provide flexibility with respect to spatial and temporal resolution, reduce costs, and are relatively easy to deploy in the field, all of which are qualities that benefit researchers and increase feasibility of data collection (Peterson et al. 2003; Rango et al. 2009; Eisenbeiss and Sauerbier 2011; Lin, Hyyppa, and Jaakkola 2011; Kelcey and Lucieer 2012; Mitchell et al. 2012; Flener et al. 2013; Mancini et al. 2013; Chabot, Carignan, and Bird 2014). The following overview illustrates the diversity of functions the UAV platform can provide in numerous fields of research.

D'Oleire-Oltmanns et al. (2012) incorporated a fixed UAV platform called, Wing Sirius I, equipped with a Panasonic Lumix GF1 digital camera to study the volumetric change of alluvium in Souss in southern Morocco near the city of Taroudant, Souss-Massa-Drâa (D'Oleire-Oltmanns et al. 2012). The UAS they utilized was an autonomously piloted UAV that captured aerial imagery of the test site at elevations of

50-600m (D'Oleire-Oltmanns et al. 2012). It was given preflight trajectories through the use of a flight program. Additionally they collected ground control points to georeference and geometrically correct their datasets by placing markers along the study area that would be captured by the UAV when imaging the study site. Using small-format aerial photography (SFAP) and triangulation methods they were able to create orthoimages and develop three-dimensional digital terrain models of the area. Using this information they were able to conduct GIS analysis and measure soil erosion by measuring volume change in the gully of the test site (D'Oleire-Oltmanns et al. 2012). D'Oleire-Oltmanns et al.'s research provides great insight into photogrammetry, specifically as it relates to capturing data and constructing orthophotos using both ground control points and georeferencing techniques. Their methodology provides meaningful information for the construction of UAV orthophotos of Brookhurst Marsh which are used to develop spectral based land cover maps.

One of the most common applications of UAV is in rangeland assessment, and it was one of the first civilian protocols to be established as soon as UAV development transferred from being strictly military (Rango et al. 2009). Because rangeland monitoring requires high spatial resolution, usually better than 25cm, UAV platforms are best for the task (Rango et al. 2009). In order to test out UAV capabilities in a rangeland environment, Rango et al. researched and bought the BAT-3 mini-UAV system which contains an onboard navigation unit. A ground operator was manually piloting the UAV. Basically, they wanted to test an off-the-shelf system that was tailored for the needs of the U. S. Natural Resources Conservation Services and similar agencies, so that these agencies could see the benefits of utilizing UAV technology (Rango et al. 2009). They

conducted the evaluation at the Jornada Experimental Range in southern New Mexico and Arizona (Rango et al. 2009). Their assessment resulted in sub 5cm spatial resolution which easily allowed for the "detection of individual plants, vegetation type, bare soil, gaps between vegetation, and patterns over the landscape not previously possible with the normal remote sensing data" (Rango et al. 2009, Pg. 6). With that they generated land cover maps of the rangeland through mosaicking and orthorectification of the UAV imagery. Similar to other research, they noted that wind and thermals could potentially cause some instability in the UAV platform and that storage limitations can be an issue since UAVs could take thousands of high quality images on a single flight (Rango et al. 2009). The conclusions presented by Rango et al. (2009) were taken into account and presented in detail in the methodology.

Case study of UAV flight modes. A detailed discourse on UAV flight modes and photogrammetric methods was developed by Eisenbeiss and Sauerbier (2011). They analyzed different methods of UAV aerial flight modes. These included the manual flight mode, the semi-automated/assisted system, and the autonomous flight mode (Eisenbeiss and Sauerbier 2011). They looked at three different image acquisition modes: manual, stop mode, and cruising mode (Eisenbeiss and Sauerbier 2011). They accomplished this by conducting four case studies at ancient archaeological sites: two Peruvian sites at Pinchango Alto and Pernil Alto, a Mayan site in Copa´n, Honduras and a Bhutanese site at Drapham Dzong (Eisenbeiss and Sauerbier 2011).

At Pinchango Alto, they utilized a UAV helicopter equipped with a Canon D20 still-video camera. In this case, they used stop mode image acquisition with an assisted flight mode (Eisenbeiss and Sauerbier 2011). They were able to derive digital surface

models and orthophotos of Pinchango Alto using the UAV acquired imagery along using the Leica Photogrammetry Suite (LPS) software package along with an in-house software set called BUN (Eisenbeiss and Sauerbier 2011). In addition, they discussed image storage as being another consideration to be taken into account and that it will depend on the needs of the specific research (Eisenbeiss and Sauerbier 2011). At Pernil Alto, they utilized the same methods and the same UAV helicopter except this one had an upgraded navigation unit and was equipped with a Nikon D2Xs 24mm lens camera unit (Eisenbeiss and Sauerbier 2011). For this assessment they employed the assisted flight mode with a ground operator and used the manual image acquisition mode at two different altitudes of 75m and 300m (Eisenbeiss and Sauerbier 2011). They followed the same photogrammetric approaches as they did for the Pinchango Alto imagery to create digital surface models and orthophotos of Pernil Alto (Eisenbeiss and Sauerbier 2011). They did not go into detail on specific workflows used within these software sets. Their experience with capturing aerial imagery at Pinchango Alto helped them conclude that the size of the area flown for aerial acquisition has to be taken into consideration. They recommended that flight lines should be extended to capture the entire object of study. They also mentioned that ground control points are necessary for camera calibration purposes (Eisenbeiss and Sauerbier 2011). At Pernil Alto, they noted that people had to be moved out of the test site during the flight so that the acquired aerial imagery would not be affected. Thier findings about planning and pre-flight considerations are all presented in detail in Phase I of this research. The photogrammetric ideas presented in this part of the study were beneficial in framing Phase III of the methodology.

Specifically, their utilization of LPS and BUN in developing digital models and orthophotos is noted in this research for the construction of land cover maps.

At Copa'n, they, again, used the same UAV helicopter but this time they used a 35mm lens along with the 24mm lens for their digital camera unit (Eisenbeiss and Sauerbier 2011). They also noted an upgraded navigation unit was used in the UAV helicopter. For this case study they used an autonomous flight mode and employed the cruising image acquisition mode (Eisenbeiss and Sauerbier 2011). One unique feature to note was that they used digital maps for their preflight planning and they pointed out that wind influences had negatively affected the imaging results. Essentially they stated that weather is an important consideration in flight planning when operating a UAV (Eisenbeiss and Sauerbier 2011). These two considerations are important and are detailed in Phase I of the next methodology.

Lastly, their final application site took them to the isolated area of Drapham Dzong, in Bhutan, where they utilized a UAV quadcopter for data collection. They had chosen it because of its lightweight characteristic which enabled it to reach higher altitudes with less energy (Eisenbeiss and Sauerbier 2011). It was also easy to transport to and from the test site. The one downside to their choice was that this UAV was more susceptible to wind turbulence. Just like the other UAV, it contained an on board navigation unit, operated under the assisted flight mode and utilized a cruising image acquisition mode. They noted that the tailwind affects image acquisition more than the downwind (Eisenbeiss and Sauerbier 2011). The digital surface model product they produced using LPS contained a 5cm spatial resolution. Using that model they were able to generate orthophotos, a three-dimensional textured model, as well as a map of the

archaeological site. Their conclusions about Quadcopter performance in moderate wind situations at this site informed Phase I of this research. Eisenbeiss and Sauerbier's (2011) workflows for collecting the aerial imagery and generating surface models are important for the methodology of this research.

In summary, Eisenbeiss and Sauerbier (2011) concluded that the UAS affects the photogrammetric analysis. Manually controlled UAVs are not as stable as assisted or autonomously controlled UAVs (Eisenbeiss and Sauerbier 2011). The stop mode image acquisition reduces overall flight time, but is not as stable in maintaining flight direction as the other image acquisition methods. Additionally, the UAVs they utilized were successfully tested under extreme weather conditions in their analysis (Eisenbeiss and Sauerbier 2011). The increased spatial resolution and accuracy of the UAV photogrammetric derived products and the ease of accessing isolated archaeological sites make the UAV a much more viable platform (Eisenbeiss and Sauerbier 2011). Lastly, the low cost to purchase and operate such platforms should be very attractive for researchers looking for a more customizable data set. The trend for UAV platforms is shifting towards multi-rotor systems because of their stability (Eisenbeiss and Sauerbier 2011). The ideas presented in this study related to pre-flight planning, UAV operation, and photogrammetry contribute significantly to this research.

UAV payload and deployment. The important feature in all UAV are their payload configurations. In remote sensing, higher spectral resolution offers a more accurate representation of an object's spectral response pattern. Spectral resolution refers to the ability of a sensor in a payload to distinguish fine wavelength intervals (Wolf, DeWitt, and Wilkinson 2014). The payload is a critical element that is related to the type

of data that can be collected (Watts, Ambrosia, and Hinkley 2012; Chabot, Carignan, and Bird 2014). Kelcey and Lucieer (2012) conducted a study where they tested low-cost consumer grade multispectral sensors aboard a UAV platform. They provided an in depth analysis on which spectral filters to use and for which purpose. They conducted this study for vegetation monitoring in order to illustrate how data quality can be improved through the utilization of different sensors by and analyzing their characteristic (Kelcey and Lucieer 2012). They employed an octocopter UAV platform and installed a miniature camera array that housed six band multispectral sensors from Tetracam Inc. and gathered UAV imagery of salt marsh communities in Ralphs Bay, Australia (Kelcey and Lucieer 2012). In order to gather high quality vegetation reflectance data, they made the necessary sensor corrections and radiometric calibrations. Their analysis went into detail about which various sensor calibrations worked best for their purposes of vegetation monitoring in the area. Essentially, their reasons for using UAV as opposed to another platform included the low preparation time and the ability of UAVs to serve as a scale gap between satellite and full scale aerial photography, along with field surveys (Kelcey and Lucieer 2012). The discourse about spectral vegetation monitoring and the use of filters for aerial imagery was very important in shaping the data collection and data analysis especially as it related to the spectral-based land cover mapping methodologies for this research.

The one advantage UAV remote sensing provides is capturing features at a higher spatial resolution than normal aerial remote sensing methods. There are a lot of studies that discuss the types of sensor payloads UAVs can carry. Lin, Hyyppa, and Jaakkola (2011) provide a great example of utilizing UAV remote sensing for high spatial

resolution mapping by outfitting it with a Light Detection and Ranging (LIDAR) system. In their study, they equipped a LIDAR system called Sensei onto their UAV Alight T-Rex 600 E copter. This UAV had a payload of 7kg, it was low cost, was able to supply local reference data with high spatial resolution, and it could collect high temporal resolution data efficiently. Its applicability was found to be very useful in dangerous situations such as measuring floods. After obtaining the necessary data using the UAV they utilized point cloud post processing methods to develop various tree models of the study area in Finland. Similar methods are showcased in the methodology of this research. Their findings indicated that high spatial resolution mapping by mini UAV LIDAR could definitely resolve the underestimation of tree heights. Along with that they developed a multi-scaled rasterization schematic which was proposed with their canopy surface model. They concluded that UAV LIDAR could essentially produce more accurate tree models, more integral pole morphologies, more applicable information for road extraction, and more definitive variables for digital terrain model refinement. Their use of a LIDAR payload offers a great example of the potential that UAV remote sensing has to offer for mapping and modeling the surface. This study shows UAV acquired aerial image applicability for high resolution spectral based land cover mapping.

In general, surfaces on the planet differ based on the reflective and emissive characteristics of the material that comprises them. UAV offers researchers the unique capability to capture these surfaces at a higher spatial resolution than other aerial and orbital platforms while offering a greater degree of flexibility (Rango et al. 2009; Eisenbeiss and Sauerbier 2011; Lin et al. 2011; Kelcey and Lucieer 2012; Chabot, Carignan, and Bird 2014). An example of an area of environmental spatial analysis that

has been challenging in the past has been modeling river bed terrain. Accurate terrain models are crucial for hydraulic modeling applications and fluvial geomorphology, but gathering spatial datasets can be difficult using conventional methods. Flener et al. (2013) proposed a new methodology to create seamless topographic models in river environments by combining both boat-based terrestrial laser surveys (TLS) and UAV aerial imagery to create optical bathymetric models of the river bed and topographic models of the floodplains. They attempted to overcome the major hurdle in mapping river environments, which lies in creating accurate and continuous representation of the submerged river bed (Flener et al. 2013). Traditional methods have included using sonar systems, but with river beds being so shallow, that method is virtually useless because of the standard 1m depth requirement. As a result, airborne remote sensing allows the mapping of larger river areas contiguously without any minimum depth requirements. They performed their study at a meander bend of the River Pulmanki in Finnish Lapland. Employing two TLS's and the UAV aerial imagery, they generated digital terrain models. The UAV they used was a 700-800 MHz class radio controlled helicopter that was outfitted with a 12. 3 megapixel Nikon D5000 camera and a 16. 2 megapixel NikonD5100 camera (Flener et al. 2013). For this study the UAV was manually controlled. The river bed mosaics produced by the UAV imagery contained elevation accuracies under 10cm (Flener et al. 2013). Their conclusion rated the TLS as being the more accurate technology for their purposes but was extremely time consuming. Flener et al. (2013) recommended that combining the TLS with a UAV is the best option in terms of accuracy, but a UAV-only schema is sufficient for basic modeling purposes.

The methodology and conclusions discussed by Flener et al. provided valuable information for the methodology and influence the findings of this research.

Advanced UAV applications. UAV remote sensing is not limited to two-dimensional modeling. The most state-of-the-art UAV application is taking place in three-dimensional digital modeling. As geovisualizations are increasing in complexity, the need for accurate spatial terrain data is increasing as well (D'Oleire-Oltmanns et al. 2012 and Mancini et al. 2013). Thus high resolution imagery taken by UAV is in increasing demand. Three-dimensional modeling offers the capability to see the topography of the surface. Mancini et al. discuss this notion by referring to one area of photogrammetry called Structure-from-Motion (SfM), which is a three-dimensional digital model generation method (Mancini et al. 2013). Specifically, they wanted to develop digital surface models using a high spatial resolution and vertically accurate dataset for coastal geomorphology. To accomplish this, they used a vertical-takeoff-and-landing (VTOL) hexacopter designed by SAL Engineering which was equipped with a Canon EOS mode 550D digital camera to capture high quality aerial images of the fore-dune located in Ravenna, Italy, on the north Adriatic coast (Mancini et al. 2013). They conducted an accuracy assessment through TLS ground referenced points and they collected one image per second with a flight time of 7 minutes images at 40m altitude (Mancini et al. 2013). They used Agisoft PhotoScan to perform the SfM algorithm on the 550 images collected to generate a spatial model of the beach-dune system (Mancini et al. 2013). Their results showed an accuracy comparison between the TLS and UAV derived data to be extremely similar and under 5cm accuracy, with UAV just edging out TLS in being slightly more accurate and they noted that their TLS surveys took much longer to

initiate than the 7 minutes it took the UAV to capture the same data (Mancini et al. 2013). The photogrammetric ideas presented by Mancini et al. were used in this research. Overall, their results provides a noteworthy example of the spatial and temporal efficiency of the UAV remote sensing platform for the development of high resolution digital modeling. It also shows the power the UAV platform can offer in developing sophisticated visualizations. Mancini et al.'s (2013) PhotoScan workflow for the construction of digital terrain models was used as part of Phase III of this research methodology.

The different studies in this section present an overview of the progress that has taken place in the field of UAV remote sensing. The UAV platform provides researchers capabilities that have demonstrated to exceed other platforms when it comes to flexibility, costs, accuracy, and time. The increasing sophistication of both UAV and payload sensors continue to offer significant advantages to collecting accurate data. Data collection is an integral part of any research, and UAV remote sensing is easing the way for researchers towards achieving their goals.

Vegetation Land Cover Analysis

This research is focused on a temporal and ecological assessment of Brookhurst Marsh at the Huntington Beach Wetlands. Time is a critical element which assesses the degree to which a certain phenomenon has changed or not changed. Time in this instance illustrates how vegetation distribution at the Huntington Beach Wetlands has altered over the last few years. Ecologically speaking, vegetation is analyzed by its spatial distribution across the study area. Consequently, one of the main foundations of all the methods used in this study is vegetation land cover analysis. The purpose of this land

cover analysis is to attempt to narrow the gap between UAV aerial image collection and limiting ground surveys for land cover based vegetation community mapping. This section details the different analytical techniques for developing spectral based land cover maps that were successfully utilized in other studies and are implemented in this research.

The inception of satellite remote sensing was revolutionized with the launch of the first Landsat satellite. This offered researchers the capability to periodically monitor phenomenon at a sub-continental scale. Vittek et al. (2014) present a land cover change assessment of West Africa between 1975 and 1990. Specifically they utilized Landsat data to track changes in forest characteristics including tree cover, tree cover mosaic, wooded land, and other vegetation cover to observe the rate at which deforestation was occurring (Vittek et al. 2014). Because this research relies on spectrally analyzing and classifying satellite remote sensing, their breakdown of satellite image analysis is very important. Their image sources were acquired from the Landsat multi-spectral scanner (MSS), between 1972 and 1980. The multispectral sensor on-board Landsat 1 and 2 satellites acquired images through four spectral bands with a spatial resolution of 80 meters. For the 1990 reference year, Landsat Thematic Mapper images acquired by Landsat 4 and 5 satellites between 1985 and 1995 were used. The Thematic Mapper images were acquired in six spectral bands with a spatial resolution of 30 meters. With the necessary data acquired, they needed to process it before using it for any type of analysis. They performed a dedicated image selection process to utilize only the highest quality images for their analysis. Continuing with their processing tasks, they had to co-register and radiometrically calibrate the images. For these tasks they used the 1990 image as their reference image and georeferenced the 1975 image in accordance with the

1990 image for accuracy. Their image processing workflow is replicated for all datasets in this research and is detailed in Phase III of the methodology.

For their data analysis, they used eCognition, a popular object based image analysis (OBIA) software package to perform their image analysis. Within eCognition they used the image segmentation tool to group pixels based on spectral similarity and spatial adjacency and they performed a multi-date segmentation by stacking the two individual sets of data (Vittek et al. 2014). Finally, they used a supervised classification with a spectral library and performed a change detection analysis. They delineated classes of "changed" and "unchanged" based on the Euclidean distance from red, near-infrared, and shortwave-infrared bands (Vittek et al. 2014). With their data they were able to derive statistics to quantify the amount of change in vegetation cover that took place in Western Africa between 1975 and 1990. While this research does not utilize eCognition, Vittek et al.'s (2014) work developing supervised classifications using spectral based classes is used in Phase IV of the methodology. Specifically, land cover maps using airplane, satellite, and UAV imagery are developed through the construction of spectral-based classes.

Ali and Pelkey (2013) undertook a study to determine vegetation cover change from invasive herbivores on the Andaman Islands located in the Indian Ocean. They calculated two different types of vegetation indices from two different satellite datasets for their analysis. They utilized the 1986-1995 from Advanced Very High Resolution Radiometer as well as 2000-2005 imagery from the Moderate-resolution Imaging Spectroradiometer (MODIS) for their research. (Ali and Pelkey 2013; NOAA 2015) They first mosaicked the AVHRR dataset that contained cloud-free Normalized

Difference Vegetation Index (NDVI) images. These images were further processed to reduce interference through bands 1 and 2 from the dataset (Ali and Pelkey 2013). They obtained NDVI composite imagery which was derived from MODIS. The resulting NDVI images from both sensors were used to conduct an analysis across four sites on the islands. They were able to identify vegetation that was affected by anthropogenic and natural effects. Their work with using temporally different NDVI images is very similar to the analysis of this research especially as it relates to utilizing specific spectral bands within the UAV and satellite imagery to perform the NDVI calculation. Ali and Pelkey's (2013) methods helped shape the data processing and data analysis portion of this research.

Literature Assessment and Research Goals

This chapter has covered the fundamentals of remote sensing, photogrammetry, the UAV platform, and temporal vegetation land cover analysis. Specifically, it has illustrated the photogrammetric approaches that were used to develop and process the UAV and airplane imagery, shown the applicability of UAV for remote sensing, and presented methodologies for vegetation land cover analysis using both satellite and UAV platforms. While UAV based aerial photography has been well documented, this study presents it as a better option over both satellite and airplane platforms. The premise established in this study is that the UAV platform is more feasible and flexible in regards to spatial and temporal remote sensing analysis.

The literature presented also shows that UAV remote sensing in Southern California has been limited, especially for wetland restoration efforts. This is due in part to the fact that federal policy is currently being developed in the United States to

incorporate UAV in the realm of commercial and academic research (Watts, Ambrosia, and Hinkley 2012, FAA 2015). This study is fashioned around delivering a land cover analysis and a comparative framework towards the viability of UAV remote sensing for field work. It provides a detailed data collection, processing, and analysis methodology that can be implemented by other conservancies. This research also provides the potential of using UAV aerial images for periodic change detection analysis.

Traditionally, vegetation land cover analysis especially as it relates to wetland monitoring at the Huntington Beach Wetlands, requires extensive land surveys involving ground-based sampling transects (Whitcraft, Allen, and Lowe 2013). These ground-based methodologies often interfere with local wildlife, are extremely time consuming especially when accurate aerial data is not available for evaluation, and can be costly for researchers (TRCA 2011). This study proposes a viable and cost-effective technique for the assessment of wetland vegetation with minimal potential impact to wildlife. While currently, no method exists to map vegetation communities and species solely from UAV imagery without any ground-based operations, this research provides a way to close that gap by illustrating its viability and accuracy in mapping vegetation land cover. This concrete research methodology can potentially be implemented by land managers. Justification and preference of the UAV platform is demonstrated through the development of spectral-based land cover maps, which are compared and evaluated to land cover maps derived from airplane and satellite based imagery. Ultimately this research augments the assessment conducted by Merkel & Associates (2011) and California State University, Long Beach Biology Department's Dr. Christine Whitcraft

(2013) by providing a unique research methodology that can potentially be implemented to update their 2014-2015 ecological assessment of the Huntington Beach Wetlands.

CHAPTER 3

METHODOLOGY

The goal of this research is to document a UAV-based data collection approach that can be repeated by conservation managers for longitudinal assessment of the Brookhurst Marsh wetland in Huntington Beach, CA. The approach developed can be implemented by conservancy personnel with minimal training. Data collection methods serve as the foundation of any research and operational monitoring program. This chapter outlines the methods used to conduct this research and form the basis for a monitoring workflow. The workflow is separated into four sections: Phase I: Planning and Training, Phase II: Data Collection, Phase III: Data Processing, and Phase IV: Data Analysis. These sections define the study area and present the procedures that went into the project preparation. Additionally, they outline the hardware and equipment used to gather the data and detail the software and tools used to process and analyze those data.

Phase I: Planning and Training

Preparation is the first step to any field data collection methodology. This section is organized into three parts: Site Selection, Pre-Flight Considerations, and Equipment and Payload. The Site Selection section details the specific study site within the Huntington Beach Wetlands that is chosen for analysis. Next, the Equipment and Payload section examines all the hardware and devices used to effectively gather the data in the field. Lastly, Pre-Flight Considerations breaks down the critical and necessary elements to account for prior to data collection.

Site Selection

Completing careful site selection is necessary in order to obtain the appropriate data. Site selection also incorporates obtaining permissions from land owners or land managers in order to operate the UAV and collect data. These are examined in the Pre-Flight Considerations sub-section. The Huntington Beach Wetlands are sectioned off into three main marshes: Magnolia Marsh (16 ha), Brookhurst Marsh (27 ha), and Talbert Marsh (11 ha) (Figure 2).

FIGURE 2. Three marshes of the Huntington Beach Wetland ecosystem.

Brookhurst Marsh was chosen because it is the largest of the three marshes in terms of area and it contains a higher variety of land cover than Magnolia Marsh and

Talbert Marsh. In addition, its location between the other two marshes is ideal for UAV operation because it is away from the Santa Ana River near the south end of Talbert Marsh and the power plants near Magnolia Marsh. Brookhurst Marsh is enclosed by Brookhurst Street on the east side, Magnolia Street on the west side, Pacific Highway on the south and a Residential district on the north along with a small waterway that leads into the Santa Ana River. The marsh is 1000 meters in length, 290 meters wide on the west side and 160 meters wide on the east side. It is a 27 ha wetland that encompasses a wide variety of land cover including water, soil, vegetation, and gravel land cover features (Figure 3).

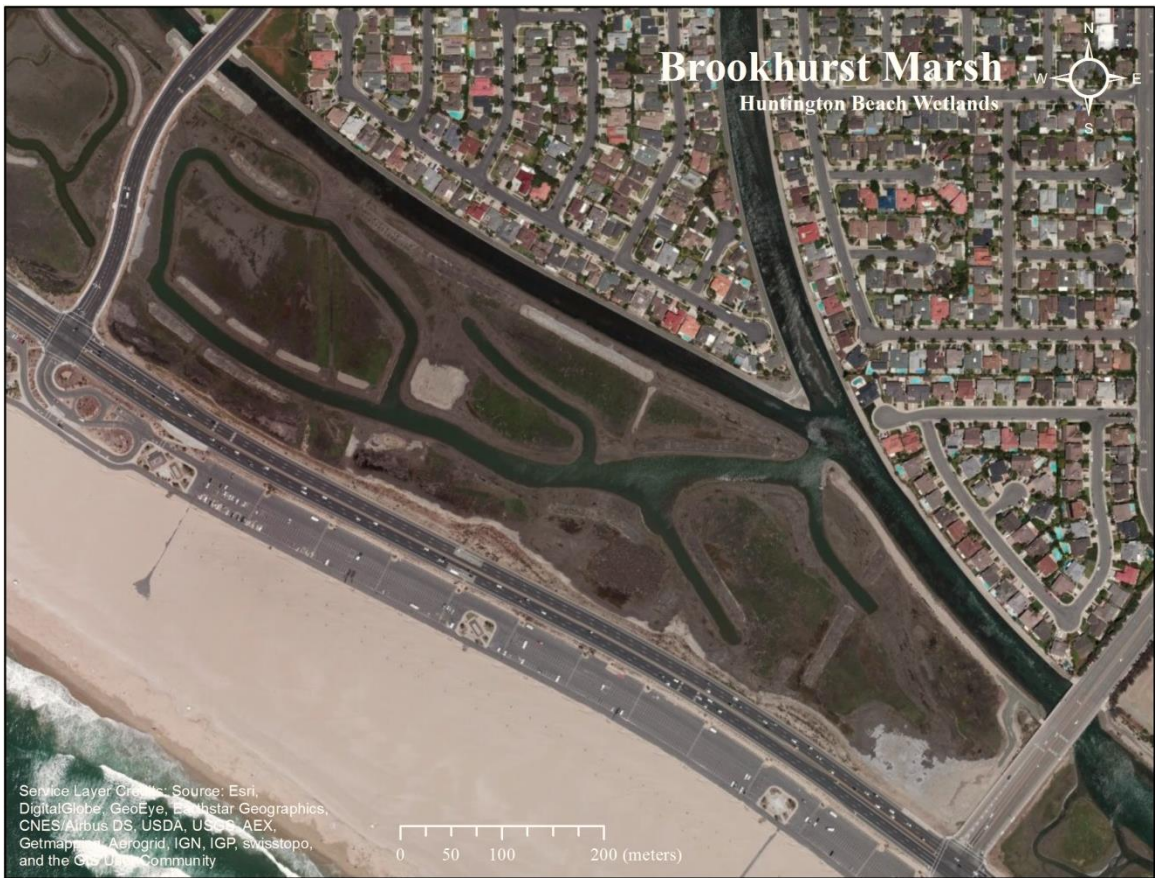

FIGURE 3. Brookhurst Marsh at the Huntington Beach Wetlands.

Equipment and Payload

In order to collect the data, steps needed to be taken to ensure proper handling, care, and use of each piece of equipment. This not only guarantees their proper functioning in the field, but also extends the longevity of the hardware for future use. More importantly, proper use of equipment will provide better results. This section is broken down into three basic elements for further clarification: Platform, Payload, and Ground Operations.

Platform. The platform is the tool used to deliver all the necessary data collection components to the study site through air, land, or water. For this study, the DJI Phantom Quadcopter was used to fly over Brookhurst Marsh and collect aerial imagery (Figure 4). The Phantom is classified as a Micro-UAV (MAV) multirotor system (Watts, Ambrosia, and Hinkley 2012). The standard Phantom 1 costs under US $400 as of May 2015 (Dajiang Innovation Technology 2015). The platform and controller specifications are presented in Table 1. Initially the standard package requires minimal assemblage of propellers, landing gears, and battery mounting. Knowing the operational limits of the UAV is important to flight performance because the addition of different size payloads can alter these limits and change the performance of the platform itself while airborne. Consequently it is necessary to conduct test flights with all payloads that will be utilized beforehand in order to assess the performance of the UAV and make any adjustments to optimize its performance as necessary.

FIGURE 4. DJI Phantom Quadcopter.

TABLE 1. DJI Phantom Quadcopter Specifications (DJI Innovation Technology 2015)

DJI Phantom Quadcopter (Out of the Box/No additional attachments)	
Operating Temperature	-10°C ~ 50°C
Power Consumption	3. 12W
Take-off Weight	<1200g
Hovering Accuracy (GPS Mode)	Vertical: 0. 8m | Horizontal: 2. 5m
Max Yaw Angular Velocity	200°/s
Max Tilt Angle	45°
Max Ascent/Descent Speed	6 m/s
Max Flight Velocity	10 m/s
Diagonal Distance (Motor Center to Motor Center)	350 mm
Phantom Prop Guard	Weight (Single): 18. 7g Size (Single): Angle: 155. 0° | Radius: 112. 32mm Whole Size with Four Prop Guards: 575. 5 mm
Power	20W
Battery Type	LiPo 11. 1 V Lithium-polymer 2200 mAh capacity
Max Flight Time	10 min
Max Payload	365 grams
DJI Phantom 1 Controller	
Working Frequency	2. 4 GHz ISM
Control Channels	7 Channels
Communication Distance	1000 m
Power	4 AA Batteries

Payload. The remote sensing payload consists of components that are attached to the platform, in this case the cameras that capture and store the data from the field. For this study, two different cameras were used to capture aerial images of the Huntington Beach Wetlands. Both cameras were set to interval mode to capture the aerial images. Interval mode is a type of capture mode that automatically captures a frame per given time period. The time period can be set depending on the settings of the camera. For aerial imaging, it is best to set the time period to the minimum the camera allows in order to capture the maximum amount of frames per flight (Wolf, DeWitt, and Wilkinson 2014). The increase in frames leads to an increase in percent overlap per frame which is ideal for aerial imagery and makes it easier for the software to generate orthophotos. Simply stated, the more frames that a given point or object appears in, the higher the geometric and photogrammetric quality of the resulting orthophoto. The first camera used was the PENTAX Optio WG-II GPS (Figure 5). This camera was used as the payload for the test flight at Brookhurst Marsh. The Pentax Optio is a standard three-band color camera that captures images at a minimum interval of ten seconds. The second camera was the Ricoh GR III and it was used to capture the final data at Brookhurst Marsh at an interval of five seconds (Figure 5). The Ricoh GR III is a three-band camera with the internal charge-couple device (CCD) filter removed so in addition to visible wavelengths the camera is sensitive to near-infrared (NIR) energy. The near-infrared wavelength is important in vegetation detection and is detailed in Phase IV. By placing a yellow filter on the camera lens, in this case a Tiffen #15 deep yellow filter (Figure 6), the blue wavelengths are filtered out resulting in a three band image comprised of green, red, and NIR information, much like the traditional Kodak color

infrared film that has been used in vegetation studies for decades (Fisher 2004; Mortimer and Davidson 2012). Specifications for the two cameras are presented in Table 2.

FIGURE 5. PENTAX Optio WG-II GPS (top) and Ricoh GR III (bottom) digital cameras.

FIGURE 6. Tiffen 43DY15 43mm deep yellow 15 filter (left). It was outfitted on the Ricoh GR III (right).

TABLE 2. Camera Specifications Comparison (Amazon. com 2015; Ricoh Imaging 2015)

	PENTAX Optio WG-II GPS	Ricoh GR DIGITAL III
Resolution	16 Megapixels	10 Megapixels
Sensor Type	1/2. 3 inch CMOS (Complementary Metal Oxide Semiconductor) (Backside Illuminated)	1/1. 7 inch CCD (Charge-Coupled Device)
Max Shutter Speed	4 seconds	1/2000 of a second
ISO Range	125, 6400	Auto, 64, 100, 200, 400, 800, 1600
Image Stabilization	Electronic	NONE
Dimensions	1. 9 x 5 x 1. 2 inches	2. 32 x 4. 29 x 1. 02 inches
Maximum Focal Length	25 mm	28 mm
Optical Zoom	5x	1x
Digital Zoom	7. 2x	4x
Battery	Lithium-Ion	Lithium-Ion
Focus Type	Manual	Autofocus & Manual
Weight (with Battery)	198 g	218 g
Additional Attachments	NONE	Tiffen 43DY15 43mm Deep Yellow 15 Filter

This study also required outfitting the Phantom with a mount that would carry the two different cameras. Because the Phantom is originally designed to carry GoPro Cameras, additional mounts and screws were utilized to enable it to carry the Pentax Optio and the Ricoh cameras (Figure 7). In the case of aerial platforms weight is an added dimension to account for. Payloads need to be light enough for the aerial platform to carry without jeopardizing operation of the platform or reducing data quality (Eisenbeiss and Sauerbier 2011; Wolf, DeWitt, and Wilkinson 2014). The quadcopter was outfitted with a proper shock and vibration absorbing mounting system to allow both the Pentax Optio and Ricoh cameras to be mounted without interfering with image

capture or flight maneuverability (Figure 8). It is important that the camera lens remain as perpendicular or vertical to the ground as possible. Any type of angle or shift in the way the camera is situated can result in distorted images or impaired flight maneuverability which can affect the photogrammetric processes for developing orthophotos (Wolf, DeWitt, and Wilkinson 2014).

FIGURE 7. DJI Phantom Quadcopter payload mounts and screws.

FIGURE 8. PENTAX Optio WG-II GPS mount (top) and Ricoh GR III mount (bottom).

Ground operations. To successfully collect a complete, high quality dataset for analysis, steps were taken to ensure proper operation of all the equipment. All necessary equipment needed to be properly assembled and prepared for deployment in the field. For the DJI Phantom quadcopter used in this research, one battery pack provided up to seven minutes of flight time. To cover the study site in a single series of flights 15 battery packs were taken into the field. Also batteries for the cameras were fully charged and camera data cards were emptied to ensure maximum storage availability for image collection. Cameras settings were adjusted on site to account for lighting conditions as they existed in the field and set to interval shooting capture mode before take-off. In addition a Trimble Juno 3B GPS unit loaded with Esri ArcPad software, and ground control markers were taken into the field to collect ground control points (GCP's) while conducting flights (Figure 9). The Trimble unit was placed at the center of the marker to capture the coordinates at that exact location. The markers were placed on the edges of Brookhurst Marsh and can be seen in the final orthophoto. Using ArcPad, the Trimble unit connects to satellites overhead and triangulates a point which stores coordinate information. This point was saved onto a map document in ArcPad and later transferred onto Agisoft PhotoScan and included in the orthophotorectification process.

Pre-Flight Considerations

There were seven logistical elements that were acknowledged and assessed before data were collected in the field. These elements are applicable to this project but can be molded to fit other research methodologies as needed. These elements are: Flight and Site Permissions, Federal Aviation Administration Regulations, Safety and Surroundings, Weather and Visibility, Surface Conditions, Seasonal Variability, and Flight Training.

FIGURE 9. Trimble Juno 3B placed on ground control marker in the field.

Flight and land permissions. Appropriate permissions have to be obtained from land owner(s) or land manager(s) before any data collection can occur. It is important for researchers to notify land owners of their intent as specifically as possible, whether this includes physically traversing on the site or just flying over it with a UAV. Additionally, they should be notified the date of the collection, the type of data collected, and the extent to which the data will be used and/or published. Furthermore, researchers need to assess the degree to which they can operate a UAV and collect data on someone's land based on the permissions granted by land owners. In the case of this study, landowners were contacted by Dr. Christine Whitcraft and permission was obtained to collect data for both the test flight (September 14th, 2014) and the final flight (October 17th, 2014). The land owners in return requested that any and all aerial imagery including orthophotos developed of the study site be shared. They also requested that all individuals on the site

stay close to the edge of the marshes so as to not damage or alter the wildlife or plants. Currently in the United States, the National Park Service has prohibited all UAV commercial operations in National Parks due to concerns for wildlife (NPS 2014).

Federal Aviation Administration (FAA) regulations. Because of the recent rise in recreational and commercial UAV/UAS use, the Federal Aviation Administration (FAA) has been developing ways to regulate their operations as they do with manned aircraft operations. Practice flights, test flights, and the field flight were all conducted in 2014 in accordance with these regulations. During that time, the FAA had a standard policy for recreational and commercial utilization of UAV's. Their 2014 regulations are outlined for both recreational and commercial model aircraft operations (Appendix A).

All flights were conducted on days where there were no Notices to Airmen (NOTAMs) or Temporary Flight Restrictions (TFRs) issued for the Southern California area. The UAV flown in this project was well within the acceptable altitude and speed limits set by the FAA (Appendix A). Beginning in 2015, the FAA updated their recreational and commercial UAV regulations. The FAA used the term small Unmanned Aerial System (sUAS) in their regulations to define UAV's that are portable enough to be carried by a person, such as the DJI Phantom quadcopter. According to these new regulations, the FAA defined recreational use as follows:

> "The recreational use of sUAS is the operation of an unmanned aircraft for personal interests and enjoyment. For example, using a sUAS to take photographs for your own personal use would be considered recreational; using the same device to take photographs or videos for compensation or sale to another

individual would be considered a commercial operation." (Know Before You Fly 2015)

They defined commercial operation as:

> "Any commercial use in connection with a business, including: Selling photos or videos taken from a UAS, Using UAS to provide contract services, such as industrial equipment or factory inspection, Using UAS to provide a professional services, such as security or telecommunications, or providing contract services for mapping or land surveys. If you want to use UAS for a commercial purpose, you have a few options. You can apply for an exemption from the FAA to operate commercially. You can use UAV with an FAA airworthiness certificate and operate pursuant to FAA rules. In both cases you would also need an FAA Certificate of Authorization (COA)." (Know Before you Fly 2015)

Because California State University, Long Beach is classified as a commercial entity, future flights would have to follow the UAV commercial regulations set forth by the FAA. Additional flights were not conducted for this research because of the new FAA commercial UAV regulations.

Safety and surroundings. Safety is another important aspect to consider when operating UAV's for data collection. Safety for other researchers in the field, other people in the vicinity, vehicles, pedestrians, and wildlife especially birds should be noted. In this case, Brookhurst Marsh encompasses a variety of these factors. Because it is adjacent to the Pacific Coast Highway and Huntington Beach, there is constant traffic from both pedestrians and vehicles especially during the noon hours. One very useful feature at Brookhurst Marsh is that it is enclosed by standard fencing on three sides

limiting access to the public. The north side of Brookhurst Marsh leads into a small river approximately 30 meters wide that buffers the residential area from the actual marsh. In regards to the entire Huntington Beach Wetlands, some notable features include a closed power plant northwest of Magnolia Marsh, Brookhurst Street and Magnolia Street in between the three marshes, and the Santa River east of Talbert Marsh (Figure 2).

Weather and visibility. Weather and visibility play a crucial role in the optimization of UAV operation and data quality (Rango et al. 2009; Eisenbeiss and Sauerbier 2011). In order to capture aerial imagery of the highest quality and ensure safe UAV operations, flights have to be conducted on days where weather will not interfere. This means that a UAV should be flown on days with very little to no cloud coverage. It is especially hazardous to fly during periods of low cloud ceiling because the probability of losing track of the UAV while in flight is higher. Additionally, cloud coverage also affects the light from the sun and could darken aerial imagery causing issues in image clarity. Another aspect to consider is wind, primarily for data quality (Eisenbeiss and Sauerbier 2011). While the DJI Phantom can function fine in winds in excess of 20mph the angular shifts it can cause to the sensors and cameras on board can alter and warp the aerial imagery. In relation to photogrammetry, this would be critical for developing orthophotos. Those aerial images captured with an aggressive tilt can result in more differences in size, shape, and area than images captured using a more vertical camera tilt angle (Wolf, DeWitt, and Wilkinson 2014). Distorted and warped imagery can reduce the image quality and accuracy of the orthophoto. While it is impossible to fly the Phantom and capture aerial photos using a near-perfect vertical camera angle, SfM programs like Agisoft PhotoScan can use images with unintentional camera tilts and

process them with little to no loss in accuracy. Finally, it is important that flights are primarily conducted in a four hour window centered on noon to maintain a near-perpendicular sun angle with the surface. If the sun is too low in the sky, there is potential for long shadows projected from even the smallest structures over the study field which could mask features of importance.

Seasonal variability. Seasonal variations affect the amount of vegetation present. On an annual basis there is a phenology of growth and decay as the season shifts from spring all the way to winter. Because of its regional location in Southern California, the Huntington Beach Wetlands have longer periods of flowering and bloom. These variations would alter the data, if they were collected in a different season. At the Huntington Beach, Wetlands, the season for optimal bloom is between April and late October/early November. All the data collected for this research is obtained during the optimal bloom period, thus limiting any sort of variation that may occur as a result of seasonal differences in vegetation abundance.

Surface conditions. Tidal influence affects the surface conditions at the Huntington Beach Wetlands (Woodfield and Merkel 2011; Whitcraft, Allen, and Lowe 2013). This was accounted for during the UAV flight scheduling. Being so close to the Pacific Ocean and the Santa Ana River, the tides in this area can fluctuate between 0.15 and one meter. Tidal flows can interfere with the aerial imagery by covering up landscape with vegetation on it resulting in incomplete assessments. The tidal height recommendation by Dr. Whitcraft was less than 0.5 meters for optimal data collection of vegetation. As a result, both flights conducted at Brookhurst Marsh were scheduled for

times of the lowest possible tide. National Oceanic and Atmospheric Administration (NOAA) tide charts were used to plan the appropriate flight times (NOAA 2015).

Flight training. Learning how to correctly operate the UAV is very important for safety and aerial image acquisition purposes. High quality aerial photography is reliant on the altitude and angle at which images are captured, consistent overlapping of images, correct camera and sensor calibration, and the accuracy of global positioning systems for georeferencing the imagery (Wolf, DeWitt, and Wilkinson 2014). In aerial photogrammetry, images should contain between 50-80% overlap (Eisenbeiss and Sauerbier 2011; D'Oleire-Oltmanns et al. 2012; Flener et al. 2013; Mancini et al. 2013; Wolf, DeWitt, and Wilkinson 2014). Photogrammetric methods for developing orthophotos are strengthened by improving image quality and continuity. High quality images are produced by practicing UAV maneuvers suited for aerial photography. These include maintaining proper horizontal speed, correct altitude, and proper flight trajectory. Moving too fast or overlapping a previously flown path can negatively affect the quality of image acquisition. Practice flights are a sure way to overcome these issues and were done in preparation for the actual flight and data collection. Four practice flights were conducted to gain experience in both flying the Phantom and learning how to operate the different cameras for aerial image acquisition. These practices helped develop the skills necessary to ensure optimum control of the UAV for data collection. It is recommended that at least one or two other people besides the operator help with data collection, so that one can help set up ground control markers and gather ground control points while the other can serve as a second pair of eyes in case the operator loses track of the UAV in the sky. Appendix B shows an example of the test aerial PhotoScan orthophoto collected on

September 14th, 2014. Tables 3 and 4 showcase the different practice, test and final flights conducted for this research.

TABLE 3. DJI Phantom Quadcopter Practice Flight Record

Flight Date	5/9/2014	9/6/2014	9/10/2014
Flight Type	Practice	Practice	Practice
Location	CSULB Quad	CSULB 22 Acres (near Japanese Gardens)	CSULB Quad
Payload	NONE	PENTAX Optio WG-II GPS	Ricoh GR III equipped with Tiffen Filter
Start Time	3:00 PM	10:00 AM	2:00 PM
Duration (Hours)	2	2	0.3
Number of Flights	4	5	1
Weather	75 Degrees, Clear Skies, No wind	86 Degrees, Clear Skies, No wind	90 Degrees, Clear Skies, No Wind
Objective	Introduction to flight operations for the Phantom	Practice flight to test out Optio camera	Practice flight to test out Ricoh Camera and filter
Number of Images Collected	NONE	196	30

TABLE 4. DJI Phantom Quadcopter Brookhurst Marsh Flight Record

Flight Date	9/14/2014	10/17/2014
Flight Type	Test	Final
Location	Huntington Beach Wetlands, 1/4th Brookhurst Marsh	Huntington Beach Wetlands, Entire Brookhurst Marsh
Payload	PENTAX Optio WG-II GPS	Ricoh GR III equipped with Tiffen Filter
Start Time	7:00 AM	9:30 AM
Duration (Hours)	1	2.5
Number of Flights	3	12
Weather	70 Degrees, Clear Skies, No wind	73 Degrees, Clear Skies, No wind
Objective	Preliminary assesment of area and data collection	Final assesment and data collection
Number of Images Collected	92	918

This section has outlined the steps taken prior to heading out to the field for field data collection. It discussed the specific steps taken for site selection, it broke down the equipment and payloads used to collect the data, and listed the key features to consider for UAV data acquisition.

Phase II: Data Collection

This section arranges the data collected into two separate types: primary acquisition and secondary acquisition. Primary data acquisition involves going out in the field and capturing data using the planned methodology illustrated in Phase I. UAV aerial imagery was the primary data acquisition source used in this research. Secondary data acquisition involves utilizing data that has already been collected and developed by another person or group. Satellite imagery and airplane imagery encompassed the secondary data acquisition.

Primary Acquisition

UAV aerial image acquisition is the basis of this study. For both the test flight and the final flight, the flight operations were the same. Flight operations involved maintaining proper flight lines and proper altitude. Because of the basic design of the Phantom, this was manually determined while flying. The benefits of the Phantom is that it has GPS calibration allowing it to maintain a constant altitude as long as no additional user inputs are made. When taking vertical aerial photographs, the flight height and a consistent overlap must be maintained to optimize the coverage and quality of the aerial imagery. The flying height is the altitude above ground level (AGL) of the camera at exposure time. The overlap is the lateral or side coverage that is common between adjacent strips of imagery (Figure 10). The amount of recommended overlap for the

aerial imagery is between 50-80 percent (Eisenbeiss and Sauerbier 2011; D'Oleire-Oltmanns et al. 2012; Flener et al. 2013; Mancini et al. 2013; Wolf, DeWitt, and Wilkinson 2014).

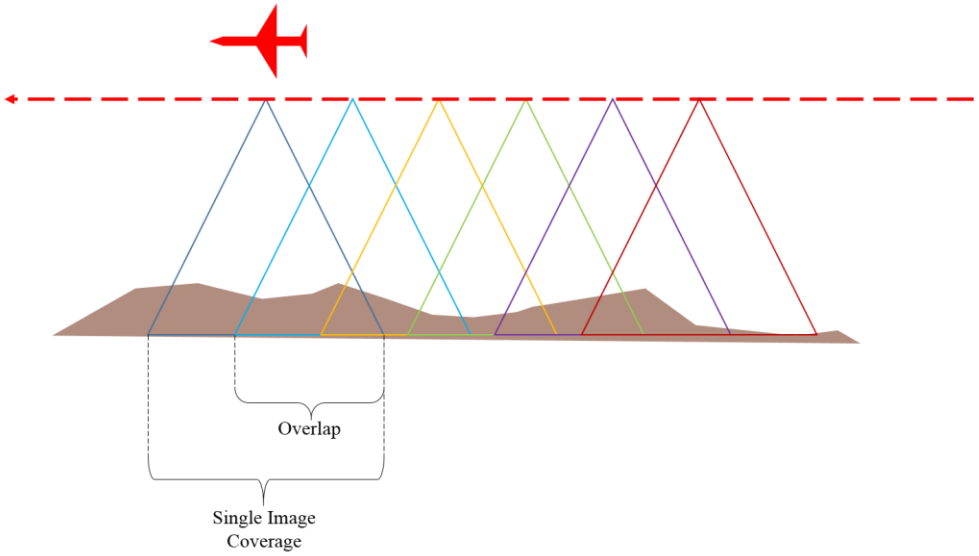

FIGURE 10. Ideal aerial remote sensing acquisition overlap.

Because of the difficult nature of judging the amount of overlap while using the Phantom, a steady rate of horizontal forward movement was maintained for each flight line. For this study, the ideal altitude while using the Phantom was between 90-120 meters. At this altitude, coverage of each image is maximized without reducing image quality. These parameters were experimented with during all the practice flights and test flight. The imaging results from these flights offered a better understanding of what corrections to make for the final flight. More advance UAS have relatively sophisticated flight computers that can track movement in real-time and can even offer preflight or autopilot capabilities to remove any user induced error. They can be programmed to fly a

preset flight plan and maintain a certain altitude. Dajaing Innovation Technology, for example, have more advanced models of the Phantom: Phantom 2 Vision Plus and the Phantom 3 Advanced. These systems cost less than US $1,300 and include built in high-definition cameras, programmable flight plans, and offer real-time telemetry and flight data (DJI Innovation Technology 2015).

For the test flight, the workflow primarily encompassed flight operations which consisted of properly piloting the UAV and following flight lines. Ground operations were only conducted during battery swaps and Pentax Optio activation. Because the DJI Phantom was equipped with the GPS enabled Pentax Optio camera, it was not necessary to capture additional GCP's for detailed georeferencing. The test flight was conducted on September 14th, 2014 and captured one-fourth of Brookhurst Marsh in three flights, all originating from the same take-off and landing point located near the northwest entrance to the wetland (Appendix B). The altitude flown for this dataset was between 90-100 meters from the surface.

For the final flight conducted on October 17th, 2014, the tasks included flight operations and a more extensive ground operation workflow than the test flight. Ground operations consisted of first properly placing ground control markers and obtaining GCP's using the Trimble GPS handheld unit. Next fresh battery packs were put in the Phantom for each flight. Because of the way the Ricoh camera was attached to the Phantom, the struts on the Phantom were held by hand to hold it upright for takeoff. At the same time the interval mode on the Ricoh GR III camera was activated right before launch. After takeoff, UAV flight time was monitored and a secondary pair of eyes helped keep track of the Phantom in the air. Test images were taken on the field with the

Ricoh camera to ensure proper exposure and focus. Because the Ricoh GR III camera does not contain any geotagging feature for captured photos it was necessary to collect GCP's at the study site. Ground operations for the final flight consisted of placing ground control markers at launch sites two, three, six, and twelve (Figure 13). The exact coordinates at the center of the ground control maker were recorded using a GPS unit. The GPS unit was left at the center of the ground control marker for 5-7 minutes in order to give it time to align with the satellites overhead for optimum accuracy (Figure 9). Four ground control points were captured using Esri ArcPad in the Trimble Juno 3B Handheld GPS unit. These were recorded using the Universal Traverse Mercator (UTM) Zone 11 North coordinate system and the World Geodetic System 1984 datum. While operating the UAV, the altitude maintained was between 100-120 meters from the surface. The flight trajectory consisted of moving in a circular pattern in order to make sure the full extent of the area was captured and image overlapping was correctly performed as best as possible. There were a total of 12 flights conducted each lasting around 6 minutes and the total acquisition time was 2. 6 hours. The final UAV acquisition started from site one near the north western-most portion of Brookhurst Marsh, next to Magnolia Street and ended southeastward at site 12 towards Brookhurst Street (Figure 13). PhotoScan provided a three-dimensional visualization of the final texture which illustrated both the height of the image taken by the camera at each 5 second interval and the overlap pattern flown by the UAV for the final image acquisition of Brookhurst Marsh (see Figures 11 and 12).

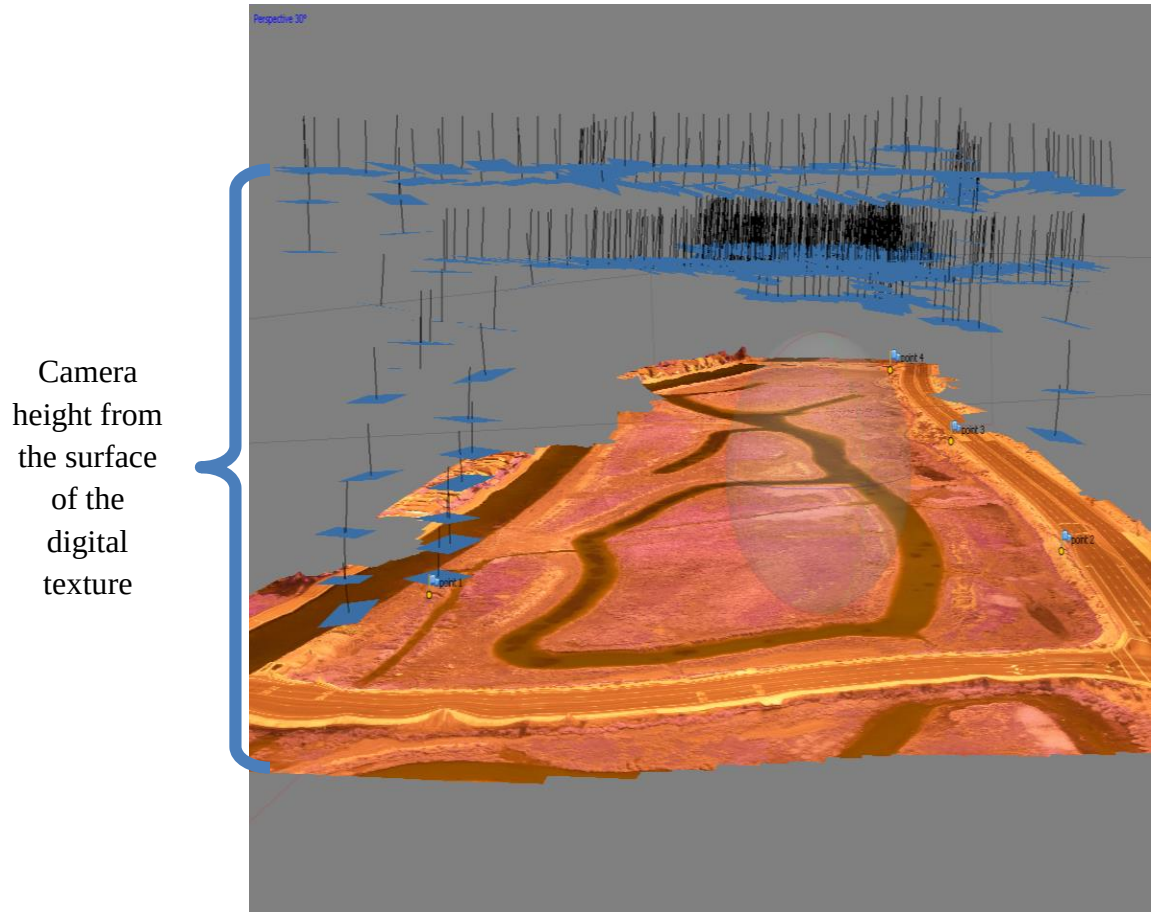

FIGURE 11. PhotoScan visualization: UAV image acquisition capture altitude. Observed using the three-dimensional height from the surface (texture) for each image. This helped determine the estimated height each photo was taken at and helped inform decisions in the photo selection process.

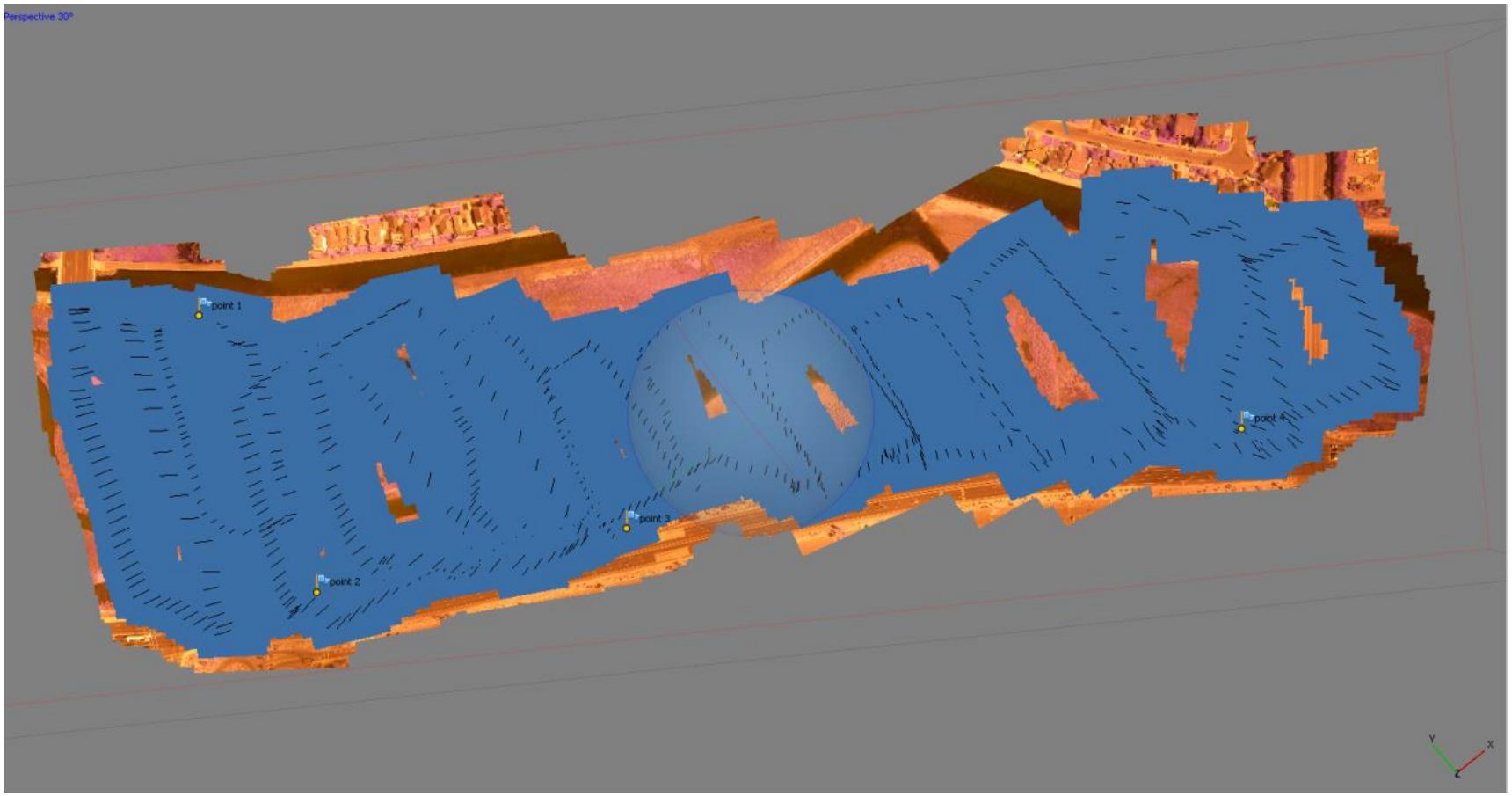

FIGURE 12. PhotoScan visualization: UAV image acquisition capture overlap. Shows all the individual images taken at Brookhurst Marsh. This offered an idea of the overlap achieved during the final UAV image acquisition.

FIGURE 13. Phantom launch locations for the final flight in Brookhurst Marsh. Of the 12 launches, GCP's were collected using the Trimble GPS unit and ground control markers at four sites: 2, 3, 6, and 12.

Secondary Acquisition

In order to understand how vegetation changed over time, previous research conducted at the Huntington Beach Wetland ecosystem was analyzed. Merkel & Associates, Inc. and Whitcraft, Allen, and Lowe (2013) developed a thorough ecological analysis of the Huntington Beach Wetland ecosystem that dates from 2007 to 2013. Their documents provided a detailed understanding as to what the state of the wetlands was in previous years and how it has changed over time.

The Huntington Beach Wetlands Conservancy obtained aerial imagery over the Huntington Beach Wetlands study area through contract flights conducted annually to photograph the site at a scale of 1:18,900 from true vertical position on true color film (Woodfield and Merkel 2011; Whitcraft, Allen, and Lowe 2013). This imagery was provided by Dr. Christine Whitcraft from the California State University, Long Beach Biology Department for the purposes of this study. These were in the form of 29 aerial images of Brookhurst Marsh which were captured in spring 2013. The 2007-2009 vector and tabular data detailing the vegetation community types and land cover at the Huntington Beach Wetlands were also provided by Dr. Whitcraft. Only the July 2009 vector data were utilized because they were the most recent dataset accessible for this research and because they were collected and generated after the completion of the physical restoration of the Huntington Beach Wetlands. These data were recoded to provide reference land cover measures to compare consistency and changes in land cover in the 2013 and 2014 airplane, satellite, and UAV datasets. Additionally, satellite imagery of the Huntington Beach Wetlands was purchased. This imagery was captured by the GeoEye-1 satellite on November 13th, 2013 and is made up of a multispectral

image and a panchromatic image. It encompasses a large swath of the Orange County coast and includes the Huntington Beach Wetlands. The spatial resolution of the multispectral imagery was 2 meters while the resolution of the panchromatic imagery was 0.5 meters.

Phase III: Data Processing

This section introduces a discussion of the software used to process the data collected and it provides a breakdown of the steps taken to ensure proper preparation of all datasets that were acquired through primary and secondary means. Subsequent surveys should follow the approach documented here for consistency and comparability of results. Processing techniques are separated by three main functions: aggregation, standardization, and configuration. Aggregation involves creating orthophotos through photogrammetric construction of separate aerial images using workflows in Agisoft PhotoScan. Standardization comprises of matching all the orthophotos and imagery to a reference map. Configuration requires correct identification of the band sequences from each data source for proper image analysis. Figure 14 illustrates the sequence of the workflow used for both data processing and data analysis using ERDAS Imagine 2014.

Software

Two software packages were used to generate orthophotos, standardize all imagery, determine band configurations, and analyze imagery – Agisoft PhotoScan and ERDAS Imagine 2014. Agisoft PhotoScan Professional 64 edition is an advanced image-based software that can create two-dimensional and three-dimensional content from still images using a Structure from Motion (SfM) algorithm (Verhoeven 2011). SfM is a type of processing technique that can estimate different types of three-dimensional structures

from two-dimensional image sequences (Verhoeven 2011). For this research, SfM was used to generate two-dimensional orthophotos from the collected UAV and airplane-based imagery. The other program used was ERDAS Imagine 2014, which is a remote sensing image processor designed for geospatial applications. ERDAS Imagine 2014 was used for standardization including georeferencing, determining band configurations, and performing image analysis classifications, all of which are presented in the following sections.

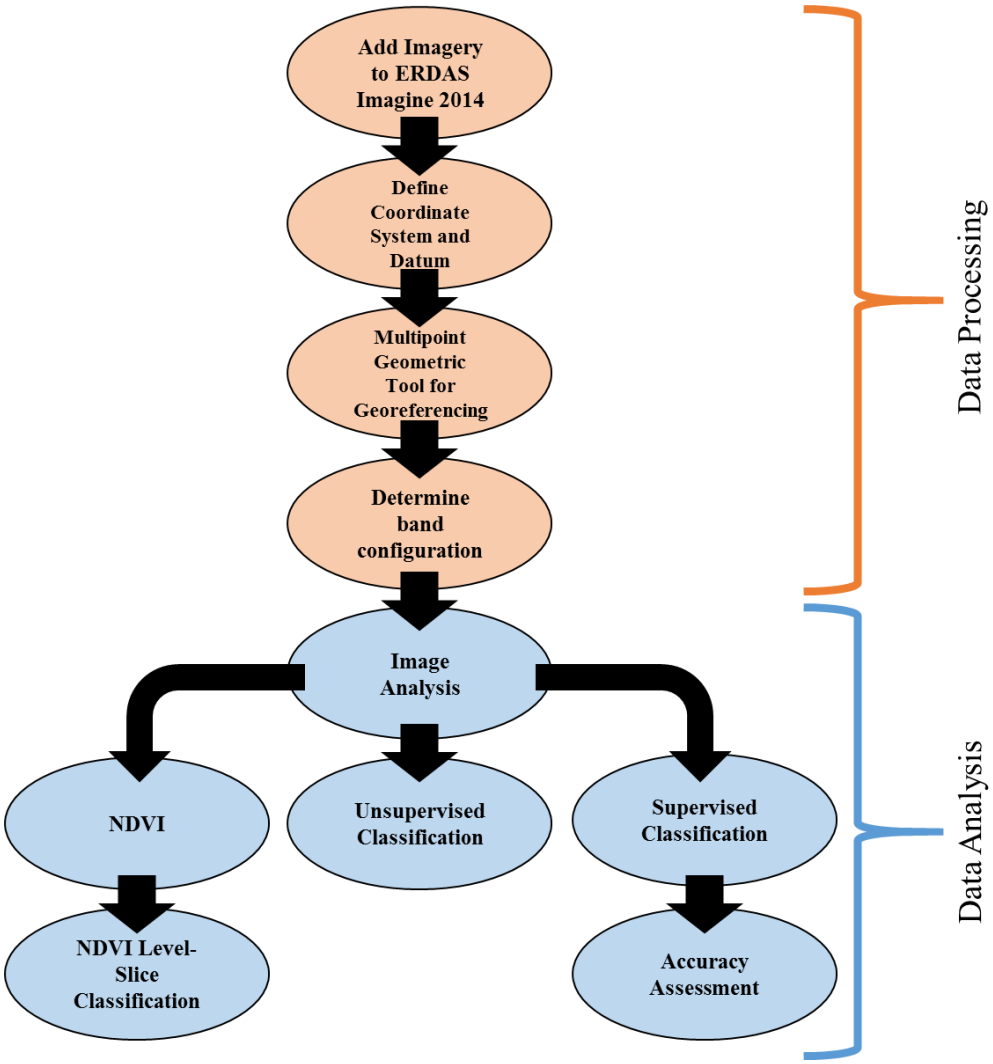

FIGURE 14. ERDAS Imagine 2014 data processing and data analysis workflow.

Aggregation

UAV and airplane imagery. With the exception of the GeoEye-1 satellite imagery, both the aerial imagery collected from the airplane and the UAV had to be mosaicked using Agisoft PhotoScan. Image analysis cannot be done without the creation of orthophotos. An orthophoto is an aerial photograph geometrically corrected such that the scale is uniform and it lacks any distortion (Taylor and Neely 1994). PhotoScan was used to generate orthophotos of the study site using both the UAV and airplane aerial imagery. Figure 15 overviews the basic steps taken to generate these orthophotos in PhotoScan.

Before using the workflows within PhotoScan, the aerial imagery had to be preselected and sorted out. This required looking at each photo and determining whether it is of sufficient quality. Any photos that were blurry, too light or too dark, or were irrelevant such as photos taken too close to the ground, were removed from the final batch. The aerial photos received from Dr. Whitcraft were already preselected into their final batch thus requiring no additional sorting. On the other hand, the UAV aerial imagery had to be sorted out. Selecting the UAV imagery required removing all photos that were not close to the flight height. The flight height was determined using PhotoScan's 3D environment (Figure 11). Any photos below the flight height were automatically removed. There were many irrelevant photos because the Ricoh GR III interval mode was activated right before the Phantom was launched into the air. As a result, it captured the entire hand launch motion as well and those photos had to be removed. The UAV imagery was reduced from 918 photos down to 698. Utilizing the workflows within PhotoScan was the next step after proper aerial image selection.

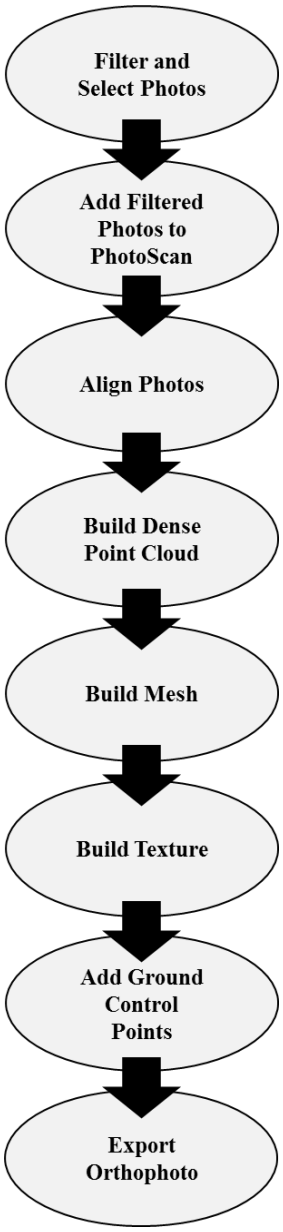

FIGURE 15. Agisoft PhotoScan orthophoto construction workflow.

PhotoScan offers a very powerful yet easy to use workflow for creating an orthophoto from a set of images. These methods are applied in a step-by-step manner and are located under the 'Workflow' tab of the main menu. First, the preselected images were imported into PhotoScan using 'Add Photos'. Next the 'Align Photos' process was

used (Figure 16). At this point PhotoScan finds the camera position and orientation for each photo and builds a sparse point cloud model (Agisoft LLC 2014). \The accuracy setting was set to "High" and Pair preselection was set to "Generic". Accuracy was set to "High" to maximize the precision of all the camera locations while Pair preselection was set to "Generic" because these photos were captured by the Ricoh GR III which does not geotag captured images. The "Generic" setting allows for the program to consider the order in which the images were taken based on the order of acquisition when processing. The Key Point limit which "indicates upper limit of feature points on every image to be taken into account during current processing stage" was set to the default of 40,000. The Tie Point Limit which "indicates upper limit of matching points for every image" was set to the default of 1000 (Agisoft LLC 2014). The outcome produced a three-dimensional sparse point cloud based on the camera position and orientation of each photo.

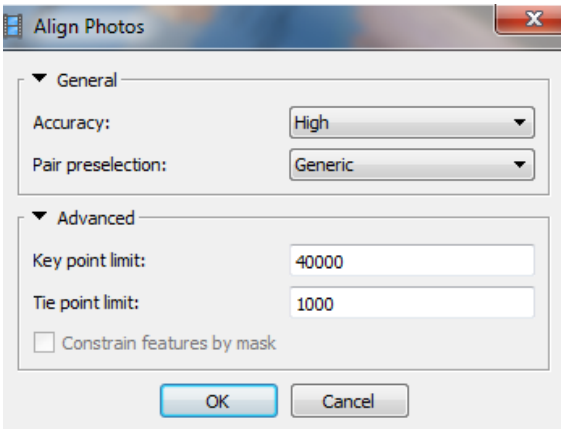

FIGURE 16. PhotoScan dialog: align photos.

One additional thing that can be done is point filtering. This involves looking at individual points or groups of points and removing them from the overall model that do

not appear to coincide with the rest of the point cloud model or are clear outliers. Because no outliers were observed and since this project deals with two-dimensional models, point filtering was not needed.

Building a dense point cloud was the next step in the workflow (Figure 17). "Based on the estimated camera positions the program calculates depth information for each camera to be combined into a single dense point cloud" (Agisoft LLC 2014). The quality of the dense cloud was set to "High" in order to maximize precision while limiting processing time. Depth filtering was set to "Aggressive" because the Huntington Beach Wetlands is a relatively flat area requiring no concern about small changes in elevation across Brookhurst Marsh. This mode is used to identify and reconstruct an area that does not contain meaningful small details, and sorts out most of the outliers (if any exist). For this study, all features of interest are horizontally distributed rather than vertically distributed thus "Aggressive" depth filtering was chosen.

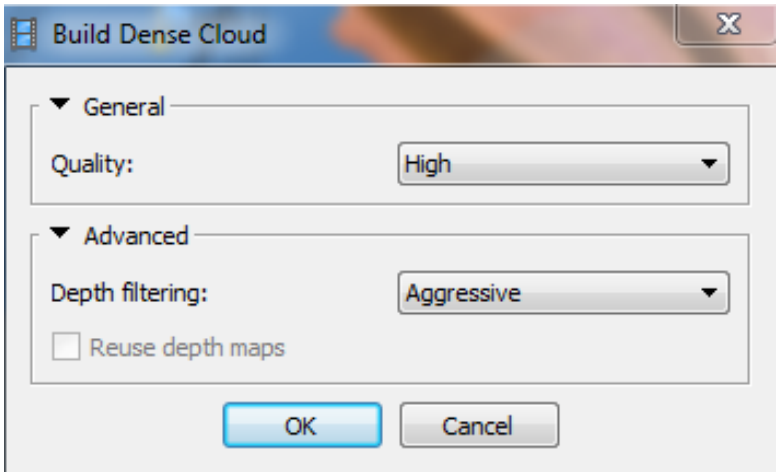

FIGURE 17. PhotoScan dialog: build dense cloud.

To offer a comparative perspective in this example, the Sparse Point Cloud generated 1,385,809 points while the Dense Point Cloud generated 387,689,564 points for the UAV imagery. For the airplane imagery, the Sparse Point Cloud generated 146,741 points while the Dense Point Cloud generated 46,371,352 points.

The next step in the workflow was "Building Mesh" (Figure 18). This is one structuring option for the dense point cloud model. A mesh is created using algorithms that interpolate features through a point-by-point basis to create a seamless visualization. For this workflow, the "Surface Type" was set to "Height field". "Height field" is used to optimize "modeling of planar surfaces, such as terrains or bas-reliefs. It should be selected for aerial photography processing as it requires lower amount of memory and allows for larger data sets processing" (Agisoft LLC 2014). "Arbitrary" is only used for three-dimensional objects and not utilized for this study. The "Source data" selected was the dense point cloud model since it yields a result with higher detail and accuracy over the sparse point cloud. The "Face count" was set to "High" to provide the best possible visualization. "Interpolation" was set to "Enabled (default)" interpolation mode as PhotoScan will interpolate some surface areas within a circle of a certain radius around every dense cloud point. Some holes in the mesh can be automatically covered using this mode while left over holes can be filled in during the post processing step. Agisoft (2014) recommends using the "Enabled (default)" setting for building the mesh for the orthophoto. Because preliminary dense point cloud classifications were not done for this research, the Point classes were set to "All" points in the model. The resulting features offered a shaded, solid, and wireframe visualization based on the dense point cloud model.

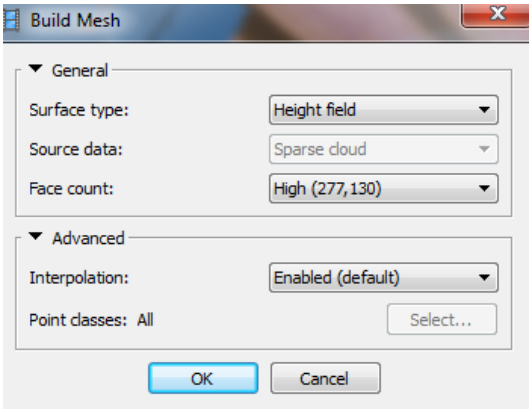

FIGURE 18. PhotoScan dialog: build mesh.

The second structuring option for the dense point cloud model is a texture. A texture is the final build of the orthophoto where GCP's can be added and the orthophoto can be exported into a raster or other image type for analysis. On the PhotoScan workflow, "Build Texture" was selected to utilize this option (Figure 19). Under the General Tab, the "Mapping mode" was set to "Orthophoto" because it produces a more compact texture representation than the "Adaptive orthophoto" mode at the expense of texture quality in vertical regions. Since there are relatively no vertical regions in Brookhurst Marsh, there was no need to select the "Adaptive orthophoto" mode.

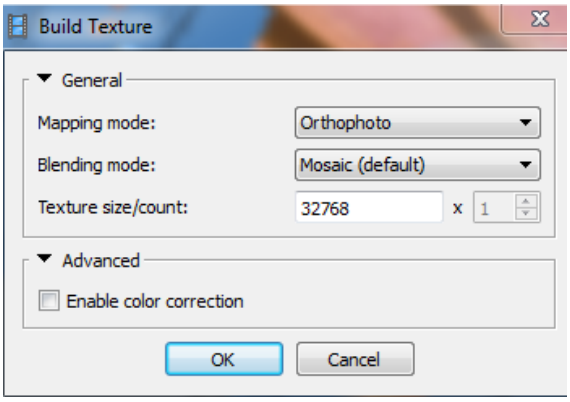

FIGURE 19. PhotoScan dialog: build texture.

The next texture generation parameter, “Blending mode” was set to “Mosaic (default)” because it offers better quality for orthophoto and texture atlas than “Average” mode since it does not mix image details of overlapping photos but uses most appropriate photo. “Mosaic texture blending mode is especially useful for orthophoto generation based on approximate geometric model” (Agisoft LLC 2014). The “Texture size/count” was set to “32768 x 1”. This specifies the width and the length of the texture in pixels and also determines the amount of total files for the texture. The texture size was quadrupled for greater precision and the count was left as default to minimize the amount of files that would need to be exported for image analysis. Under the Advanced tab, color correction was not enabled because these were all high quality photos. The textured icon was enabled for viewing the final texture after completion. Once the texture was built, GCP’s were added by transferring the data collected from the Trimble Juno 3B through Esri ArcPad. From there an orthophoto of the texture was exported for analysis in ERDAS Imagine 2014. This process was repeated for the aerial imagery obtained from Whitcraft, Allen, and Lowe (2013) and Merkel & Associates, Inc. (2011).

GeoEye-1 satellite imagery. The GeoEye-1 satellite imagery was delivered as two separate files. The satellite imagery includes both 0. 5 m panchromatic and 2 m multispectral imagery. Panchromatic imagery consists of only one band and is displayed as a high resolution grayscale image (CRISP 2001). In a panchromatic image, the brightness of a pixel corresponds to the intensity of solar radiation which is the visible portion of the electromagnetic spectrum reflected by the ground resolution cell represented in that pixel. Multispectral imagery consists of multiple spectral bands of data which can be viewed as a color composite image (CRISP 2001). Pan sharpening an

image fusion technique that combines both the multispectral imagery and the panchromatic imagery to produce a high spatial resolution color image, was used to increase the resolution of the multispectral imagery (Intergraph Corporation 2013; Mishra and Zhang 2013). ERDAS Imagine 2014 was used to merge the two datasets. The Subtractive Resolution Merge and the High Pass Filter (HPF) Resolution Merge algorithms were utilized for this process (Appendix C). The Subtractive Resolution Merge is a pan sharpen merge that retains the colors of the multispectral image while maintaining the spatial detail of the pan image (Intergraph Corporation 2013). The HPF process involves a convolution using a high pass filter on the high resolution pan data and then combines this with the lower resolution multispectral data (Intergraph Corporation 2013). All the values were left as default, and the weighting factor was maximized to provide the best result. This number determines how much "weight" is given to the filtered high resolution input in the final result. Higher numbers result in a very crisp output, while lower numbers result in a smoother output. The default value results in moderate crispness (Intergraph Corporation 2013). Both value distribution of these merged image sets were analyzed and because they were relatively different from the original multispectral imagery, they were not used in Phase IV. Instead the original multispectral imagery was utilized.

Standardization

In order to successfully analyze and compare all three datasets they need to be standardized and georeferenced. Without standardization, comparison and analysis among the different datasets is not possible (Lu et al. 2003; Balakeristanan and Said 2012; Vittek et al. 2014). Standardization is the process of defining all datasets to use the

exact same datum, coordinate system, reference basemap, and extent. This process was completely done using ERDAS Imagine 2014. First, all the datasets have to use the same projections. As mentioned in Phase II, the spatial information used in this research was the Universal Traverse Mercator (UTM) Zone 11 North coordinate system and the World Geodetic System 1984 datum. Datasets have to either have their projections defined for the first time or redefined to fit the right projection. The "Reproject" tool in ERDAS Imagine 2014 was used for this task.

Next, all three types of imagery have to be georeferenced to a common basemap in order to match each other's spatial extent. Geographic data was aligned to a known coordinate system so it could be viewed, queried, and analyzed with other geographic data. The reference extent of both the GeoEye-1 satellite imagery and the aerial imagery were chosen to match UAV imagery using the "Mask" tool in ERDAS Imagine 2014. Both the UAV and airplane imagery was referenced to the GeoEye-1 satellite imagery. Using the Multipoint Geometric Correction tool in ERDAS Imagine 2014, points were visually chosen on the UAV and airplane imagery and then automatically linked to the GeoEye-1 satellite imagery in order to spatially match it. Points that contained features that stood out were chosen to be linked. Twenty points from each the UAV imagery and the airplane imagery were chosen and referenced to the GeoEye-1 Satellite imagery. Once all the links were complete, the image was transformed so that it properly overlaid on top of the GeoEye-1 satellite image.

Spectral Configuration

Configuration and determination of the spectral resolution in the related datasets is crucial for any sort of image analysis, especially when it relates to vegetation detection.

The representation of an object's spectral response pattern increases in accuracy when using a dataset with higher spectral resolution. Spectral information of an image is stored in bands (USDA 2013; Wolf, DeWitt, and Wilkinson 2014). For example, the spectral resolution of color film corresponds to three spectral bands: blue, green, and red. For more complex image sensors, devices can image an object ranging from several bands to hundreds of bands (Pidwirny 2006; USDA 2013; Wolf, DeWitt, and Wilkinson 2014). The GeoEye-1 multispectral imagery consisted of four bands. The aerial imagery consisted of three bands because it was captured using a true color camera. Band information for the UAV imagery, GeoEye-1 satellite imagery, and the aerial photography was determined and verified using ERDAS Imagine 2014. Spectral band information is presented in Table 5.

TABLE 5. Image Spectral Information

	Airplane Imagery	GeoEye-1 satellite Imagery	UAV Imagery
Band 1	Red	Blue	Green
Band 2	Green	Green	Red
Band 3	Blue	Red	Near-Infrared (NIR)
Band 4		Near-Infrared (NIR)	

For the UAV imagery, a standard true color image captured using the Ricoh GR III includes the three basic bands blue, green, and red. But as described in Phase I, the imagery captured for this dataset utilized a lens filter outfitted on the Ricoh camera. Using a lens filter is advantageous because it allows for strategic targeting of specific bands on the spectrum (Kelcey and Lucieer 2012). The two general types of color camera filters are absorption filters and interference filters (Mortimer and Davidson

2012). Interference filters are built using thin film coatings onto an optical lens and they reflect unwanted wavelengths while absorption filters are built using colored glass lens that absorb unwanted wavelengths (Fisher 2004; Mortimer and Davidson 2012). The Tiffen 43DY15 43mm Deep Yellow 15 Filter is a type of color lens absorption filter that alters the color of an image by absorbing certain wavelengths of light (Tiffen Company LLC 2015). This filter absorbs the passage of some blue wavelengths in order to enhance the remaining wavelengths to improve the detail of vegetation features in the UAV aerial imagery. This Tiffen filter is also a tone control filter. It acts on color variations to produce tonal differences by lighting objects that are yellow and darkening objects that are its color compliment, violet. This filter is designed to produce progressively deeper and artificially more dramatic representations of blue sky and enhances landscape and marine scenes in aerial photography (Tiffen Company LLC 2015).

Band combinations for the UAV aerial images captured using this filter were determined using both the "Inquire" tool and the "Spectral Profile" tool in ERDAS Imagine 2014. The Inquire tool was used to look at the pixel values of each image type individually to determine the correct band combinations. The File Pixel values and the Look Up Table (LUT) values of pixels were analyzed to make these determinations. Analyzing select locations where features of one kind are known to exist, such as locations with high abundance of vegetation, were used as part of the process. Viewing the LUT values at those locations offered a clear indicator of how the band combinations looked. The band with the highest LUT values indicated that it was the near-infrared band. The next highest LUT value indicated it was the red band, and the lowest LUT value indicated that it was the green band. After looking at the LUT values of the test

filter images along with the actual UAV aerial images the correct band combination was determined for the UAV imagery (Table 5). The same process was repeated for the airplane imagery and the GeoEye-1 satellite imagery for verification (Table 5).

Phase III has outlined all the steps taken to properly process all the datasets that were used for this research. These processes included developing orthophotos of the UAV and airplane imagery using the workflows from Agisoft PhotoScan. Next, it detailed the processes done to standardize and georeferenced all datasets using ERDAS Imagine 2014. Finally, it illustrated how the spectral resolution of each respective dataset was configured and verified using ERDAS Imagine 2014. All these processes were vital to the next Phase, data analysis. The results of these analyses are presented in the next chapter.

Phase IV: Data Analysis

This section details how the analysis of the processed imagery was conducted to develop spectral based land cover maps. The main goal was to use methods that evaluated vegetation occurrence and density and demonstrated the overall land cover change that has taken place at Brookhurst Marsh. This section breaks down the analysis into four portions: Vegetation Distribution, Classification, Accuracy Assessment, and Land Cover Change Analysis. Vegetation distribution refers to visualizing the degree of vegetation land cover in the UAV and GeoEye-1 dataset using the Normalized Difference Vegetation Index (NDVI) formula. The classification section details the different methods used to develop the land cover maps of Brookhurst Marsh. The accuracy assessment section breaks down the measures used to assess the supervised

classifications. Land cover change analysis shows the formulas used to calculate and compare percent change using the 2009 data as reference.

Vegetation Distribution

In order to assess the change that has taken place at Brookhurst Marsh, the vegetation land cover distribution was calculated for each dataset in order to see the spatial distribution of it across the study area. While there are many methods to accomplish this task, this study used the NDVI to assess the occurrence of vegetation. Remote sensing phenology studies use data gathered by sensors that measure wavelengths of light absorbed and reflected by green plants (USDA 2013; USGS 2015). Certain pigments in plant leaves strongly absorb wavelengths of visible red light. NIR wavelengths are strongly reflected by leaves. As plants cycles from early spring to late fall, these reflectance properties also change. Many sensors carried aboard aerial platforms measure red and near-infrared light waves reflected by plants. Using mathematical formulas, raw data measured from these sensors about these light waves can be transformed into vegetation indices. A vegetation index describes the degree of the relative density and health of vegetation for each pixel in a given image (Ali and Pelkey 2013; USDA 2013; USGS 2015).

One of the most widely used vegetation index is the Normalized Difference Vegetation Index (NDVI). NDVI values range from +1. 0 to -1. 0. Areas containing water, rock, sand, or snow usually show very low NDVI values between -1 to 0. 1. Sparse vegetation such as shrubs, grasslands, and crops can result in moderate NDVI values around 0. 2 to 0. 5. Higher NDVI values around 0. 6 to 0. 9 relate to dense vegetation, such as those found in forests or healthy crops. NDVI values can be viewed

across time to establish growing condition standards in a region for a given time of year (USDA 2013; USGS 2015). Health of vegetation can be temporally analyzed by identifying where vegetation is thriving and where it is under stress. It can also help detect vegetation changes due to anthropogenic activities such as deforestation, natural disturbances such as wild fires, or changes in plants' phenological cycle (USDA 2013; USGS 2015).

ERDAS Imagine 2014 provides an assortment of band operation toolsets that can be used to analyze imagery, one of which includes the NDVI operation. The per-pixel NDVI calculation was performed using the formula in Figure 20.

$$NDVI = \frac{(NIR - RED)}{(NIR + RED)}$$

FIGURE 20. Normalized difference vegetation index (NDVI) formula.

Because this formula requires the use of the NIR band, only the UAV imagery and the GeoEye-1 satellite imagery could be utilized since they both contain that band in their respective band sequences. ERDAS Imagine 2014 does a pixel-by-pixel calculation using this formula to create a new black and white image output that ranges from dark to bright depending on the pixel value. Brighter areas showcased vegetation, areas that are dark grey illustrate unvegetated areas and darker areas show pixels containing water.

Using the Normalized Difference Vegetation Index, pseudo color classified images of the GeoEye-1 satellite imagery and the UAV imagery were developed. This level-slicing procedure was based on the pixel location in Brookhurst Marsh and the ability of the image specialist to interpret and classify the groups of pixels appropriately.

There were 256 bins in the original NDVI images and each bin represented different pixel clusters of a specific NDVI value. Pixel clusters in that bin were classified into the three classes that were utilized in all the other classification methods in this research: water, vegetation, and unvegetated. Vegetation included any of the local grasses, shrubbery, and any other plant features. Unvegetated included any features that did not belong in the first two classes including barren land, open soil, sidewalks, roadways, and housing. The classes were determined by looking at individual bins and the pixels they contained. The majority of the pixels that seemed to represent a certain information class were classified accordingly. Pixels closer to the class breakpoints were harder to classify and thus required a trial-and-error method for completion. The distribution of the three different classes for these NDVI level-slices was compared between the GeoEye-1 and the UAV imagery.

Classification

Digital classification of imagery is the process of isolating, grouping, and arranging the reflectance statistics of pixels based on what they actually represent in the real world (Eastman 2003). The three basic types of classification techniques are object based classification, unsupervised classification, and supervised classification. This research utilized unsupervised and supervised classifications in order to analyze land cover variations at Brookhurst Marsh using aerial images captured using airplanes, satellites, and UAV's. Additionally, the vector and tabular data provided by Dr. Whitcraft were reclassified into the three main land cover classes. All these products were developed using ERDAS Imagine 2014 and are shown in Chapter 4.

Unsupervised classification. Unsupervised classifications utilize specific algorithms to make determinations about what objects within an image should be classified as (Eastman 2003). When using the unsupervised classification function within ERDAS Imagine 2014, it uses the ISODATA algorithm. This stands for Iterative Self-Organizing Data Analysis Technique and it's iterative in that it continually performs an entire classification and recalculates statistics (Intergraph Corporation 2013). It is self-organizing because of the way in which it locates the clusters that are intrinsic in the actual data (Intergraph Corporation 2013). Basically, clusters are formed using the minimum spectral distance formula which is part of the ISODATA clustering method. It begins with either random cluster means or the means of an existing signature set. Each time the clustering repeats, the means of these clusters are moved and the new cluster means are used for the next iteration. This clustering method repeats itself until a maximum number of iterations is performed or the convergence threshold is reached between two iterations. Each dataset was grouped into 30 different spectral clusters and the convergence threshold was set to 0.950. The convergence threshold is the maximum percentage of pixels whose cluster assignments can go unchanged between iterations. In other words, as soon as 95% or more of the pixels stay in the same cluster between one iteration and the next, the algorithm will stop processing. The maximum iteration was set to 10 to decrease processing time and maintain accuracy. The clustering option is set to initialize from the statistics of the image. After performing the unsupervised classification, all 30 spectral were individually classified into the three land cover classes: water, vegetation, and unvegetated using the original image as reference. All three types of datasets were used to develop unsupervised land cover maps.

Supervised classification. Unlike the unsupervised classification, the supervised classification is completely dependent on the skills and cognition of the image specialist or analyst and requires familiarity with the actual study site (Eastman 2003; Mitchell et al. 2012). Signature sets were developed for the three base classes: water, vegetation, and unvegetated using the original imagery as reference. Spectral signatures were developed using the Region Grow Tool in ERDAS Imagine 2014. Region grow is a method of collecting spectral signatures for image classification based on geographic constraints (Intergraph Corporation 2013). These constraints are set anywhere between 100,000 to 10,000,000,000 pixels depending on the actual type of signature that had to be collected. These were done on a pixel-by-pixel level and were constructed by analyzing each feature in the imagery. Images were divided into quadrants and multiple signatures were collected for each individual feature to minimize any error and discrepancy in signature development.

Once all the signatures were compiled, the final signature sets were evaluated using the DN values as a function of band sequences to verify the accuracy of the spectral examples collected from the image sets. These signature sets must be consistent using multiple features during comparison in order to complete verification. Once verified, the supervised classification was performed, by setting the parametric rules as maximum likelihood and the non-parametric rules as parallelepiped. In the parallelepiped decision rule, the values of the candidate pixel are compared to upper and lower limits. These limits can be either the minimum and maximum values of each band in the signature set or the mean of each band including their standard deviations (Intergraph Corporation 2013). The advantage of using this rule set is that it is fast and efficient. The maximum

likelihood decision rule is based on the probability that a pixel belongs to a particular class. It assumes that these probabilities are equal for all classes and that the input bands have normal distributions (Intergraph Corporation 2013). Out of the parametric rules this is the most accurate in ERDAS Imagine 2014. Figure 21 shows the decision rule workflow that ERDAS Imagine 2014 uses to complete supervised classifications. The output of this tool resulted with a supervised classification image that incorporated the three land cover classes along with a distance image file that was used to assess the accuracy of the classification based on the original signature sets.

Accuracy Assessment

Separate accuracy assessments were completed to further verify the validity of these supervised classifications (Eastman 2003). The distance image file evaluates the supervised classified image and illustrates the variation between each classified pixel as it actually relates to the features in the field (Intergraph Corporation 2013). Brighter pixels (containing the higher distance file values) are spectrally farther from the signature means for the classes to which they are assigned. They are more likely to be misclassified. Darker pixels are spectrally nearer, and more likely to be classified correctly. Since supervised training was used, the darkest pixels are usually related to the training samples. Thresholding is the process of identifying pixels in a classified image that are most likely incorrectly classified (Intergraph Corporation 2013). This was accomplished by viewing the distance file value histogram and determining the chi-square parameter. If the chi-square distribution was relatively smooth with a tail on the right side, then that classification was correct and the values or pixels in the tail could be removed.

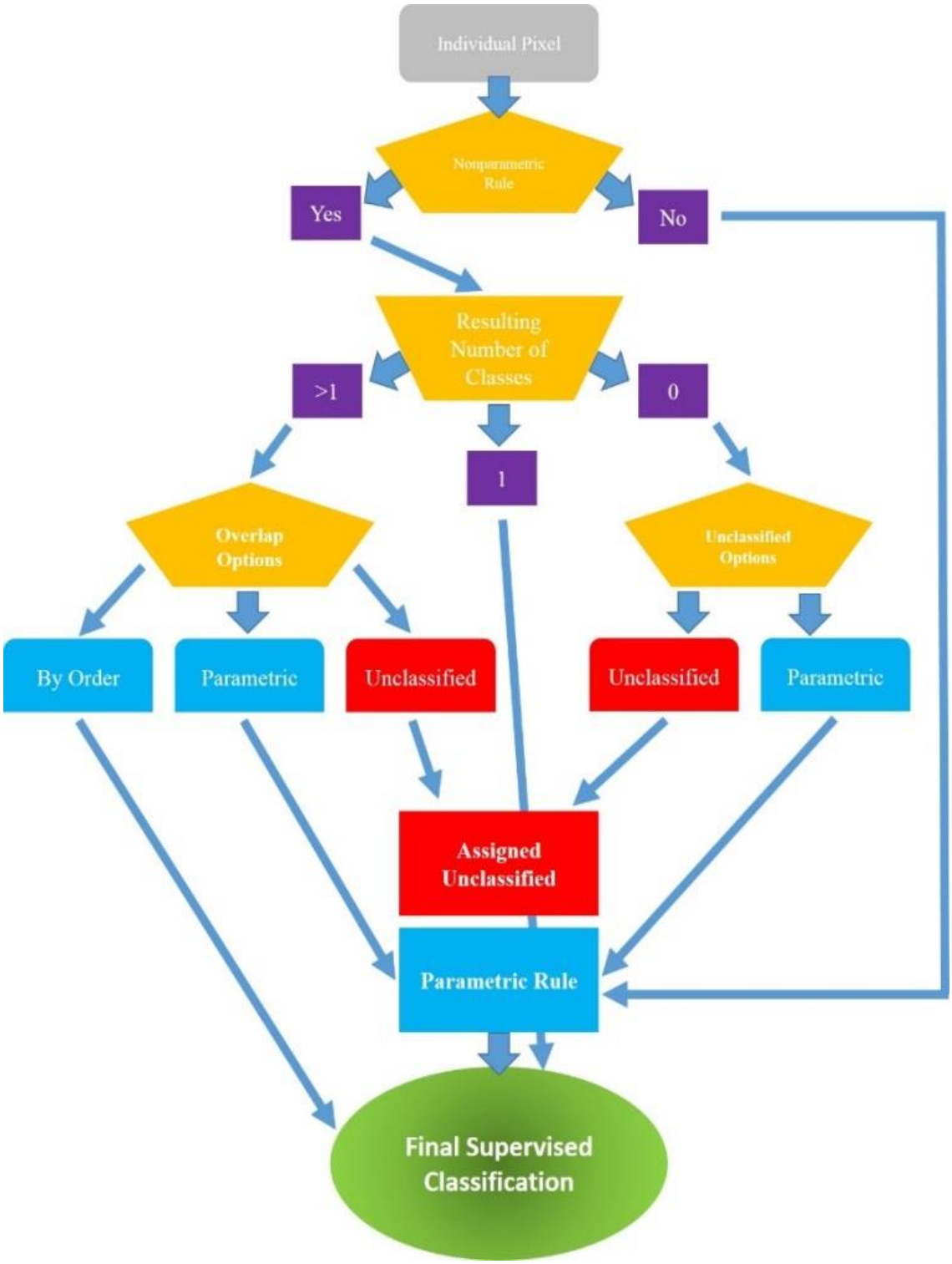

FIGURE 21. ERDAS Imagine 2014 supervised classification decision ruleset. Adapted from the ERDAS Field Guide (Intergraph Corporation 2013).

The confidence level used was 0.05, which means that 0.05% of the pixels were believed to be misclassified by the software. Accuracy assessments in the form of pixel reference were completed for each classification. Finally, accuracy reports were created through the method of selecting random test pixels from the image for evaluation. These test pixels were chosen at random by ERDAS Imagine 2014. From there, these test pixels were individually sorted into the three main classes by only using the original image as reference. Twenty five test pixels were generated by the software and classified for an accuracy assessment for each supervised classification.

After determining the classes for all the test points based on the original imagery, ERDAS Imagine 2014 calculated the precision of the selection of the pixel classes by checking to see if the test point classification matched the supervised classification in the form of an error matrix. The error matrix shows the amount of classified test pixels that matched the supervised classification. The Kappa Coefficient is used to statistically analyze the accuracy derived from the error matrix (Gómez and Montero 2011). The same standard Kappa Coefficient formulas which are assessed in Gómez and Montero's (2011) analysis were utilized in ERDAS Imagine 2014. These standard formulas were used to assess the accuracy of the supervised classifications in this research.

First, the overall accuracy (O^c) from the error matrix was calculated. This is defined as a proportion of the sum of the elements in the error matrix where each element represents the number of pixels classified by the image specialist and the pixels classified by the software ($\sum_{i=1}^{k} n_{ii}$) over the number of pixels being tested ($|T|$), (Figure 22).

$$O^c = \frac{\sum_{i=1}^{k} n_{ii}}{|T|}$$

FIGURE 22. Kappa coefficient: overall Accuracy (O^c) formula (Gómez and Montero 2011).

Next, the percentage of pixels classified correctly (p_e), defined as the proportion of the number of test pixels that matched the image specialist's classification and the original supervised classification ($\sum_i n_i n_i$) over the total number of test pixels (n), was calculated (Figure 23).

$$p_e = \frac{\sum_i n_i n_i}{n}$$

FIGURE 23. Kappa coefficient: correct classified pixels percentage formula (p_e) (Gómez and Montero 2011).

Finally, the Kappa Coefficient (K), which is defined as the proportion of the difference between the overall accuracy (O^c) and the percentage of items that were classified correctly (p_e) over the percentage of items that were classified incorrectly, was generated (Figure 24).

$$K = \frac{O^c - p_e}{1 - p_e}$$

FIGURE 24. Kappa coefficient (K) formula (Gómez and Montero 2011).

The Kappa Coefficient determines what percentage of the supervised classification process avoids errors that a completely random classification would generate by

outputting values between 0 and 1 (Intergraph Corporation 2013). The closer the value is to 1, the more accurate that supervised classification is considered to be. Accuracy assessments using the Kappa Coefficient were completed for the satellite, airplane, and UAV supervised classifications.

Land Cover Change Analysis

Land cover change was assessed using the percent change of water, vegetation, and unvegetated land cover classes in Brookhurst Marsh. Percent change refers to the degree to which a variable increases or decreases in value. The percent change figures were used to assess the land cover change using the conditions of Brookhurst Marsh in 2009 (Balakeristanan and Said 2012; Vittek et al. 2014). Pixel proportions of each land cover type for each classification were used because the raw numbers for each type of imagery used different metrics. These were obtained using ERDAS Imagine 2014. In a particular classification, all the pixels classified as a certain land cover class (P_c) were divided by the total number of pixels (P_t) in that classification to obtain the proportion of pixels classified as that certain land cover class (P_p) (Figure 25). These proportions were then converted into percentages and are shown in Chapter 4. Land cover percentages were also calculated for the recoded July 2009 vector data by deriving the total area of each land cover class type from the tabular information.

$$P_p = \left(\frac{P_c}{P_t}\right) * 100$$

FIGURE 25. Land cover class percentage formula (P_p).

Since physical restoration was completed in July 2009, the ideal land cover conditions most likely existed at the marsh at that time which is why the 2009 vegetation community map is used as reference to assess accuracy and land cover change among the datasets. Percent change figures were calculated from the pixel proportions of land cover for each classification. Each percent change figure (C) was calculated using the difference between the proportion of pixels classified as a certain information class in a particular classification (P_c) and the proportion of pixels classified as that same information class in the 2009 vegetation community map (P_v). This difference was divided by the same figure referring to the proportion of pixels for the 2009 vegetation community map (P_v) in order to normalize the percent change figures and enable comparison among the datasets (Figure 26).

$$C = \left(\frac{P_c - P_v}{P_v}\right) * 100$$

FIGURE 26. Percent change formula (C).

The average percent change (C_{avg}) refers to the proportion of the sum of the absolute value of percent change figures relating to water (C_w), vegetation (C_v), and unvegetated (C_u) land cover over the total number of land cover class types which in this case was three (Figure 27). The percent change figures were used to assess the degree of change among datasets at Brookhurst Marsh.

$$C_{avg} = \frac{\sum |C_{wvu}|}{3}$$

FIGURE 27. Average percent change formula (C_{avg}).

This chapter provides a detailed description of the methods used in this research. The methodology presented was designed so that it can be implemented by the Huntington Beach Wetland Conservancy as an effective method of analyzing land cover at the Huntington Beach Wetlands and determining changes taking place at a high spatial and temporal level.

CHAPTER 4

RESULTS

This chapter presents the visual products and statistical analyses produced. The orthophotos, Normalized Difference Vegetation Indices (NDVI), NDVI level-slices, unsupervised classifications and supervised classifications were derived from the UAV imagery, GeoEye-1 satellite multispectral imagery, and airplane imagery. The 2009 vegetation community vector data developed by Whitcraft, Allen, and Lowe (2013) was classified into water, vegetation, and unvegetated land cover classes and used for visual comparison to the every spectral based land cover maps developed for this study. The NDVI images along with the NDVI level-slices of each product that were derived from the UAV PhotoScan orthophoto and the GeoEye-1 satellite imagery are provided. Results of the unsupervised and supervised classifications performed on the UAV PhotoScan product, the GeoEye-1 satellite multispectral imagery, and the airplane PhotoScan orthophoto are provided. Both types of classifications were compared to the classified 2009 vegetation community map and the NDVI level-slice land cover maps. Accuracy assessments of each supervised classification are provided for the airplane, GeoEye-1 satellite, and UAV as well. These techniques and products demonstrate the effectiveness of studying vegetation distribution and land cover in a coastal wetland environment. More importantly these results illustrate the comparability and utility of the UAV products to those derived using the airplane and satellite platforms.

Aerial Imagery and Derived Products

The pixel resolution of the UAV – derived orthophoto was 0.03 m^2 (Figure 31). The orthophoto derived from the airplane acquired imagery was 0.1m^2 (Figure 29). Both were georeferenced to the GeoEye-1 satellite multispectral imagery. The airplane imagery was captured in spring 2013, and as such differs from the land cover depicted in the UAV – derived orthophotos captured in October 2014. Of note are the pronounced white barren areas that were not visible in either the GeoEye-1 multispectral imagery or the UAV orthophoto. This was a veneer of salt as a result of tidal fluxes in Brookhurst Marsh in 2013. The flight path did not follow a straight line across the bottom half of Brookhurst Marsh when capturing the aerial photos in spring 2013. As a result, 11.3% percent of Brookhurst Marsh was missing from the overall extent in the airplane – derived orthophoto. The sequential images drift to the right as a result of crabbing of the aircraft and not only resulted in missing images in the southwestern portion of the marsh but also created warped distortions across multiple sections of the orthophoto. For example, in PhotoScan's attempt to use photogrammetric methods to accurately map the southwestern portion of Brookhurst Marsh, the street and curb were pushed further inward towards the marsh creating a noticeable distortion in the imagery. This clearly is a major issue that has to be addressed to the HBWC if they wish to continue utilizing piloted flights in the future to obtain aerial imagery.

The multispectral satellite imagery had a coarser resolution than the panchromatic imagery. The High Pass Filter Merge of the multispectral and panchromatic image is shown in Appendix C. The histograms of the HPF Merge image, the Pan Sharpening technique and the original GeoEye-1 multispectral image contained relatively similar

mean values but displayed significant differences in shape (Figure 28). This indicated that there were spectral changes in the image, which was a by-product of the merging process and would alter the analytical results if used in this research. In order to maintain the spectral integrity of the original multispectral imagery, the HPF merge and the Pan Sharpening merge images were not used. The original, multispectral imagery with a spatial resolution of two meters was utilized for this analysis (Figure 30).

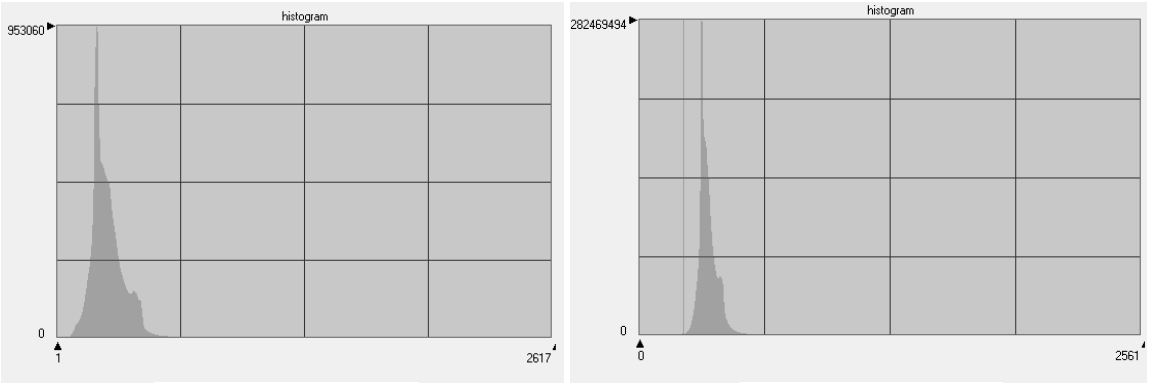

Mean = 264.365 Mean = 254.955

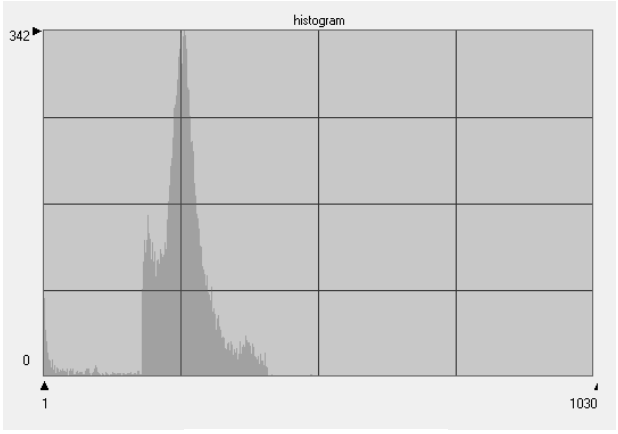

Mean = 255.188

FIGURE 28. Multispectral and panchromatic merge technique histograms. Subtractive Resolution merge histogram and mean value (Top Left). High Pass Filter (HPF) merge histogram and mean value (Top Right). GeoEye-1 multispectral imagery histogram and mean value (Bottom).

The UAV orthophoto captured images using a lens filter (Figure 32). In the format presented here vegetation appears in shades of purple, while shades of orange show different land features such as roadways, barren soil, and sand. Turbid water shows up as much darker colors. The ground control markers in the UAV orthophoto were also visible when zoomed in demonstrating the level of detail inherent in this product. This level of spatial detail made it easier to determine the class that pixels belonged to while developing the NDVI-level slice class break points and supervised classification training samples. The major issue with the UAV imagery collected for this research was in the northern portion of the marsh. Close to five percent of Brookhurst Marsh was missing from this imagery which were a result of the flight path flown from launch locations six through nine (Figure 13). The radius of these flight paths didn't completely cover the northern extent of Brookhurst Marsh and resulted in some missing extents of the final UAV orthophoto. Because of the recent change in the FAA ruling for commercial UAV usage, it was not possible to conduct flights to correct this issue and capture the missing extent of Brookhurst Marsh. Nonetheless, the upper northern sections of Brookhurst Marsh are primarily covered by water which was taken into account in the land cover analysis.

The vegetation community vector data was constructed by Dr. Whitcraft by combining an unsupervised classification of the 2009 airplane imagery along with the corresponding 2009 ground transect data (Figure 32). This vector data aided in assessing the validity of the UAV, GeoEye-1, and 2013 airplane land cover maps. The 2009 vegetation community data contained specific spatial and tabular information about the distribution of vegetation communities. It detailed eight different types of vegetation

communities found in Brookhurst Marsh at that time. These included brackish marsh, coastal salt marsh, coastal scrub, dune scrub, freshwater marsh, mulefat scrub, southern willow scrub, and non-native vegetation. Coastal salt marsh was the predominant vegetative community found in Brookhurst Marsh in 2009. The original 2009 vector data was reclassified into a land cover map using ERDAS Imagine 2014 to reflect the three classes that were also used in the land cover maps for the UAV, GeoEye-1, and 2013 airplane datasets. The borders of the vegetation class in this map were color coded to highlight the location of the different vegetation communities as they existed in 2009. The vegetation land cover class from the reclassified 2009 vegetation community map coincided fairly well with the vegetation distribution observed in all three UAV and GeoEye-1 spectral based land cover maps.

Normalized Difference Vegetation Index (NDVI)

The Normalized Difference Vegetation Index image was generated for both the GeoEye-1 satellite multispectral imagery and the UAV orthophoto using ERDAS Imagine 2014 (see Figures 34 and 35). Brighter areas on the grayscale images indicate areas encompassing heavy concentrations of vegetation. Shades of gray refer to areas of barren and urban features while darker pixels indicate locations covered with water. Due to the lack of a near-infrared band in the airplane imagery, an NDVI calculation was not completed. NIR bands only existed in the GeoEye-1 satellite and UAV images and their histograms show a fairly normal distribution of values (Figure 33). The overall distribution of vegetated areas between the two NDVI images show visual similarities and offered a good baseline visual on what land cover distributions to expect from the classifications. The UAV NDVI imagery offered a more detailed and smoother look at Brookhurst Marsh than the GeoEye-1 NDVI image.

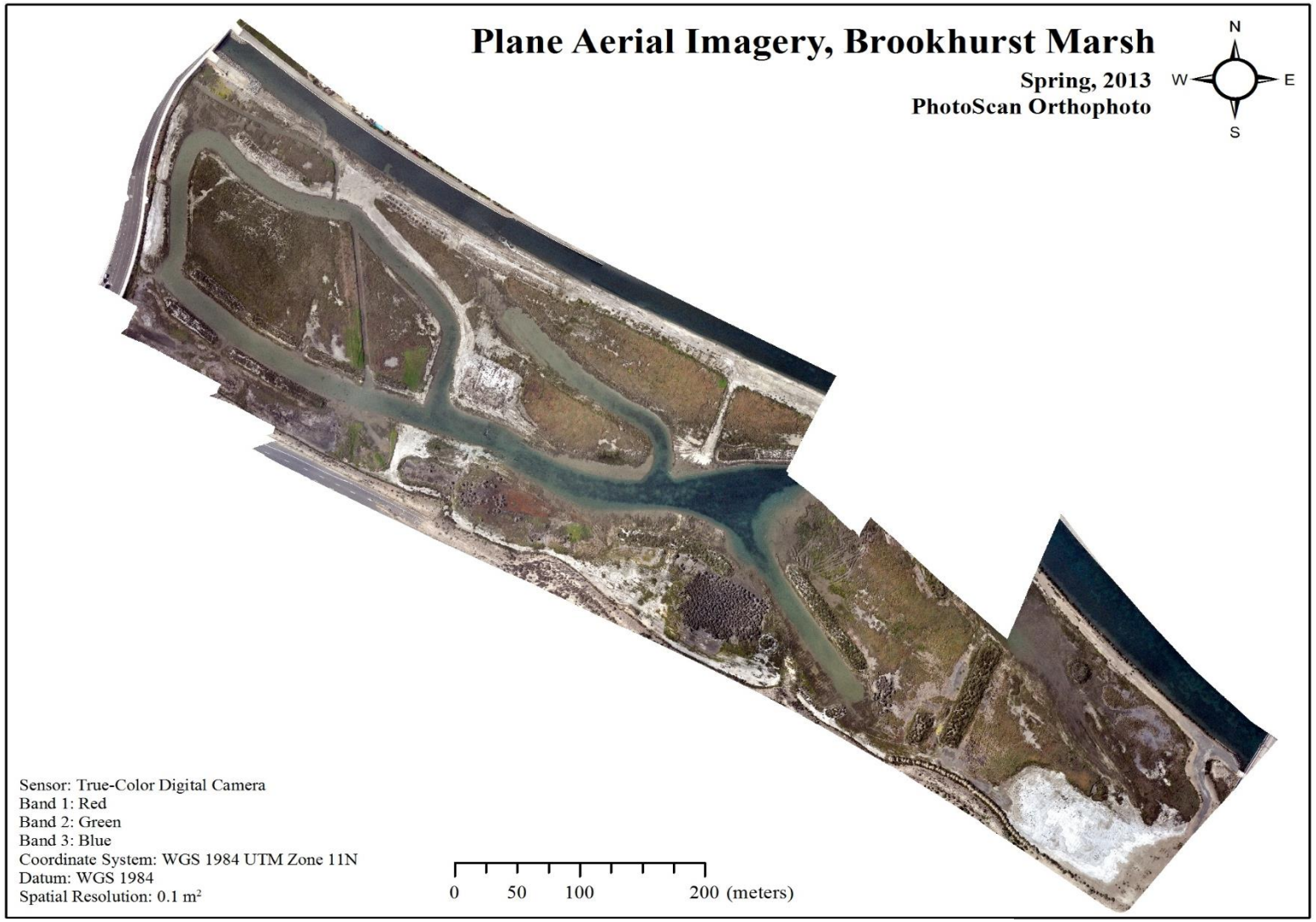

FIGURE 29. Spring 2013 airplane PhotoScan aerial imagery.

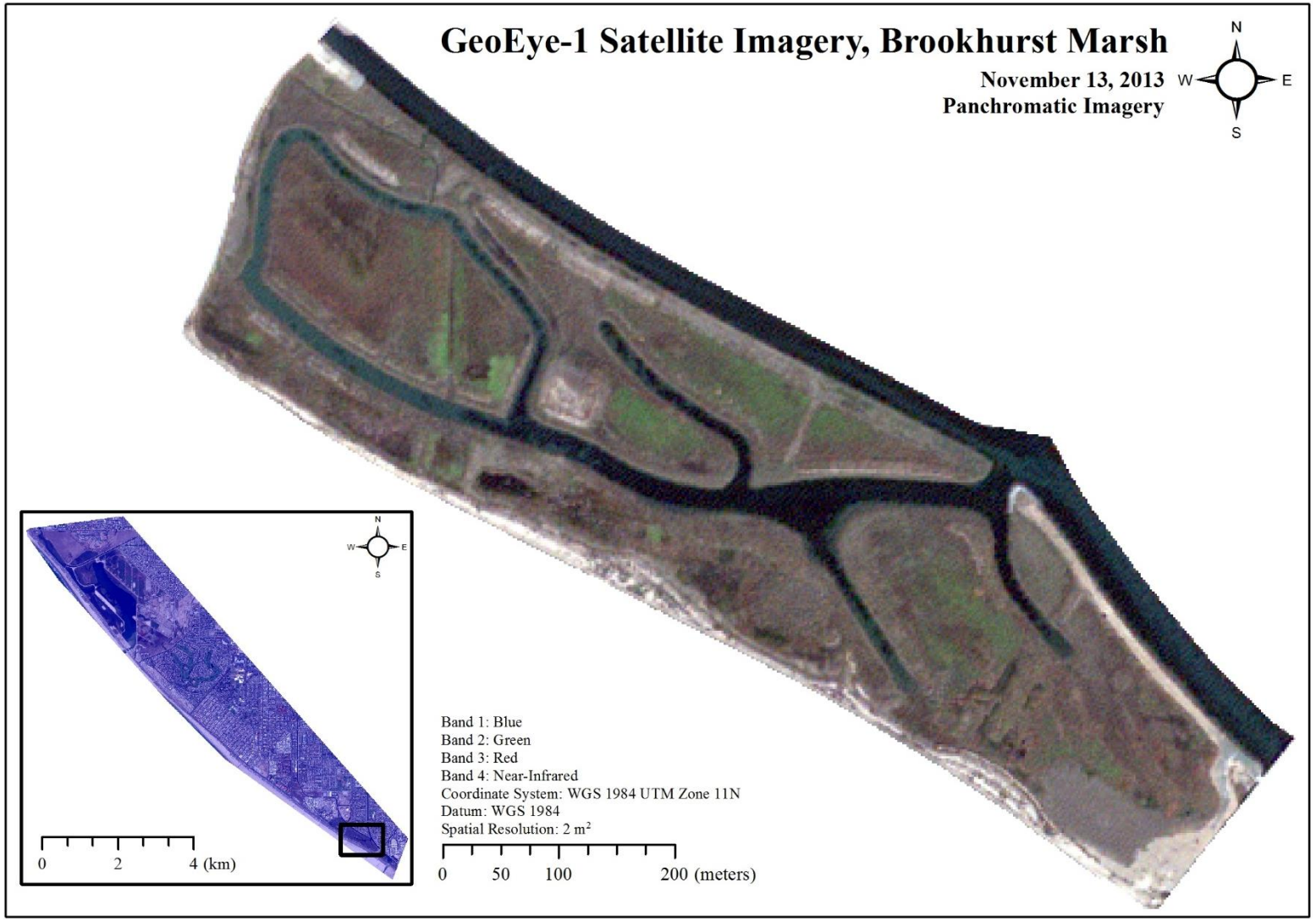

FIGURE 30. November 2013 GeoEye-1 multispectral satellite imagery.

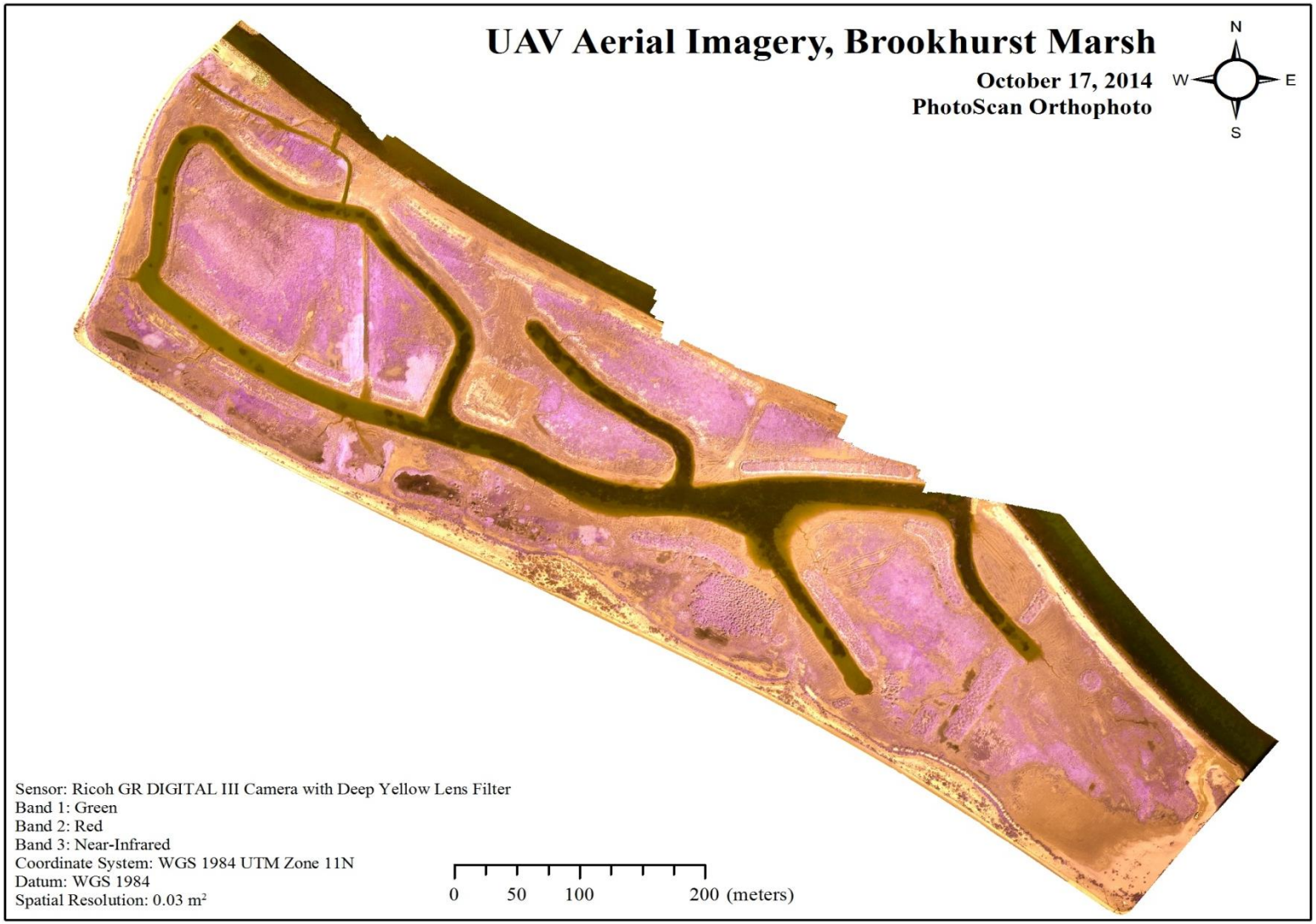

FIGURE 31. October 2014 UAV PhotoScan aerial imagery.

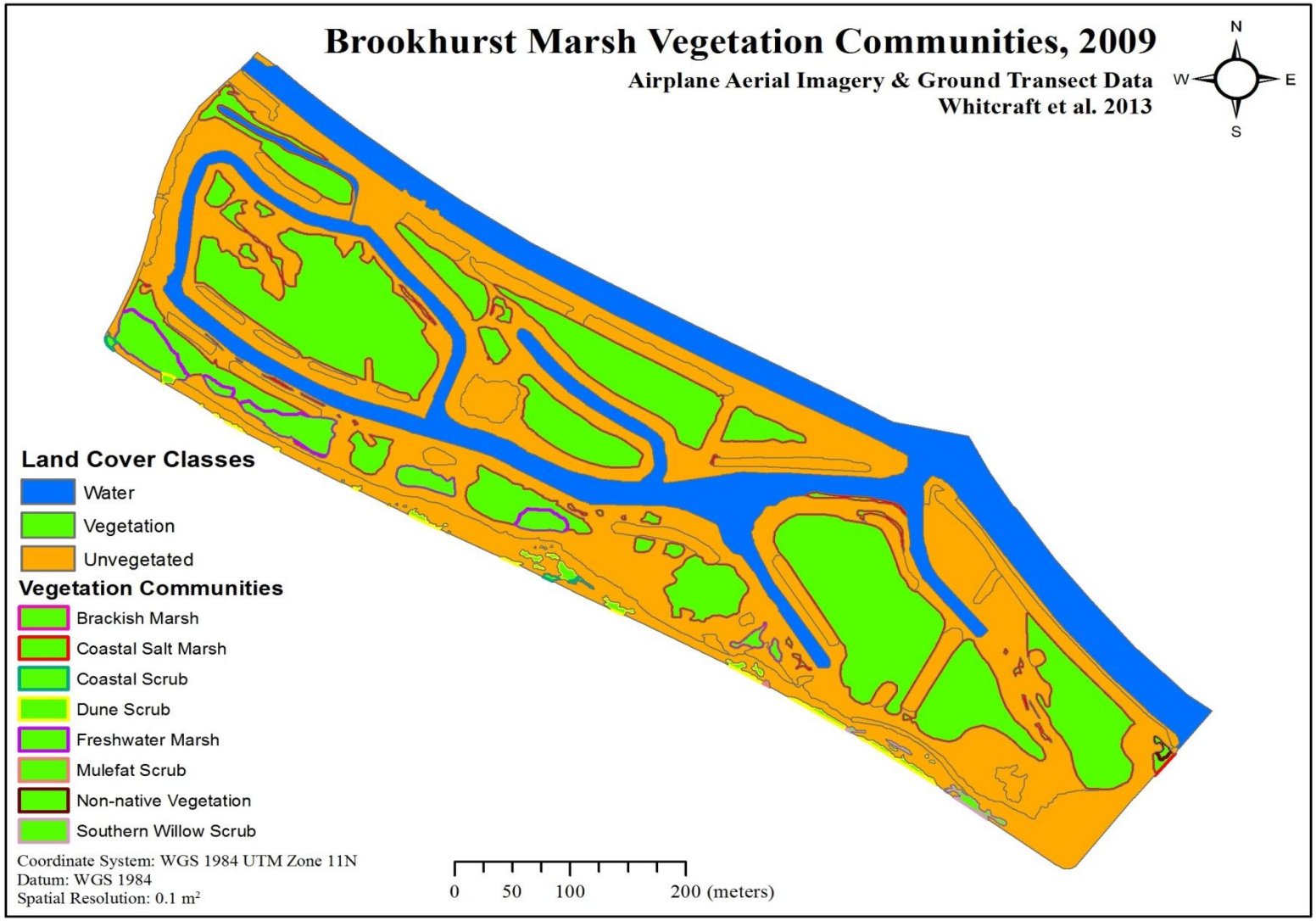

FIGURE 32. July 2009 vegetation community land cover map. Reclassified land cover map of the original vector data originally developed by Whitcraft, Allen, and Lowe (2013).

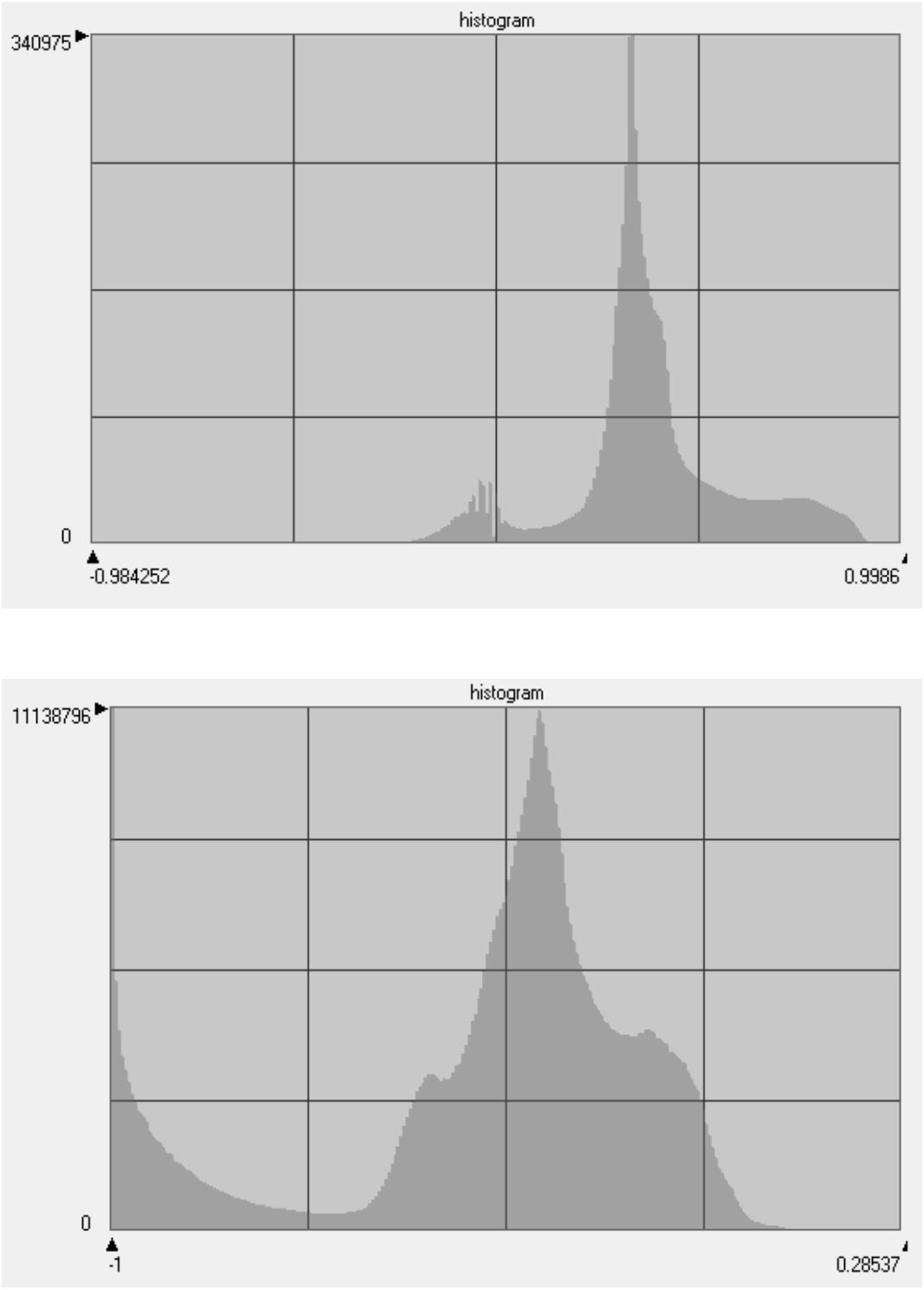

FIGURE 33. GeoEye-1 NDVI histogram (top) and UAV NDVI histogram (bottom).

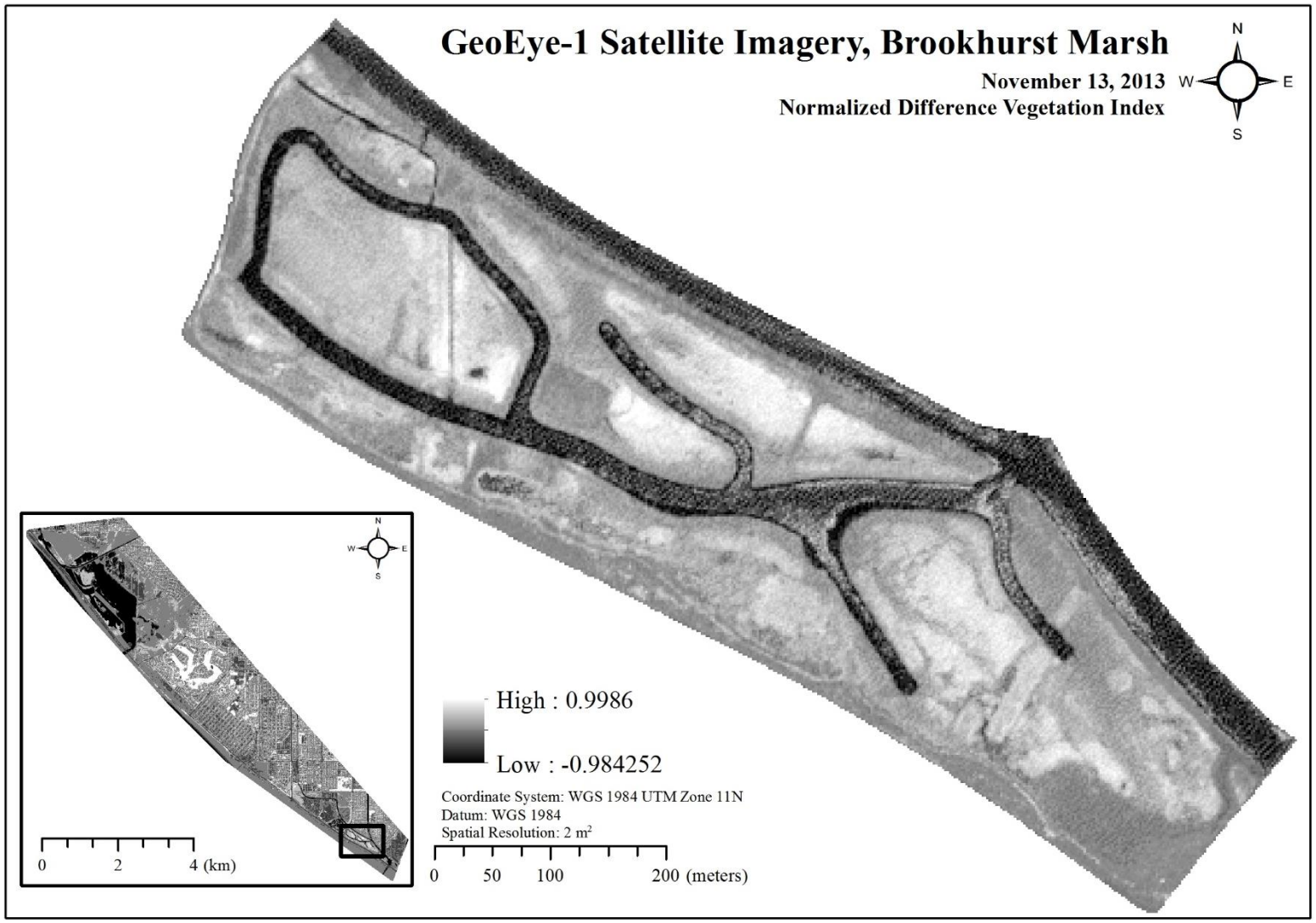

FIGURE 34. NDVI of the GeoEye-1 satellite multispectral imagery. Developed using ERDAS Imagine 2014.

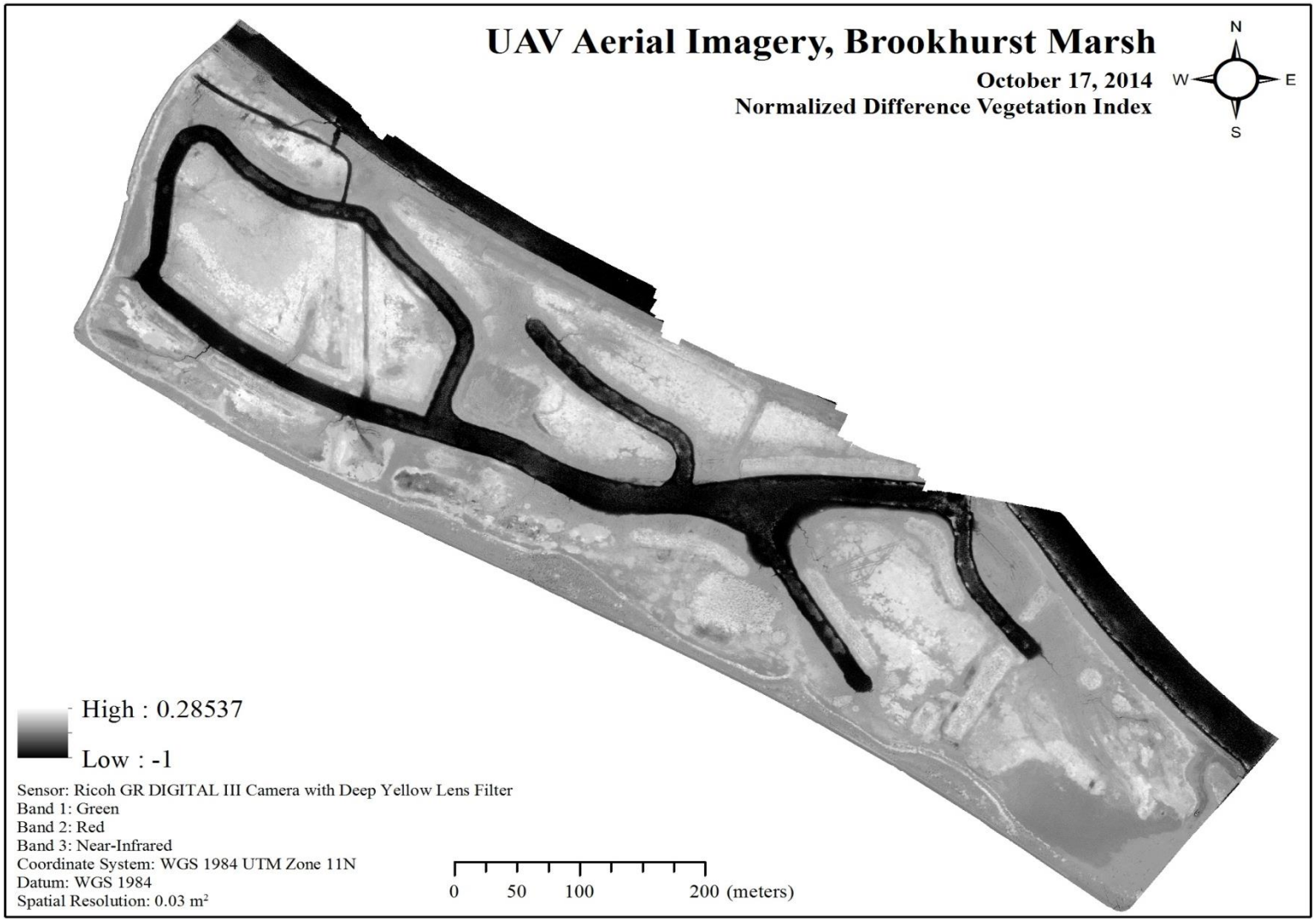

FIGURE 35. NDVI of the UAV aerial imagery. Developed using ERDAS Imagine 2014.

Classification Products

Three classification methods were implemented using ERDAS Imagine 2014 to show and compare the land cover distribution at Brookhurst Marsh. These included a NDVI level-slice, an unsupervised classification, and a supervised classification. The goal of using these methods was to demonstrate that the UAV has the potential to rival satellite and airplane image acquisitions through the comparison of spectral based land cover distribution percentages. The errors and discrepancies within each classification are detailed in the next chapter. Table 6 shows the land cover distribution percentages of Brookhurst Marsh for each type of classification that was derived from all the datasets. For this study, it was assumed that the land cover results for the 2009 vegetation community map were completely accurate so that reference measures, changes in land cover, and accuracy comparisons among the three datasets could be presented.

TABLE 6. Brookhurst Marsh Land Cover Distribution

	Water	Vegetation	Unvegetated
2009 Vegetation Community Map	20.79%	32.29%	46.92%
2013 Airplane Unsupervised Classification	35.24%	14.95%	49.81%
GeoEye-1 Satellite Unsupervised Classification	20.74%	28.12%	51.14%
UAV Unsupervised Classification	20.45%	29.61%	49.94%
GeoEye-1 Satellite NDVI Level-Slice Classification	23.39%	24.79%	51.82%
UAV NDVI Level-Slice Classification	25.52%	28.79%	45.69%
2013 Airplane Supervised Classification	47.42%	27.75%	24.83%
GeoEye-1 Satellite Supervised Classification	22.72%	25.85%	51.43%
UAV Supervised Classification	20.56%	28.87%	50.57%

NDVI Level-Slice

The NDVI level-slices of both the GeoEye-1 satellite multispectral imagery and the UAV imagery were visually consistent with the other two methods of classification. Specifically, these two land cover maps showed some visual vegetation distribution consistency with the 2009 vegetation community map, the unsupervised classifications and the supervised classifications. Table 7 shows the percent increase or decrease in water, vegetation, and unvegetated land cover as defined by the difference in land cover percentages using the 2009 vegetation community map as reference. Both NDVI level-slices showed a percent increase in water land cover and a percent decrease in vegetation land cover since 2009. The percent increase in water cover was greater for the UAV NDVI level-slice than the GeoEye-1 level-slice.

The average percent change for the GeoEye-1 NDVI level-slice was slightly greater than the UAV NDVI level-slice which could be caused by few potential reasons that could relate to accuracy and land cover change. It is possible that the UAV NDVI-level slice was a more accurate land cover representation of Brookhurst Marsh for October 2014 than the GeoEye-1 NDVI level-slice was for Brookhurst Marsh in November 2013. This could be because the UAV imagery has a higher spatial resolution than the GeoEye-1 multispectral imagery which makes it easier to determine information classes for individual pixels. The second reason for the GeoEye-1 NDVI level-slice having a greater average percent increase than the UAV NDVI level-slice could be the result of small changes in land cover distribution which are probable over a 4 or 5 year period.

It should be noted that there were some discrepancies within these land cover maps. Table 8 breaks down the class breakpoints along with the classification they

represent for both the UAV and the GeoEye-1 satellite NDVI level-slices. Because a trial-and-error method was used to determine the class association for each scaled NDVI value in the NDVI image, not all the pixels could be attributed to that chosen classification from the 256 individual bins. This was especially so for the bins centered on the breakpoints of the three classes. Selective bias exists when determining which class an NDVI value belongs to and was reduced by utilizing prior knowledge of the features in Brookhurst Marsh. Figures 36 and 37 show the GeoEye-1 and UAV NDVI level-slice maps.

TABLE 7. Percent Change: NDVI Level-Slice

	Water	Vegetation	Unvegetated	Average Percent Change
2013 GeoEye-1 NDVI Level-slice & 2009 Vegetation Community Map (Reference)	12.51%	-23.23%	10.44%	15.39%
2014 UAV NDVI Level-slice & 2009 Vegetation Community Map (Reference)	22.75%	-12.16%	-2.62%	12.51%

TABLE 8. NDVI Level-Slice Class Breakpoints

	2014 UAV NDVI Level-slice	2013 GeoEye-1 Satellite NDVI Level-slice
Water	-1 to -0.548112	-0.465302 to 0.32474
Unvegetated	-0.543091 to -0.201665	0.332486 to 0.54936
Vegetation	-0.196644 to -0.194993	0.557106 to 0.897909

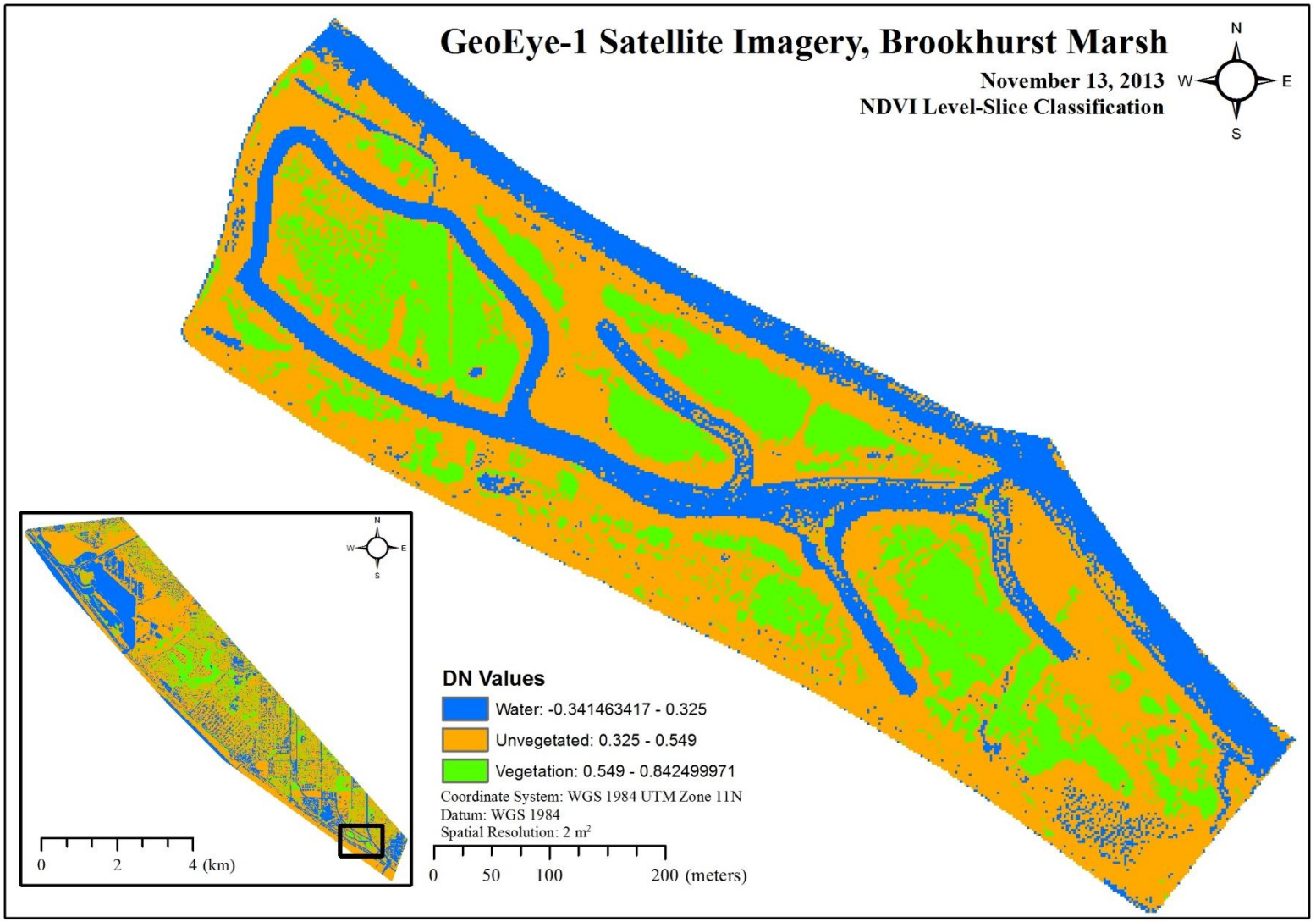

FIGURE 36. NDVI level-slice classification of the GeoEye-1 satellite imagery. Developed using ERDAS Imagine 2014.

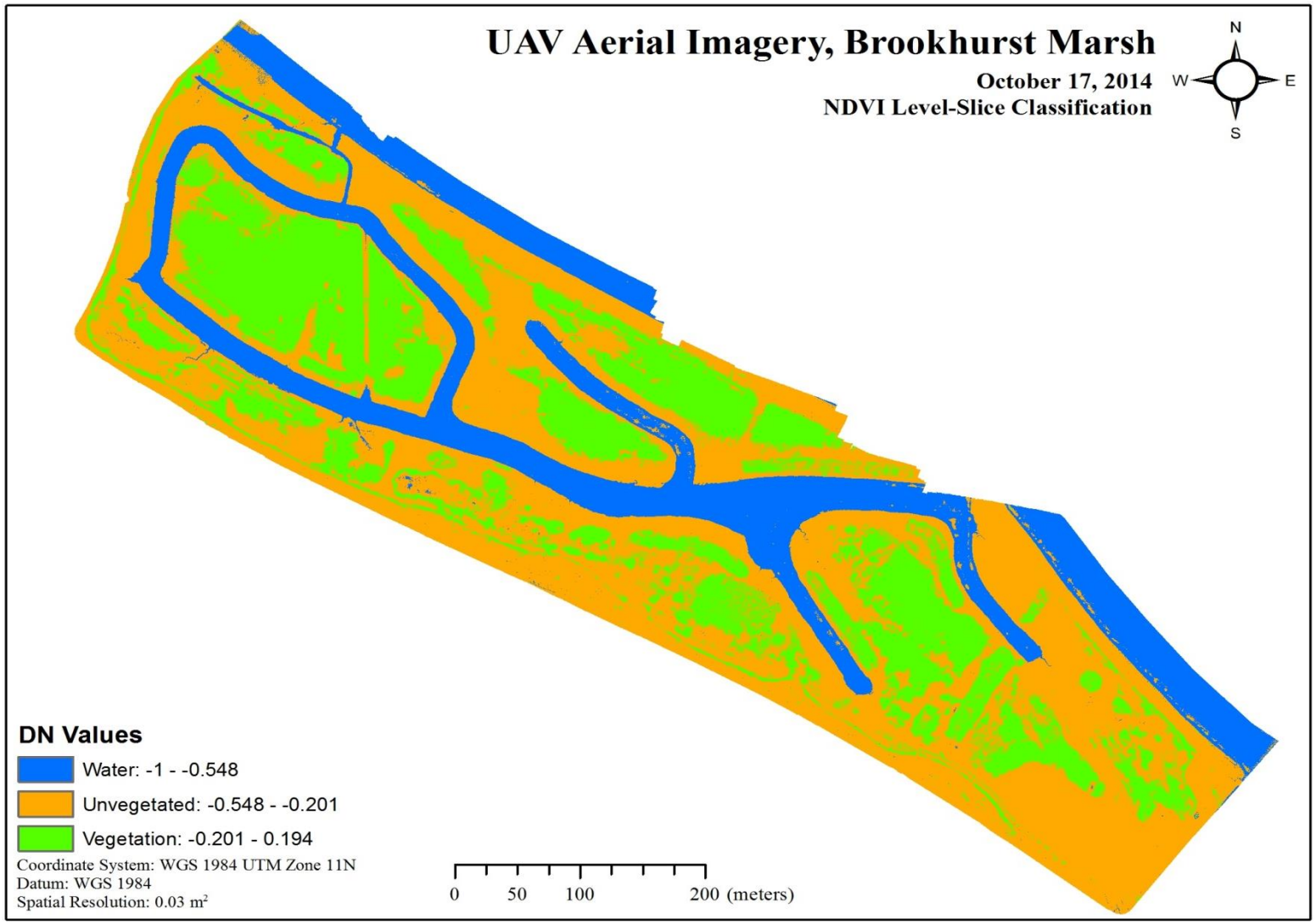

FIGURE 37. NDVI level-slice classification of the UAV aerial imagery. Developed using ERDAS Imagine 2014.

Unsupervised Classification

The unsupervised classified images used the statistics of the actual imagery to generate 30 distinct spectral clusters, which were then individually classified to the three main land cover classes: water, vegetation, and unvegetated. Figures 38, 39, and 40 show the unsupervised classifications all three sets of imagery. The GeoEye-1 and UAV unsupervised land cover classes were visually and proportionally consistent. Both identified water at 20%, recognized vegetation between 28-29%, and identified unvegetated surfaces between 50-51% (Table 6). The similarity in land cover distribution percentages verified that the procedures used for the unsupervised classification in ERDAS Imagine 2014 were consistent for both the UAV and the GeoEye-1 images. This similarity also spoke to the minimal change that took place at Brookhurst Marsh from November 2013 to October 2014. These figures also potentially indicated that there was a slight increase in vegetation over that period of time which bodes well for the monitoring measures placed on Brookhurst Marsh. Furthermore, the UAV and GeoEye-1 unsupervised classifications showed visual consistency with the 2009 vegetation community map and the NDVI-level slice land cover maps. The airplane unsupervised land cover classification suffered significantly when compared to the other two unsupervised maps. There was about a 14% difference in the vegetation class and water class for the airplane unsupervised map when compared to the GeoEye-1 and UAV unsupervised maps (Table 6). The most significant reason for these differences was caused by a lack of a NIR band. While performing the unsupervised classification, the software could only utilize the visible bands in the true color airplane imagery to develop spectral clusters which resulted in spectral redundancy.

Similar to the NDVI level-slice maps, the average percent change for the UAV unsupervised classification was less than both airplane and GeoEye-1 unsupervised land cover maps (Table 9). Again, this could be a good indicator of the UAV unsupervised map being a more accurate representation of Brookhurst Marsh land cover for October 2014 than either the airplane (Spring 2013) or GeoEye-1 (November 2013) unsupervised classifications were for their respective time periods. This also demonstrates the strength of using higher spatial resolution UAV datasets since the average percent change for it was the lowest among the three unsupervised classifications. The numbers for all three show a percent decrease in vegetation land cover since 2009 (Table 9).

TABLE 9. Percent Change: Unsupervised Classifications

	Water	Vegetation	Unvegetated	Average Percent Change
2013 Airplane Unsupervised Classification & 2009 Vegetation Community Map (Reference)	69.50%	-53.70%	6.16%	43.12%
2013 GeoEye-1 Satellite Unsupervised Classification & 2009 Vegetation Community Map (Reference)	-0.24%	-12.91%	8.99%	7.38%
2014 UAV Unsupervised Classification & 2009 Vegetation Community Map (Reference)	-1.64%	-8.30%	6.44%	5.46%

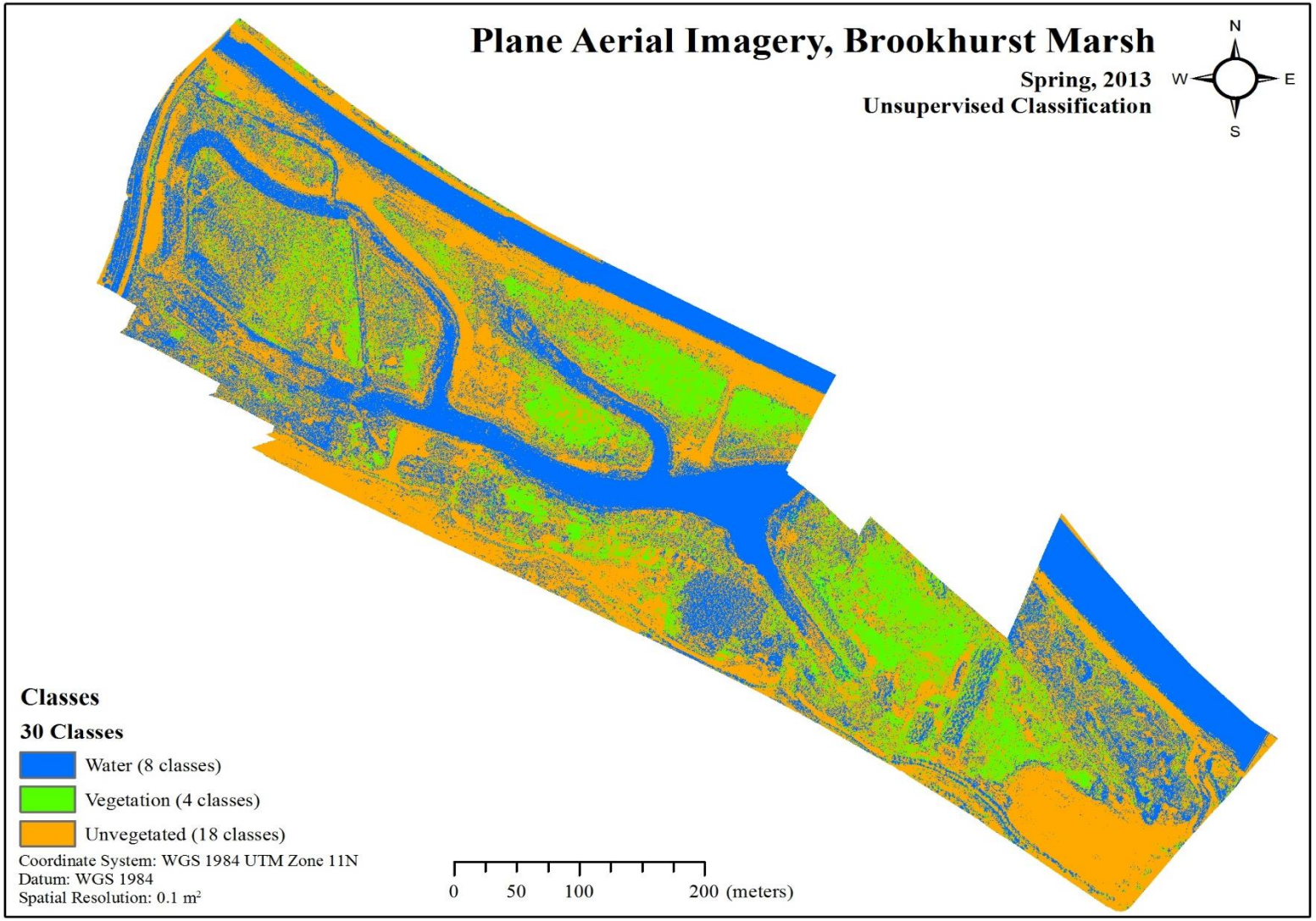

FIGURE 38. Unsupervised classification of the airplane aerial imagery. Developed using ERDAS Imagine 2014.

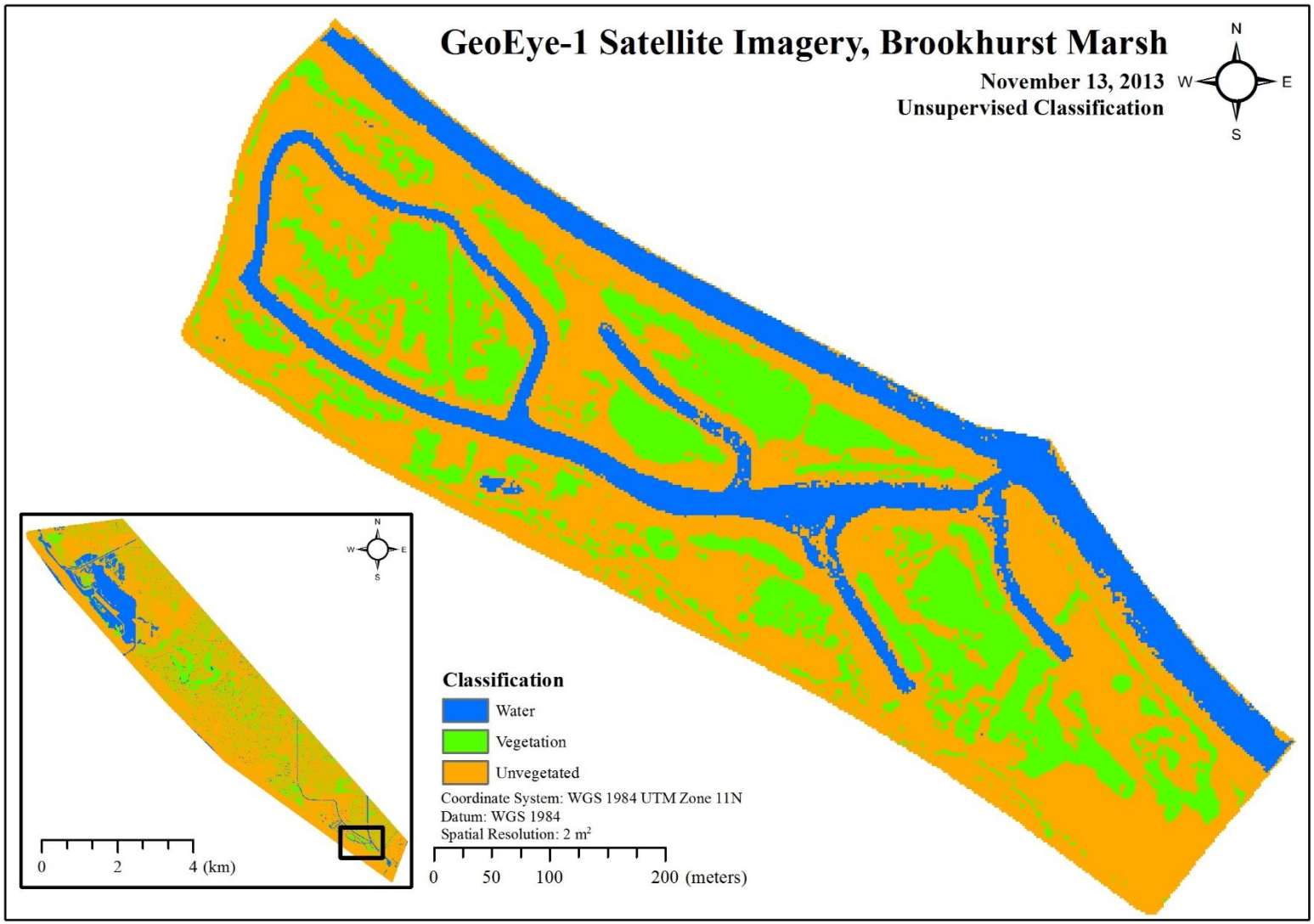

FIGURE 39. Unsupervised classification of the GeoEye-1 satellite imagery. Developed using ERDAS Imagine 2014.

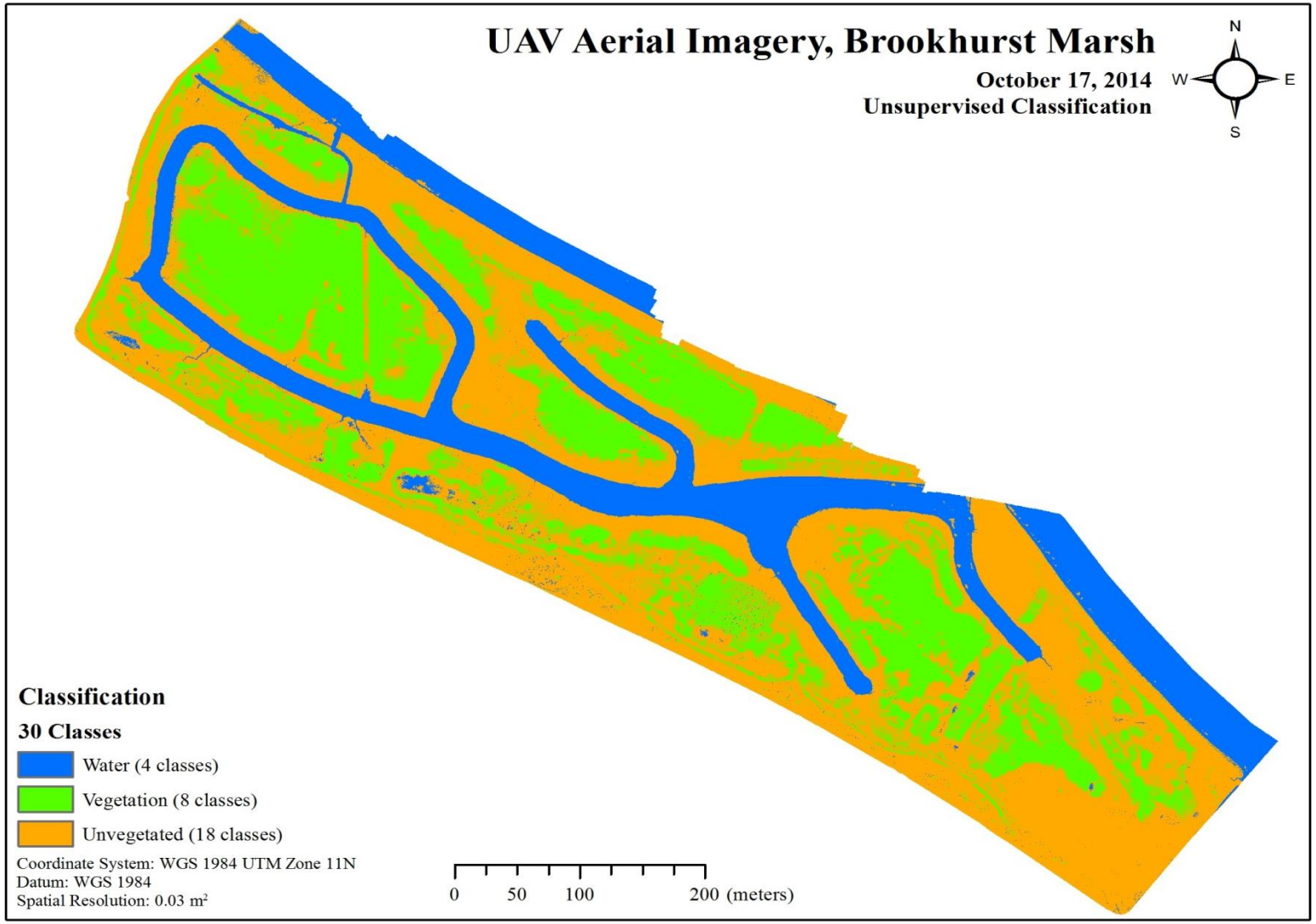

FIGURE 40. Unsupervised classification of the UAV aerial imagery. Developed using ERDAS Imagine 2014.

Supervised Classification

Figures 41, 42, and 43 show the airplane, GeoEye-1, and UAV supervised classifications. Both land cover maps showed water between 20-22% and unvegetated surfaces between 50-51% in Brookhurst Marsh (Table 6). The vegetation distribution was 28.87% for the UAV supervised land cover map while the GeoEye-1 satellite supervised classification showed vegetation distribution 25.85% (Table 5). Similar to the NDVI level-slice maps and the unsupervised classifications, the figures in Table 10 show that the UAV supervised classifications had the lowest average percent change most likely due to its' high spatial resolution characteristic. For all three supervised classifications, vegetation land cover showed an overall percent decrease since 2009 (Table 10). Again, the average percent change can also be attributed to errors and differences in classifying the 2009 land cover map and the supervised classifications.

TABLE 10. Percent Change: Supervised Classifications

	Water	Vegetation	Unvegetated	Average Percent Change
2013 Airplane Supervised Classification & 2009 Vegetation Community Map (Reference)	128.09%	-14.06%	-47.08%	63.08%
2013 GeoEye-1 Satellite Supervised Classification & 2009 Vegetation Community Map (Reference)	9.28%	-19.94%	9.61%	12.94%
2014 UAV Supervised Classification & 2009 Vegetation Community Map (Reference)	-1.11%	-10.59%	7.78%	6.49%

Again due to the limited reliance on the visible bands of the airplane imagery and a lack of spectral difference, the airplane supervised land cover map shows a lot of visual errors in attempting to distinguish intertidal mudflat areas and water (Figure 29). Even though the GeoEye-1 and UAV supervised training samples had minor issues with distinguishing water and unvegetated land cover classes, they showed strong overall visual consistency with the 2009 vegetation community map, the NDVI-level slice land cover maps, and the unsupervised classifications.

Accuracy assessment. The three types of accuracy assessments that were conducted to evaluate the supervised classified images are the distance image files, thresholding, and overall accuracy reports. While distance images are not a complete measurement of accuracy, they provide a general overview of distributions between the classification and the original imagery. The supervised classification distance file histograms for all three types of imagery indicated a chi-squared distribution which was to be expected if the maximum likelihood classification was performed correctly (Appendix D). In regards to thresholding, both the GeoEye-1 and UAV imagery displayed a smooth chi-square histogram distribution at the 0.05 confidence level for all three signature classes. On the other hand, the airplane imagery struggled with defining water and vegetation signature classes. These spectral signature classes were showing polymodal (multiple peaks) chi-squared distributions which are indicative of inaccurate class feature representations. These were the caused by insufficient spectral differencing due to a lack of a NIR band in the airplane imagery.

Generating the assessment report for all three types of imagery offered a better perspective on the degree of accuracy for the supervised classifications. Table 10

provides the overall accuracy percentages and corresponding kappa coefficient figures for the three supervised classifications. It should be emphasized that these accuracy reports were user driven. The accuracy figures can fluctuate based on the skill of the image specialist in determining the appropriate class for the test pixels based on the original imagery. The higher the overall accuracy percentage for the supervised classification the more accurate those supervised training classes were at representing land cover at Brookhurst Marsh for the respective time periods. The kappa coefficient, which ranges between 0 and 1 with 1 being the most accurate, indicates the proportion of errors a classification avoids that a completely random classification would generate. Both the GeoEye-1 and UAV supervised classifications had the same overall accuracy but the UAV had the highest kappa coefficient (Table 10). This meant that the GeoEye-1 had markedly more issues spectrally classifying individual pixels than the UAV supervised classification. Similar to the results of the thresholding, the airplane supervised classification's overall accuracy and kappa coefficient numbers were the lowest because of insufficient spectral differencing in the original imagery (Table 10).

TABLE 10. Supervised Classification Overall Accuracy and Kappa Coefficients

	Overall Accuracy	Kappa Coefficient
2013 Airplane Supervised Classification	60%	0.34
2013 GeoEye-1 Satellite Supervised Classification	84%	0.64
2014 UAV Supervised Classification	84%	0.72

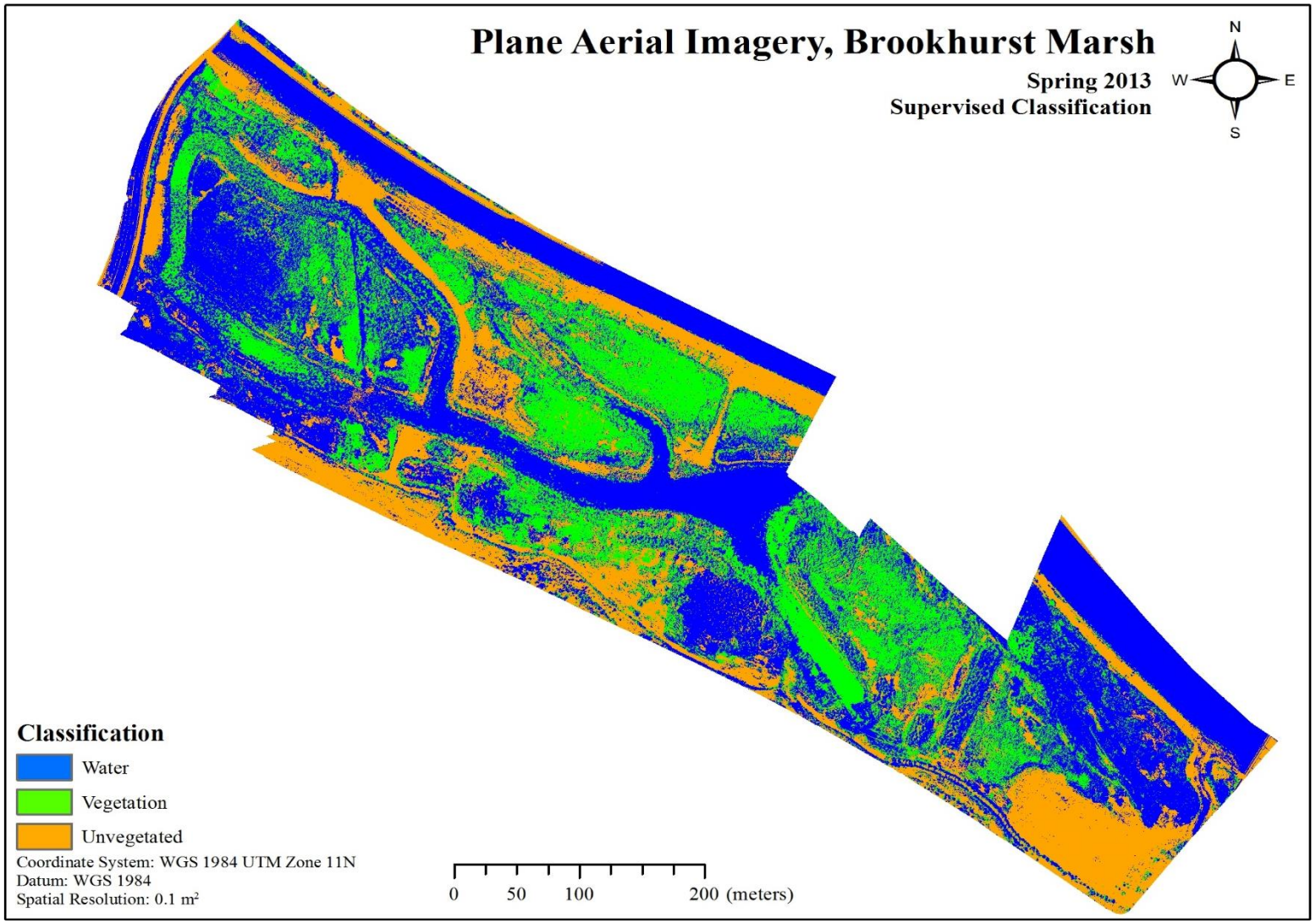

FIGURE 41. Supervised classification of the airplane aerial imagery. Developed using ERDAS Imagine 2014.

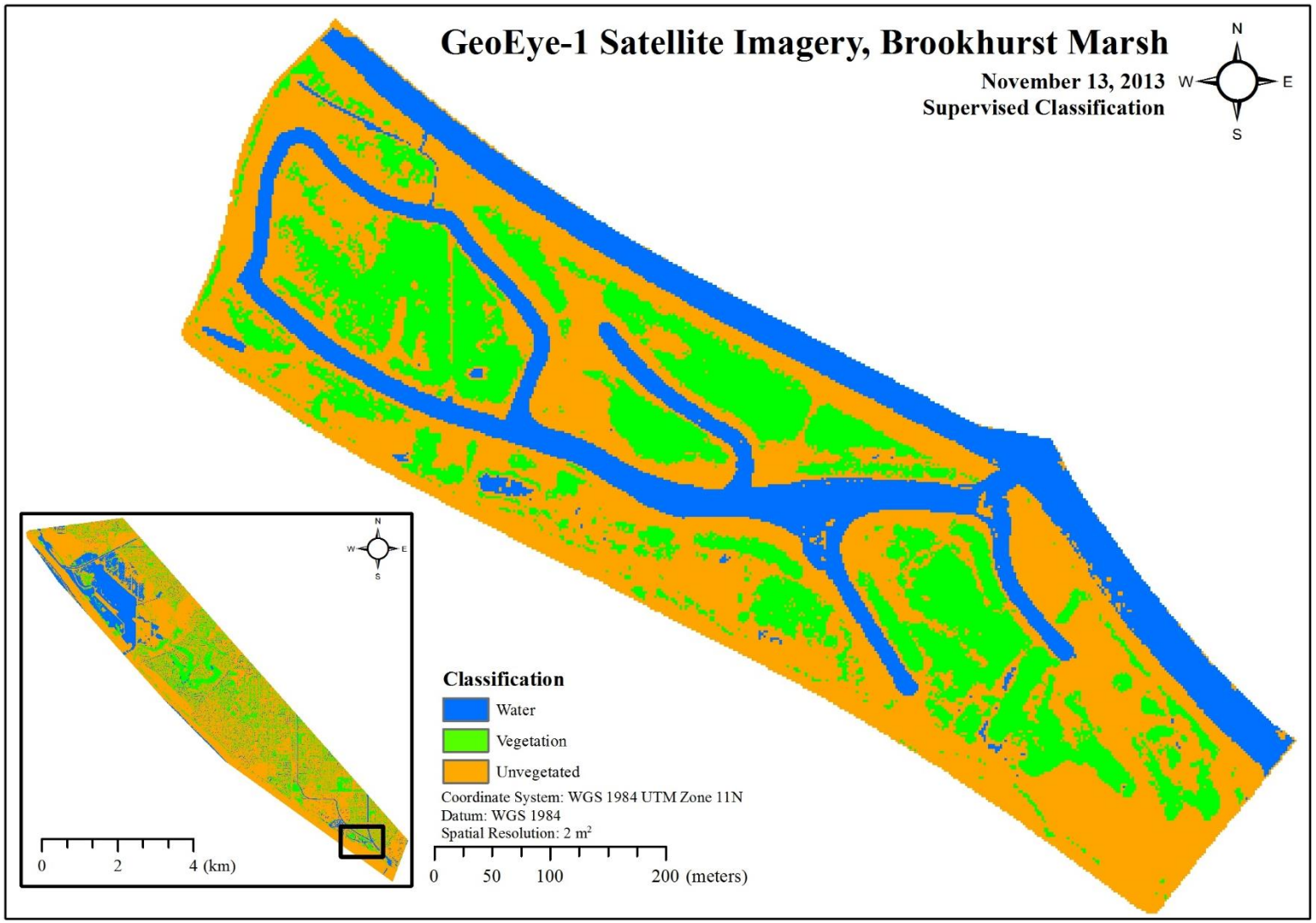

FIGURE 42. Supervised classification of the GeoEye-1 satellite imagery. Developed using ERDAS Imagine 2014.

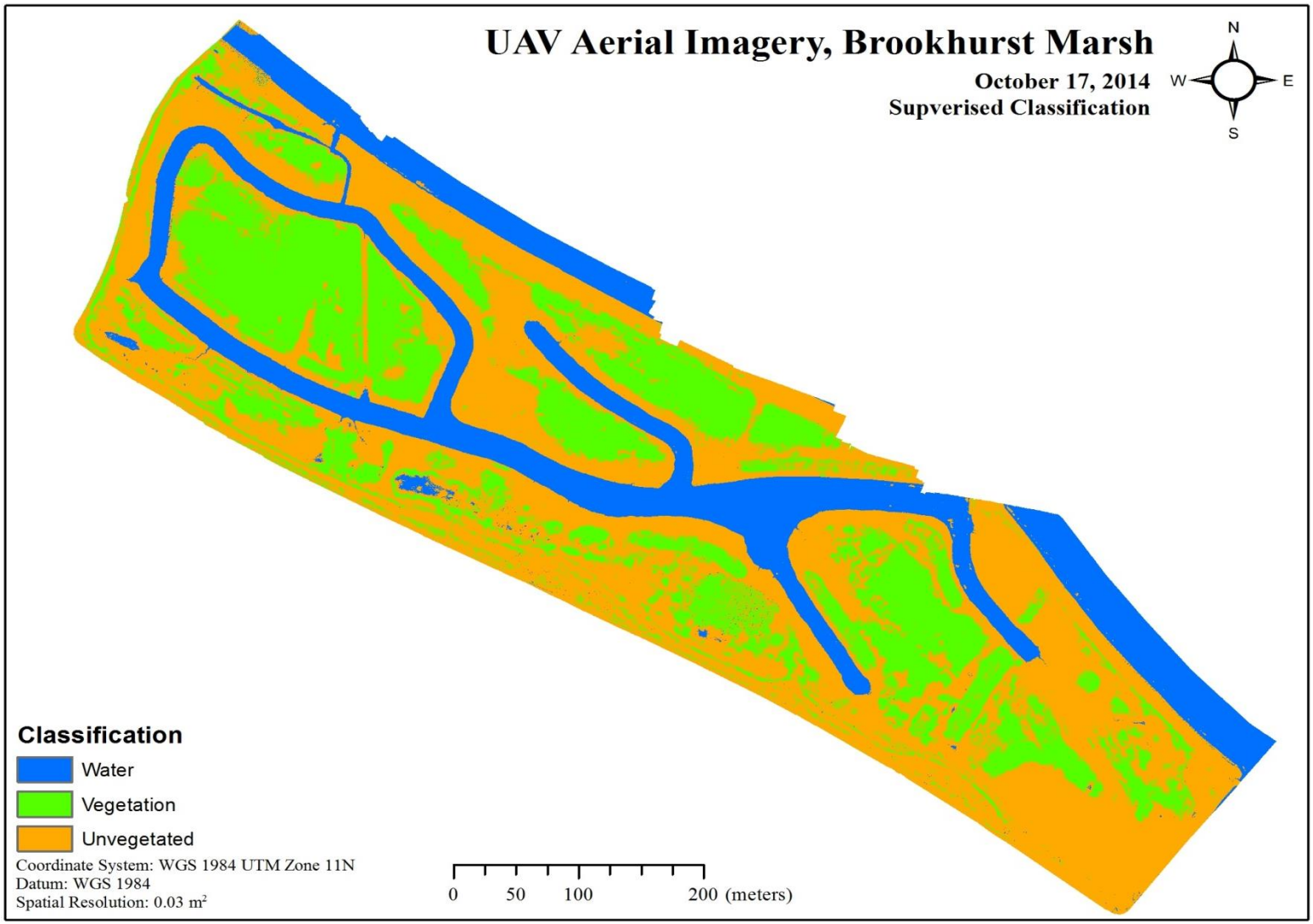

FIGURE 43. Supervised classification of the UAV aerial imagery. Developed using ERDAS Imagine 2014.

This chapter provides the analytical and statistical results of the comparison between classifications of the different data products. These included the base products: the airplane PhotoScan aerial orthophoto, the GeoEye-1 multispectral satellite imagery, and the UAV PhotoScan aerial orthophoto. The 2009 vegetation community vector data was reclassified into a land cover map for visual and statistical reference to the spectral based land cover maps of the UAV, GeoEye-1, and airplane datasets. The Normalized Difference Vegetation Index analysis produced the GeoEye-1 NDVI and UAV NDVI images, along with the GeoEye-1 and UAV NDVI level-slice land cover maps. Finally, unsupervised classification and supervised classifications were performed for all three datasets and lastly accuracy assessments were completed for each corresponding supervised classification. Each land cover map was referenced to the 2009 vegetation community map to determine percent change statistics relating to increases or decreases in water, vegetation, and unvegetated land cover types in Brookhurst Marsh.

CHAPTER 5

DISCUSSION

This study demonstrates the applicability of a method for conducting aerial surveys using Unmanned Aerial Vehicles (UAV). This research demonstrates and compares methods of image analysis through different classification techniques in order to limit the degree of ground survey data required for annual community and species mapping at the Huntington Beach Wetlands and by extension, to other wetland environments.

Assessment and Significance

This research has demonstrated some important features of remote sensing as they relate to UAV acquired aerial imagery. Images derived from the UAV platform offers both spatial and temporal advantages over airplanes and satellites. It should be noted that UAV platforms, especially quadcopters are best suited for research limited to small spatial extents. Studies of areas on the order of a few square kilometers can benefit from UASs. Image analysis of both the GeoEye-1 satellite and UAV imagery demonstrated that commercial off-the-shelf (COTS) cameras, modified to capture NIR wavelengths can yield comparable results to satellite sensors if the images are captured using a UAV platform and processed using a systematic approach. In this study, the high spatial resolution UAV imagery has shown to offer a more detailed land cover assessment for water, vegetation, and unvegetated surfaces at Brookhurst Marsh over airplane and satellite derived imagery. Basically, a higher level of spatial detail makes the detection

and distinction of vegetation cover much easier. It should be noted that aerial imagery captured by airplane and satellite platforms have a coarser spatial resolution than the imagery captured by the UAV because of the respective altitude from which these images were taken at. While achieving sub-centimeter resolution is possible through both airplane and satellite platforms, the UAV platform provides temporal resolution capabilities far beyond those available with airplane and satellite platforms. Instead of having to rely on the repeat time for satellites or scheduling flights with a private pilot, a UAV can be readily deployed over the marsh and capture aerial imagery whenever updated surveys are needed and when plant phenology is favorable for identifying specific plant species or communities.

This study demonstrated a viable first step towards vegetation community and even species mapping. There was visual consistency in vegetation land cover between the reclassified 2009 vegetation community map and all three UAV and GeoEye-1 spectral based land cover maps. Consequently, the similarity of land cover percentages and consistency in location of water, vegetation and unvegetated surfaces between the UAV and GeoEye-1 satellite images was indicative of the spectral potential that UAV imagery can offer. The relative consistency between the GeoEye-1 and the UAV supervised classifications also illustrated that the land cover has not changed significantly and even more importantly the vegetation cover has remained consistent if not increased from November 2013 to October 2014 at Brookhurst Marsh. This consistency also speaks to the success of the HBWC in implementing preservation policies that encouraged vegetation growth during that period of time. The vegetation land cover percentages in the NDVI level-slice, the unsupervised, and supervised land cover maps of

the GeoEye-1 satellite multispectral imagery displayed more variation than the UAV land cover maps. The water and vegetation land cover percentages showed variation to a lesser degree in all the UAV land cover maps as well. These small percentage variations can be attributed to either human errors in processing and calculation, the spatial resolution of the datasets, or actual differences in land cover between November 2013 and October 2014. The location of some of the pixels classified as vegetation in the airplane unsupervised classification were sporadically consistent with the vegetation locations of the unsupervised classifications derived from the other two platforms. The GeoEye-1 satellite and UAV aerial image unsupervised classifications also showed a much clearer representation of the different land cover classes than the NDVI level-slices.

All land cover maps showed a percent decrease in vegetation cover when compared to the 2009 vegetation community map. While this could indicate that vegetation cover has decreased in Brookhurst Marsh since 2009, it was most likely the case of overestimation of vegetation land cover in the 2009 vector data. As concluded in the study completed by Wade et al. (2003), there were no significant differences in vector data and raster-based land cover assessments but some cases illustrated statistically higher efficiency and accuracy when using raster data to assess land cover. All three spectral based UAV land cover maps showed the smallest average percent change when compared accordingly to the airplane and satellite maps. This speaks well for the accuracy of the UAV imagery as the smallest average percent change makes it the closest statistical match to the 2009 vegetation community land cover map. Additionally, the visual similarity and land cover percentage agreement of the three land cover classes

among the 2009 vegetation community land cover map, NDVI level-slice maps, and the unsupervised and supervised classifications for both the UAV and GeoEye-1 satellite imagery is significant because it shows that the NDVI level-slice method can be comparable to the other classification methods. This is important and ideally beneficial for environmental agencies requiring timely data because the NDVI level-slice method of developing land cover maps takes less time to implement than a complete supervised classification.

As demonstrated in this research, aerial photography provides an overall picture of land over change within Brookhurst Marsh. Along with this, permissions from land owners that only require a few hours installing ground transects are more easily attainable than those consisting of days. This study has also shown that the aerial imagery collected from Dr. Whitcraft was much more spectrally limited for land cover analysis than the UAV or satellite imagery. This airplane imagery was inadequate because the spatial extents were incomplete, the image quality was somewhat poor due to atmospheric effects, and the utilization of a true color digital camera without any proper filtration of the lens could not capture NIR wavelengths. All these factors yielded poor spectral based land cover maps. The UAV imagery was more comparable to the satellite imagery than the airplane imagery was to the satellite imagery based on the land cover statistics of water, vegetation, and unvegetated surfaces derived from these maps. With access to higher spatial imagery as offered by the low cost UAV platform used in this study, the vegetation community maps developed by Dr. Whitcraft and Merkel & Associates can potentially be improved. The agreement in land cover with the 2009 vegetation

community map and the GeoEye-1 maps demonstrates that the UAV platform can be ideal for future annual mapping and assessment of Brookhurst Marsh.

Errors and Limitations

This study contained limitations as they relate to data collection, data processing, and data analysis. As mentioned earlier, the spatial extent of both the UAV imagery and the airplane imagery did not completely encompass the extent of Brookhurst Marsh. With data collection, the main constraint with using the DJI Phantom quadcopter was that it was manually piloted using only line of sight. There were no real-time feedback capabilities in this system that could inform an operator of altitude, speed, angle, and perspective while capturing aerial imagery. All this was done using visual cues from the ground. This limitation can be solved by using a UAS that is fully autonomous or one that offers flight planning capabilities such as the advanced Phantom models offered by Dajiang Innovation Technology. As a result of manual flight operation and acquisition, the northeast portions were slightly cut off in the UAV imagery.

There were many more limitations for the airplane imagery used in this study. A significant amount of images in the northeast and southwest portions of the marsh were not captured during the initial flight in spring 2013. Additionally, there were visible distortions along the edges of the marsh because of incomplete overlapping during the image collection by the pilot. A lack of a NIR band also created some difficulty in assessing this airplane imagery. These difficulties rose from the fact that the visible bands derived from a true color image are highly correlated. This high correlation makes the information derived from them redundant since they originate from the same range on the electromagnetic spectrum (CRISP 2001; Eastman 2001; Pidwirny 2006). A NIR

band would allow for some spectral variation which could yield better results for the spectral based land cover maps as shown with the successful construction and analysis of the GeoEye-1 and UAV spectral based land cover maps. This also meant that a NDVI could not be computed nor could an NDVI level-slice be performed for this aerial imagery.

Due to time constraints, ground based observations for the purposes of assessing the potential for vegetation community and species level mapping could not be performed. Merkel & Associates and Dr. Whitcraft did not collect ground transect data for 2014 hence constraining this analysis from potentially developing vegetation community maps derived from the October 2014 UAV acquired imagery. It would have been important to see if the Ricoh GR III camera along with this Phantom quadcopter could be successfully utilized to develop vegetation community maps. As seen with the 2009 vegetation community map, Merkel & Associates along with Dr. Whitcraft used a combination of aerial imagery and ground transects to develop these maps. While they used the same unsupervised image classification technique, they do not detail the specific methods they used to create estimates based on the ground transect data. Having their methodology could have helped inform the construction of the unsupervised and supervised land cover maps for this research. This information would also be required for future research and vegetation community map development.

There were also some issues in calculating the percent change figures for all the land cover maps. The land cover proportions from the 2009 vector data were used to normalize the percent change for each type of land cover map. The 2009 vector data is not perfect for a few reasons. In the final reports developed by Merkel & Associates

(2011) and Whitcraft, Allen, and Lowe (2013), there were no measures utilized to check the accuracy and validity of their land cover distribution results. It is assumed that their analysis was representative of the land cover conditions in 2009 to provide a baseline reference to compare land cover measures and accuracy. Additionally, each area of individual classes in the 2009 vegetation community map was derived from data in vector format, which means that it is probable that the class areas from the 2009 map could have been under or overestimated since vector data is based on individual observations rather than continuous data that is inherent in raster-based imagery (Wade et al. 2003).

A lack of access to earlier aerial imagery of the marsh is another factor that limited this research. If the UAS utilized for this study is shown to successfully develop vegetation community maps, then this type of map could be compared to historical aerial imagery and older vegetation community maps such as the 2009 vegetation community map. This type of analysis could essentially provide a better perspective on the degree of change that has taken place at the vegetation community level in Brookhurst Marsh. It could potentially help inform the Huntington Beach Wetlands Conservancy of the types of measures that have aided in the preservation and growth of the vegetation communities at different periods of time in Brookhurst Marsh.

As far as the analysis portion is concerned, supervised training samples are dependent on the manual interpretation skills of the image specialist and the tools used to create those samples with the image analysis software. The methods used to develop the supervised signatures in ERDAS Imagine 2014 displayed difficulty at times distinguishing the spectral differences between water features and unvegetated features in some areas for all three types of aerial images. This was especially evident in the

intertidal mudflat areas where the water was shallow enough that it resembled unvegetated features such as soil or barren land. It was increasingly difficult to develop distinct signature classes for the airplane imagery because of these indistinguishable spectral resemblances. The same was occasionally seen in the GeoEye-1 satellite imagery where there were examples of intertidal mudflat areas which caused some of the errors in the supervised classification.

Because the airplane imagery and the GeoEye-1 satellite imagery were taken in 2013, it was difficult to judge what some features might have looked based on the 2014 field observations. Of course drastic changes would most likely not have occurred but changes to a lesser degree are much more probable. Since some features were indistinguishable between one another in both the airplane and GeoEye-1 satellite imagery, it would have been valuable to have the knowledge of the features and their distributions as they existed in 2013, when these datasets were captured. In turn, this knowledge would have helped out in the field while capturing the UAV imagery by offering a better indication of the types of features that exist in Brookhurst Marsh. It would have also assisted during the data analysis phase because it could help inform the construction of spectral signature classes for the land cover features. Additionally, this knowledge could further assist in the possible quantification of the degree of changes in the conditions at the marsh. Again, it is difficult to make assumptions based off of other sourced aerial imagery since the field conditions might not have been as similar as they were when the UAV data was captured in October 2014.

There were also some errors with the NDVI level-slice images. Each of the 256 bins in the original NDVI image represented a certain NDVI value which pertained to a

group of pixel clusters. Some of these pixels near the edge of the class breakpoints belonged to multiple information classes. The GeoEye-1 NDVI level-slice was noisier than the UAV NDVI level-slice land cover map when it came to making distinctions between water and suspended sediments along with incorrectly classifying known unvegetated pixels as water in the southeastern most portion of the marsh. For both images, there were multiple locations especially in the southeast portion and central portion of the marsh where pixels were clearly misidentified as water or unvegetated classes. The average percent change figures for the UAV and GeoEye-1 was the highest in the NDVI level-slices in comparison to the unsupervised and supervised land cover maps' average percent values which showed some limitation of the accuracy this method produced. There was an overall consistency in location of the vegetation classes between the GeoEye-1 and UAV NDVI level-slice maps which spoke to the reliability of how this method was performed.

The unsupervised classification of the airplane imagery was the noisiest in regards to what the actual conditions on the field should have looked at the time. Again, the issues came from the fact that the actual imagery lacked an NIR band which affected the decisions that ERDAS Imagine 2014 made about the spectral clusters. An insufficient spectral difference limited the software to solely rely on the true color wavelengths of the airplane imagery which resulted in a poor unsupervised classification. The issues of clusters being misclassified incorrectly existed in all three image sets but were most prevalent in the airplane imagery because of the previously mentioned issues. Again, some of the suspended sediments in the water around Brookhurst Marsh were very similar in spectral reflectance to soil landscape. The unsupervised calculation over

classified cells as water rather than vegetation for the airplane orthophoto. For both the GeoEye-1 and UAV unsupervised classifications, the southernmost portions of the marsh exhibited some inconsistency mainly with known vegetation and unvegetated surfaces being classified as water pixels. The GeoEye-1 unsupervised classification showed some additional discrepancy by classifying areas where water existed as unvegetated pixels.

With the supervised classifications, the discrepancies from the airplane displayed a similar erroneous result as seen with the unsupervised land cover map. Pixels were predominantly over classified as water over both vegetation and unvegetated surfaces. These discrepancies rose from the spectral redundancy of the airplane imagery which resulted in difficulty in differentiating the water, vegetation, and unvegetated land cover classes when the training samples were being developed. Additionally, defining signature classes for the supervised classification became increasingly difficult especially when looking at specific pixels because of the haze like effect in the airplane imagery. As mentioned earlier, the individual images contained these hazy effects that were possibly caused by clouds overhead or limited sunlight on the area when the airplane was flown in April 2013. The GeoEye-1 supervised classification showed more visual improvement over the unsupervised classification. The UAV supervised classification was able to correctly classify more pixels as vegetation in the southern portion of the marsh over the unsupervised classification. Similar to the unsupervised classification, the inconsistencies for both the GeoEye-1 and the UAV supervised classifications were seen in the southern portions of the marsh where pixels were classified as water in areas that were actually vegetation and unvegetated in the original imagery.

Future Research

Overall, the visual and statistical consistency among the UAV and GeoEye-1 spectral based land cover maps and the reclassified 2009 vegetation community map was a strong indicator that the methods used in this research are viable for ecological assessment at Brookhurst Marsh. Furthermore, the spectral limitations in the airplane imagery, which has been used by the Huntington Beach Wetland Conservancy, yielded very poor unsupervised and supervised classifications. This combined with the successful comparability of the UAV land cover maps should be evidence enough for the implementation of UAS remote sensing for the ecological and temporal assessment of the Huntington Beach Wetlands.

The next step in this research can potentially come with the development of vegetation community and/or species maps. As illustrated with the 2009 vegetation community land cover map, HBWC along with Dr. Whitcraft have been using aerial imagery captured by airplane for their analysis in developing these types of maps over the past few years. The development of vegetation community maps required extensive manual interpretation and ground surveys which in turn necessitated resources in the form of time and effort. Ground surveys are necessary for obtaining metrics (e.g. abundance, percent cover, species richness, community composition) that are unattainable through aerial remote sensing (Woodfield and Merkel 2011; Whitcraft, Allen, and Lowe 2013). Using aerial photography, physical access to the marsh is not required during sensitive times of the year such as bird breeding season (Woodfield and Merkel 2011; Whitcraft, Allen, and Lowe 2013). The UAV platform can potentially reduce the time needed to spend ground surveying and potentially reduce the instance of

harm coming to wildlife that inhabit the marsh. The accuracy and flexibility of the UAS can augment the efforts of the HBWC in monitoring the Huntington Beach Wetlands.

CHAPTER 6

CONCLUSION

This research provides a detailed methodology for Unmanned Aerial Vehicle (UAV) aerial image acquisition for the purposes of vegetation analysis at the Huntington Beach Wetlands. These methods provide a systematic approach to planning and training, data collection, data processing, and data analysis in order to assess the land cover and vegetation in Brookhurst Marsh. This systematic approach demonstrates the advantages of UAV acquired aerial imagery in comparison to imagery captured using satellite and airplane platforms. Essentially, these methods build the first step towards a foundation for creating vegetation community based classifications and cartographic products.

The method includes four steps. Phase I describes planning and data collection training and includes recommendations for site selection, calibrating and prepping all necessary equipment, and considering all pre-flight factors including permissions, safety, weather, and training. Phase II provides steps required for consistent data collection. This includes all primary and secondary acquisitions. Specifically, these encompassed the UAV, airplane, and GeoEye-1 satellite aerial imagery of Brookhurst Marsh. Phase III comprised of all data processing tasks including standardization, georeferencing, photogrammetric image assembly, and band configuration. Lastly, Phase IV consisted of all the image analysis techniques used. These entailed reclassifying the 2009 vegetation community vector data into a land cover map, calculating the Normalized Difference

Vegetation Indices (NDVI), creating the NDVI level-slices, and performing the unsupervised and supervised classifications along with generating accuracy reports.

The results across all three types of spectral based land cover maps and the reclassified 2009 vegetation community map illustrate distributional consistency among the vegetation, unvegetated, and water land cover classes between the UAV aerial imagery and the GeoEye-1 satellite multispectral imagery. These consistent results also demonstrated that the degree of land cover change has been minimal from November 2013 to October 2014. These results also showed some semblance of distributional consistency among pixels classified as vegetation in the airplane unsupervised and supervised land cover maps when compared to the UAV and GeoEye-1 classifications. But the two main limitations in the airplane aerial imagery stemming from a lack of a NIR band which limited the degree of spectral difference that could be utilized along with poor flight trajectory which created image distortions resulted in very poor unsupervised and supervised land cover maps. The level of high spatial and temporal resolution was highlighted by the UAV acquired aerial imagery and provides a great advantage for future acquisitions over satellite and airplane platforms at Brookhurst Marsh. The visual similarity between the 2009 vegetation community land cover map and the three spectral based land cover maps for the UAV and GeoEye-1 speak to the consistency and success of preservation methods employed by the Huntington Beach Wetland Conservancy. Additionally, the consistency and distributional agreement of all three land cover classes between the UAV and GeoEye-1 NDVI level-slices and their respective supervised classifications suggested that the NDVI level-slice method can potentially be utilized for

a rapid and accurate first-step vegetation assessment by environmental conservancies looking to develop spectral based land cover maps.

Suggestions for Potential Work

The methods described and implemented in this research require further development and progression with respect to data collection and data analysis. First it would be important to assess the Unmanned Aerial System (UAS) utilized for this study in conjunction with concurrent ground surveys for developing an updated vegetation community based map of Brookhurst marsh. Consequently, capturing updated UAV aerial imagery of Brookhurst Marsh and gathering concurrent vegetation ground survey data will be required for future analysis. If the UAS utilized in this research, which incorporated the Ricoh GR III and Phantom quadcopter, coupled with vegetation ground transect data prove to be insufficient for mapping vegetation communities, then aerial image acquisition should be enhanced with the use of more sophisticated UASs. This would entail using larger UAV platforms that can hold a heavier and ideally a more sophisticated payload than what was utilized for this study (Watts, Ambrosia, and Hinkley 2012). Examples of such UAS include the Phantom 2 Vision Plus or the Phantom 3 Advanced which have the ability to automatically plan and execute flight operations for more precise aerial image acquisition missions.

This research provides a first step towards mapping vegetation communities. Future work will undoubtedly necessitate the utilization of ground transect methodologies as conducted by Whitcraft, Allen, and Lowe (2013) or similar wetland vegetation monitoring protocols as established in their report by the Toronto and Region Conservation Authority (2011). Developing vegetation community and species level

maps of Brookhurst Marsh require ground surveys to an extent (Woodfield and Merkel 2011; Whitcraft, Allen, and Lowe 2013). Essentially the land cover analysis presented here can be taken further with vegetation ground survey data and could potentially help in the development of vegetation community mapping. Furthermore, a more sophisticated development of spectral signatures of select communities or species through the investigation of textures in the UAV aerial imagery could be a valuable addition for future research in mapping Brookhurst Marsh's vegetation habitat distribution. Research in object-based image analysis (OBIA) for species and community spectral differencing through using software such as eCognition could be an easier and efficient means to creating vegetation community maps (Willhauck 2000; Niemeyer and Canty 2003; Shi, Wang, and Xu 2011). The OBIA software environment, eCognition 9. 0, is used to develop rulesets such as spectral signatures for remote sensing image analysis (Trimble 2015). A creation of an extensive spectral library developed using this type of software can provide the framework for automation. This type of enhanced streamlined method of analysis coupled with a sophisticated remote sensing UAS could potentially reduce the use of the ground survey methodology previously used by Whitcraft, Allen, and Lowe (2013) and Merkel & Associates, Inc (2011). Ultimately, it could potentially provide significant and efficient ecological and temporal insights detailing plant phenology and land cover at Brookhurst Marsh.

Because of the temporal flexibility as illustrated by this study, of the UAV remote sensing platform, future analysis involving change detection could be more feasible. Change detection is the process of identifying differences in the state of an object or phenomenon by observing it at different times (Singh 1989, Lu et al. 2003; Théau 2012;

Vittek et al. 2014). It involves the application of multi-temporal datasets to quantitatively analyze the temporal effects of a phenomenon such as land cover distribution or changes in plant phenology (Théau 2012). Datasets can potentially be acquired using a UAV at designated times. For example, a UAV can be deployed on a monthly basis to assess the change in vegetation distribution over the course of a year, or they can be deployed daily to assess the change at the marsh on a weekly basis. The end goal would be to streamline UAV remote sensing aerial image acquisitions and spectral based land cover analysis with the ground survey methods developed by Whitcraft, Allen, and Lowe (2013) to create accurate time-sensitive vegetation community and/or species maps of the Huntington Beach Wetlands.

APPENDICES

APPENDIX A

FAA REGULATIONS

These are the 2014 regulations set forth by the United States Federal Aviation Administration (FAA) regarding the use of Unmanned Aerial Vehicles in commercial airspace for recreational purposes (FAA 2014). These rules were followed during all UAV aerial image acquisition procedures:

- Fly below 400 feet and remain clear of surrounding obstacles, flight speed cannot exceed 200 kts of true airspeed
- Keep the aircraft within visual line of sight at all times
- Remain well clear of and do not interfere with manned aircraft operations
- Don't fly within 5 miles of an airport unless you contact the airport and control tower before flying
- Don't fly near people or stadiums
- Don't fly an aircraft that weighs more than 55 lbs unless it is certified by an aeromodeling community-based organization
- Don't be careless or reckless with your unmanned aircraft as it could result in a fine for endangering people or other aircrafts

APPENDIX B

UAV TEST AERIAL IMAGERY

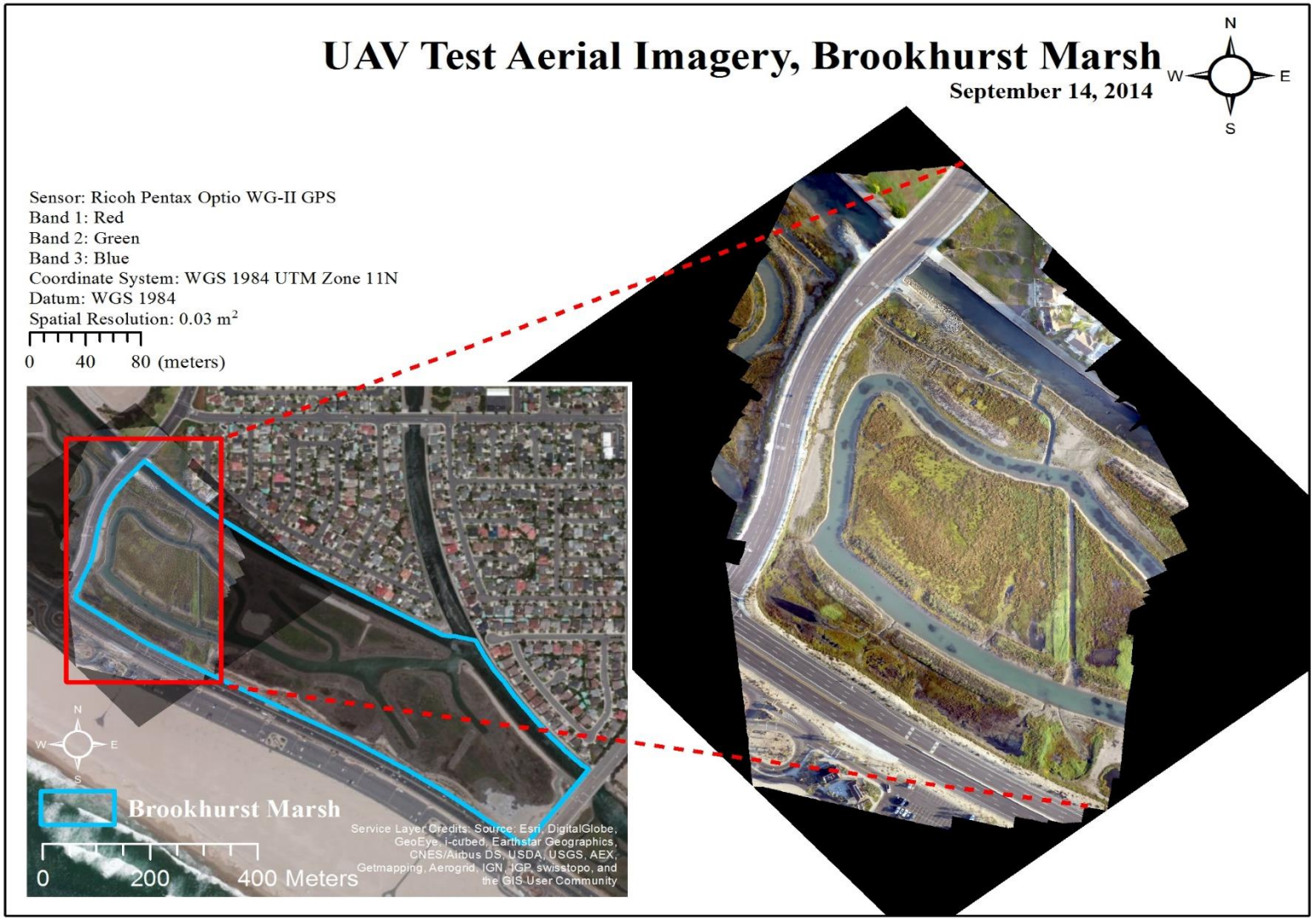

FIGURE 44. Test UAV aerial orthophoto. Captured using the Pentax Optio digital camera and developed using Agisoft PhotoScan.

APPENDIX C

SATELLITE PANCHROMATIC AND PAN-SHARPENED MODELS

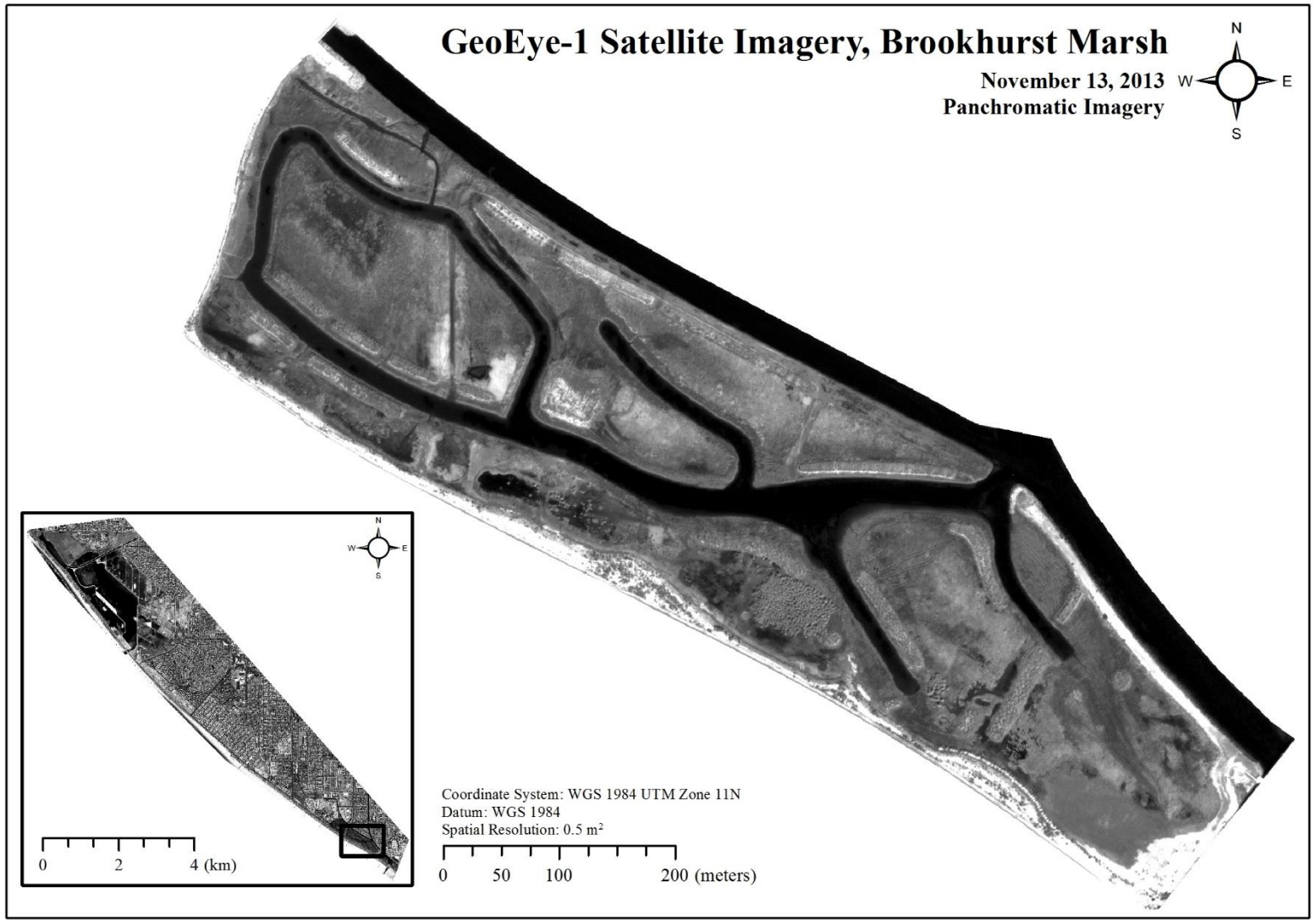

FIGURE 45. 2013 GeoEye-1 panchromatic satellite imagery. Has a spatial resolution of 0.5 m^2.

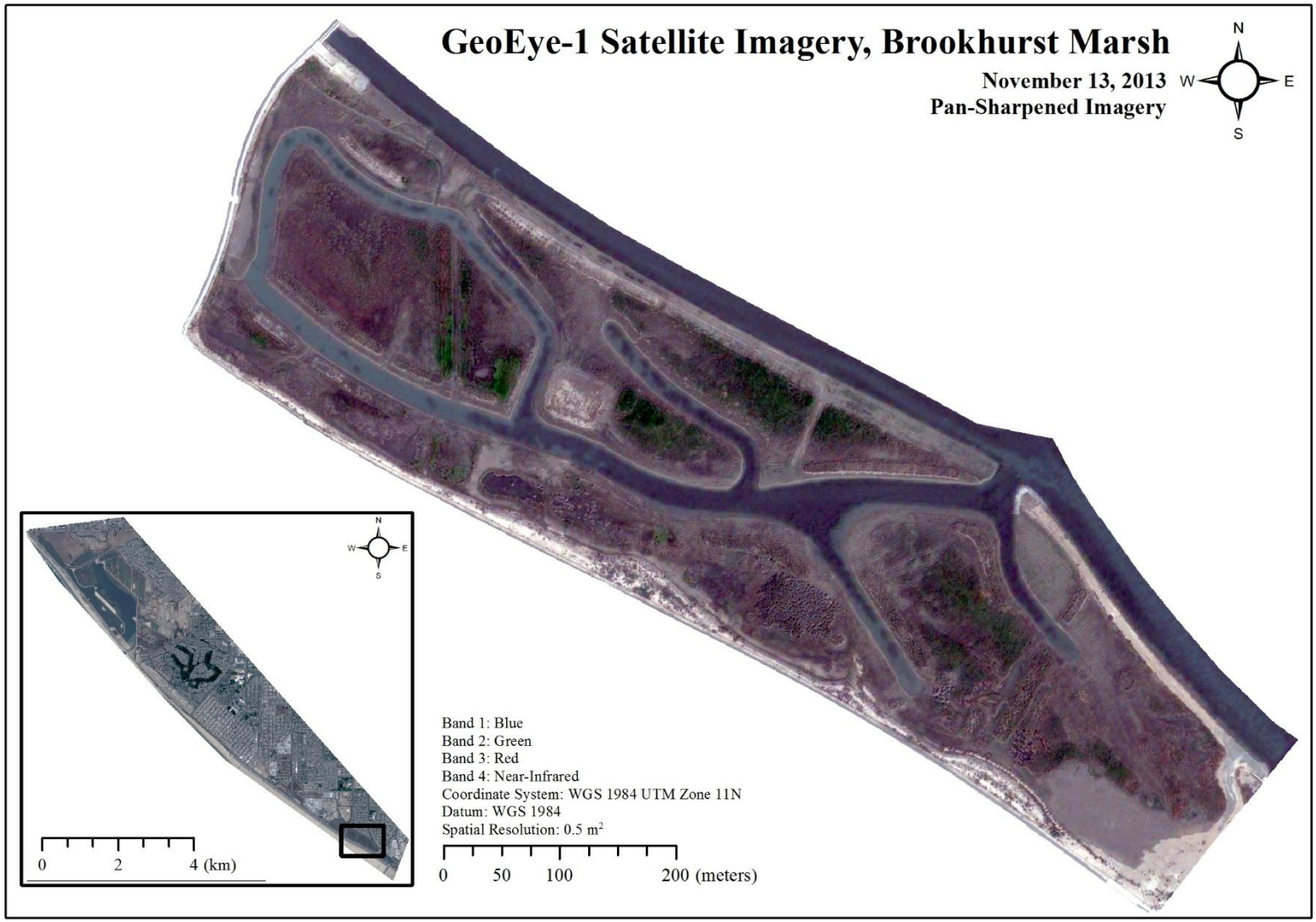

FIGURE 46. Subtractive resolution merge of the GeoEye-1 satellite imagery. Developed ERDAS Imagine 2014.

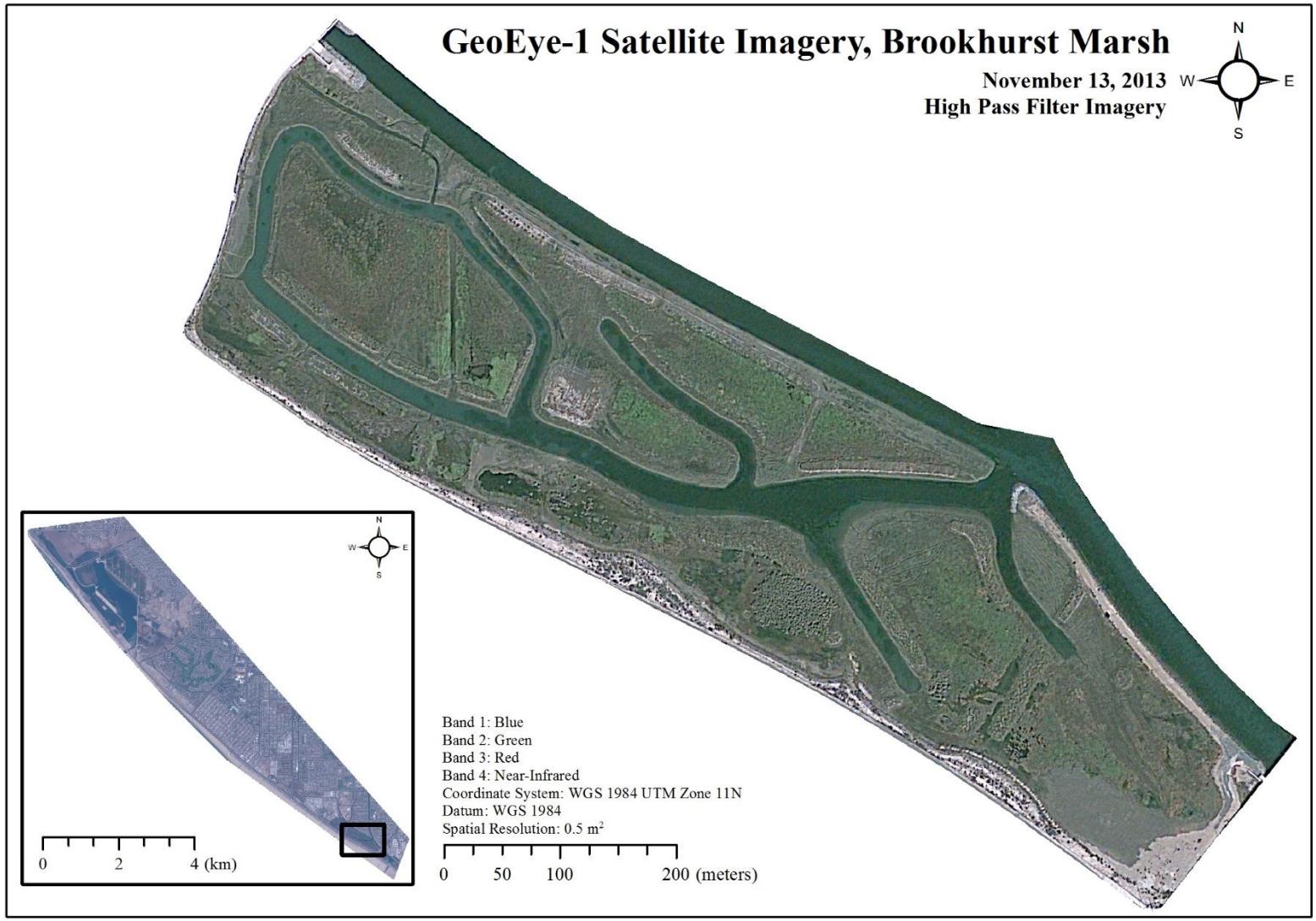

FIGURE 47. High Pass Filter (HPF) merge of the GeoEye-1 satellite imagery. Developed using ERDAS Imagine 2014.

APPENDIX D

SUPERVISED CLASSIFICATION ACCURACY HISTOGRAMS

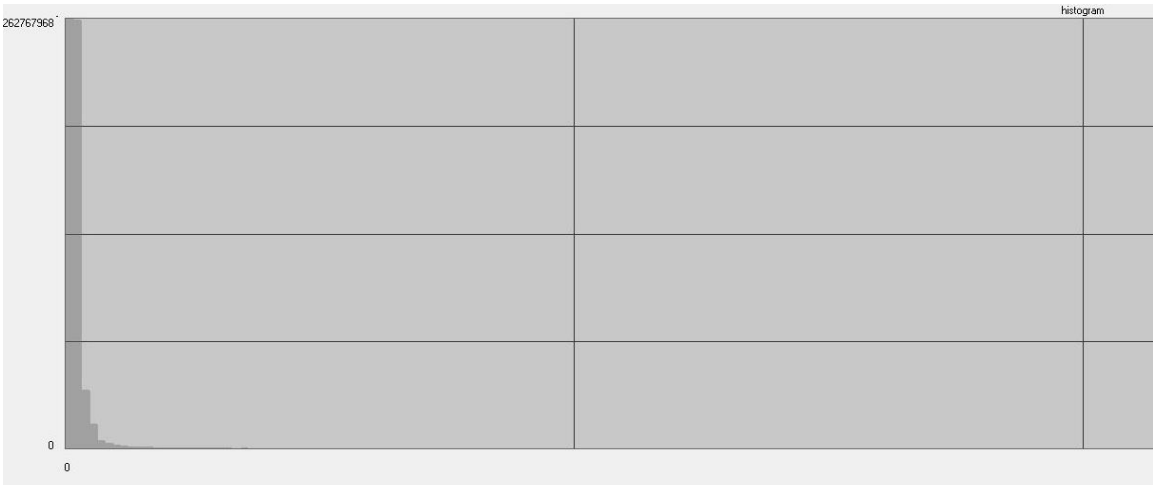

FIGURE 48. Distance histogram of the airplane aerial supervised classification. The histogram shows a chi-square distribution indicative of proper classification procedures.

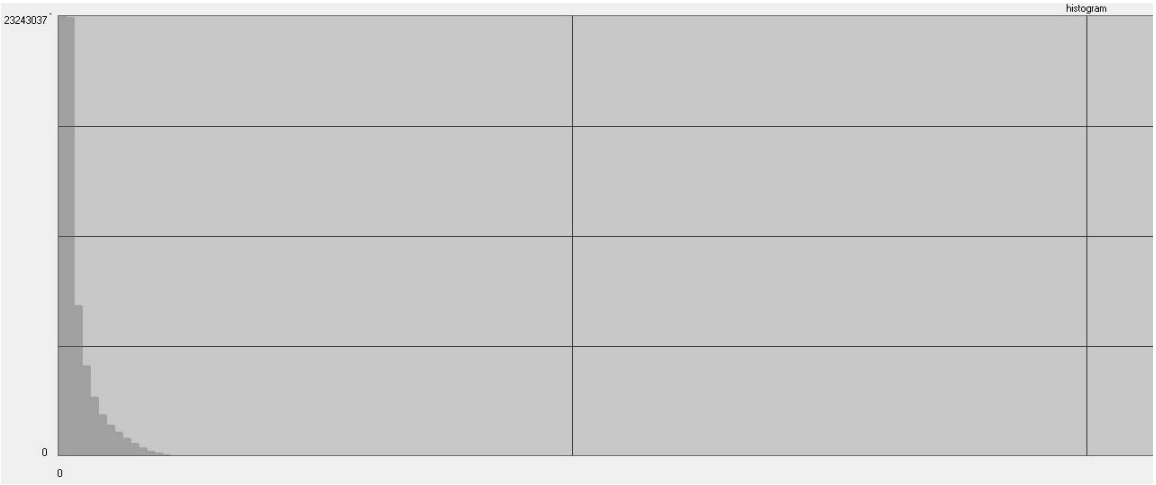

FIGURE 49. Distance histogram of the GeoEye-1 satellite supervised classification. The histogram shows a chi-square distribution indicative of proper classification procedures.

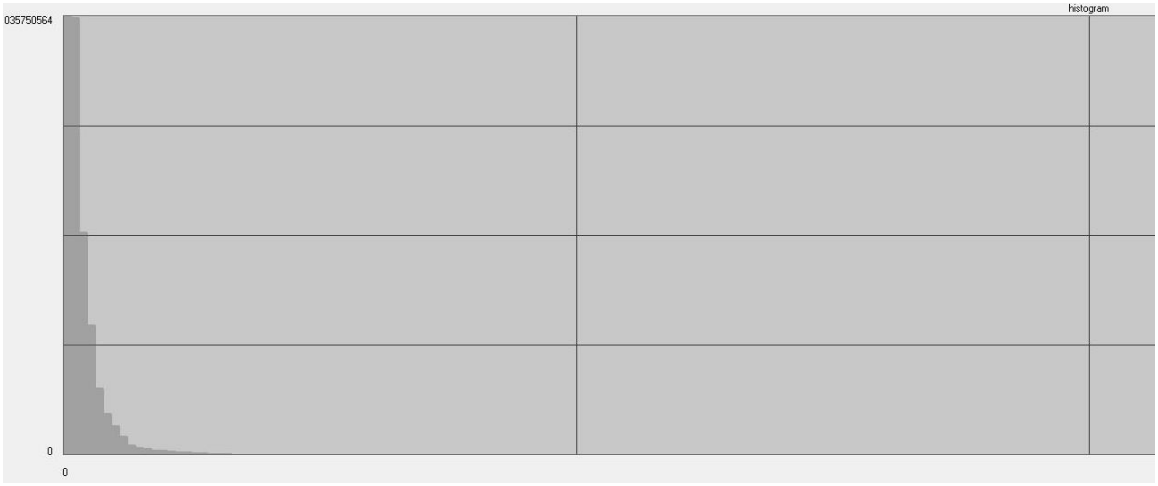

FIGURE 50. Distance histogram for the UAV supervised classification. The histogram shows a chi-square distribution indicative of proper classification procedures.

BIBLIOGRAPHY

BIBLIOGRAPHY

Abdullah, Q. A. 2010. Mapping matters. *American Society for Photogrammetry & Remote Sensing* 1106-1108.

Agisoft LLC. 2014. Agisoft PhotoScan User Manual Professional Edition, Version 1.1. http://www.agisoft.com/pdf/photoscan-pro_1_1_en.pdf (last accessed 12 June 2015).

Ali, R., and N. Pelkey. 2013. Satellite images indicate vegetation degradation due to invasive herbivores in the Andaman Islands. *Current Science* 105 (2): 209-214.

Amazon.com. 2015. Ricoh GR DIGITAL III 10 MP CCD Digital Camera with 28mm F/1.9 GR Fixed Lens and 3-Inch LCD. http://www.amazon.com/Ricoh-GR-DIGITAL-Digital-Camera/dp/B002W6Z80C (last accessed 12 June 2015).

Balakeristanan, M. L., and M. A. M. Said. 2012. "Land Use Land Cover Change Detection Using Remote Sensing Application for Land Sustainability." *International Conference on Fundamental and Applied Sciences, 2012* 425-430. Kuala Lumpur, Malaysia: American Institute of Physics.

Centre for Remote Imaging, Sensing & Processing (CRISP). 2001. Interpreting Optical Remote Sensing Images. http://www.crisp.nus.edu.sg/~research/tutorial/opt_int.htm (last accessed 12 June 2015).

Chabot, D., V. Carignan, and D. M. Bird. 2014. Measuring habitat quality for least bitterns in a created wetland with use of a small unmanned aircraft. *Wetlands* 34: 527–533.

Coiacetto, E. 1996. A model for use in the management of coastal wetlands. *Landscape and Urban Planning* 36 (1): 27-47.

Digital Globe. 2015. GeoEye-1. https://www.digitalglobe.com/sites/default/files/DG_GeoEye1.pdf (last accessed 12 June 2015).

D'Oleire-Oltmanns, S., I. Marzolff, K. Peter, and J. Ries. 2012. "Unmanned Aerial Vehicle (UAV) for Monitoring Soil Erosion in Morocco." *Remote Sensing* 4 (12): 3390-3416.

Eastman, J.R. 2001. Guide to GIS and image processing. *Clark University, USA* 1: 17–34.

EBay. 2014. What are some uses for Infrared Camera Lens Filters. http://www.ebay.com/gds/What-Are-Some-Uses-For-Infrared-Camera-Lens-Filters-/10000000177629136/g.html (last accessed 12 June 2015).

Eisenbeiss, H. and M. Sauerbier. 2011. Investigation of UAV systems and flight modes for photogrammetric applications. *The Photogrammetric Record* 26 (136): 400-421.

Federal Aviation Administration (FAA). 1981. Advisory Circular Subject: Model Aircraft Operating Standards. http://www.faa.gov/documentlibrary/media/advisory_circular/91-57.pdf (last accessed 12 June 2015).

------. 2015. Model Aircraft Operations. https://www.faa.gov/uas/model_aircraft/ (last accessed on 12 June 2015).

Fisher, R. 2004. Spectral Filtering. *CVonline: The Evolving, Distributed, Non-Proprietary, On-Line Compendium of Computer Vision* http://homepages.inf.ed.ac.uk/rbf/CVonline/LOCAL_COPIES/FISHER/specfilt.htm (last accessed 12 June 2015).

Flener, C., M. Vaaja, A. Jaakkola, A. Krooks, H. Kaartinen, A. Kukko, E. Kasvi, H. Hyyppä, J. Hyyppä, and P. Alho. 2013. Seamless mapping of river channels at high resolution using mobile LiDAR and UAV-photography. *Remote Sensing* 5 (12): 6382-6407.

Godet, L., and A. Thomas. 2013. Three centuries of land cover changes in the largest French Atlantic wetland provide new insights for wetland conservation. *Applied Geography* 42: 133-139.

Gómez, D. and J. Montero. 2011. Determining the accuracy in image supervised classification problems. In *Proceedings of the 7th Conference of the European Society for Fuzzy Logic and Technology* 342-349.

Hassan, F. M., H. S. Lim, and M. Z. Mat Jafri. 2011. Cropcam UAV images for land use/land cover mapping over Penang Island, Malaysia using neural network approach. *Pertanika Journal of Science and Technology* 19: 69-76.

Hassani, M. and J. Carswell. 1992. Transition from analogue to digital photogrammetry. *Advances in Remote Sensing* 1 (3): 66-70.

Huntington Beach Wetlands Conservancy (HBWC). 2013. http://www.hbwetlands.org/ (last accessed 12 June 2015).

Intergraph Corporation. ERDAS Field Guide. 2013. http://e2b.erdas.com/products/erdas-imagine/ProductLiterature.aspx (last accessed 12 June 2015).

Kelcey, J., and A. Lucieer. 2012. Sensor correction of a 6-band multispectral imaging sensor for UAV remote sensing. *Remote Sensing* 4 (12): 1462-1493.

Know Before You Fly. 2015. Recreational Users, Business Users, Public Entities. http://knowbeforeyoufly.org/ (last accessed 12 June 2015).

Lewis, D., S. Phinn, and L. Arroyo. 2013. Cost-effectiveness of seven approaches to map vegetation communities - a case study from northern Australia's tropical savannas. *Remote Sensing* 5 (1): 377–414.

Lin, Y., J. Hyyppa, and A. Jaakkola. 2011. Mini-UAV-borne LIDAR for fine-scale mapping. *IEEE Geoscience and Remote Sensing Letters* 8 (3): 426-430.

Lowry, J. H, Jr., R. D. Ramsey, K. Boykin, D. Bradford, P. Comer, S. Falzarano, W. Kepner, J. Kirby, L. Langs, J. Prior-Magee, G. Manis, L. O'Brien, T. Sajwaj, K. A. Thomas, W. Rieth, S. Schrader, D. Schrupp, K. Schulz, B. Thompson, C. Velasquez, C. Wallace, E. Waller, and B. Wolk. 2005. Southwest regional gap analysis project: final report on land cover mapping methods. Logan: Utah State University, RS/GIS Laboratory.

Lu, D., P. Mausel, E. Brondizio, and E. Mora. 2003. Change detection techniques. *International Journal of Remote Sensing* 25 (12): 2365-2407.

Mancini, F., M. Dubbini, M. Gattelli, F. Stecchi, S. Fabbri, and G. Gabbianelli. 2013. Using unmanned aerial vehicles (UAV) for high-resolution reconstruction of topography: the structure from motion approach on coastal environments. *Remote Sensing* 5 (12): 6880-6898.

Matthews, N. A. Aerial and close-range photogrammetric technology: providing resource documentation, interpretation, and preservation. 2008. *Technical Note 428. U.S. Department of the Interior, Bureau of Land Management, National Operations Center, Denver, Colorado* 1-53.

Mishra, R. K., and Yun Zhang. 2013. A comparison of commercial pan-sharpening techniques for HR satellite imagery. *ESRI International User Conference*. http://proceedings.esri.com/library/userconf/proc13/papers/470_149.pdf (last accessed 15 March 2015).

Mitchell, J. J., N. F. Glenn, M. O Anderson, R. C. Hruska, and A. H. Charlie. 2012. *Unmanned aerial vehicle (UAV) hyperspectral remote sensing for dryland vegetation monitoring hyperspectral image and signal sensing.* Idaho: Idaho National Laboratory.

Mortimer, A and M.W. Davidson. 2012. Light Filtration. *Olympus America, Inc., Microscopy Resource Center* http://www.olympusmicro.com/primer/ lightandcolor/filter.html (last accessed 12 June 2015).

National Oceanic and Atmospheric Administration (NOAA). 2015. NOAA Tide Predictions California. http://tidesandcurrents.noaa.gov/tide_predictions.html?gid=235 (last accessed 12 June 2015).

National Park Service. 2014. National Park Service Press Release. http://home.nps.gov/news/release.htm?id=1601 (last accessed 12 June 2015).

Niemeyer, I., and M.J. Canty. 2003. Pixel-based and object-oriented change detection analysis using high-resolution imagery. *Proceedings of 25th Symposium on Safeguards and Nuclear Material Management* 1-8.

Peterson, D. L., J. A. Brass, W. H. Smith, G. Langford, S. Wegener, S. Dunagan, P. Hammer, and K. Snook. 2003. Platform options of free-flying satellites, UAVs or the International Space Station for remote sensing assessment of the littoral zone." *International Journal of Remote Sensing* 24 (13): 2785-2804.

Pidwirny, M. 2006. Introduction to Geographic Information Systems. *Fundamentals of Physical Geography.* 2nd ed. http://www.physicalgeography.net/fundamentals/2e.html (last accessed 12 June 2015).

Rango, A., A. Laliberte, J. E. Herrick, C. Winters, K. Havstad, C. Steele, and D. Browning. 2009. Unmanned aerial vehicle-based remote sensing for rangeland assessment, monitoring, and management. *Journal of Applied Remote Sensing* 3: 1-15.

Ricoh Imaging UK LTD. 2015. Optio WG-2 GPS - Specifications. http://www.ricoh-imaging.co.uk/en/digital-compact/specifications/optio-wg2-gps.html (last accessed 12 June 2015).

Ryan, D. 2012. Unmanned Aerial Vehicles: A New Approach for Coastal Habitat Assessment. *European Space Agency (ESA) Conference Bureau*. http://congrexprojects.com/docs/12m47_docs2/22-uav-pres-ogeo-14-09-12.pdf?sfvrsn=2 (last accessed 12 June 2015).

Schuyt, K. and L. Brander. 1997. What Are Wetlands? *Living Waters Conserving the Source of Life: The Economic Values of the World's Wetlands*. Gland, Switzerland: IUCN 8-11.

Shi, J., Jinling Wang, and Yaming Xu. 2011. Object-based change detection using georeferenced UAV images. *In Proceedings of the International Conference on Unmanned Aerial Vehicle in Geomatics (UAV-g)* Zurich, Switzerland: Swedish Federal Institute of Technology Zurich 38-1/C22: 1-6.

Taylor, J.L. and K. Neely. 1994. Orthography at the geometronics service center moving from analog to digital. *Remote Sensing and Ecosystem Management Proceedings of the Fifth Forest* 253-261.

The Tiffen Company, LLC. 2015. 49MM 8 YELLOW 2 FILTER. http://www.tiffen.com/displayproduct.html?tablename=filters&itemnum=498Y2 (last accessed 12 June 2015).

------. 2015. 350X450MM GEL FILTER/#15. http://www.tiffen.com/displayproduct.html?tablename=kodakaccessories&itemnum=EK1348440 (last accessed 12 June 2015).

------. Camera Filters. http://www.tiffen.com/camera_filters.htm (last accessed 12 June 2015).

Théau, J. 2012. Change Detection. *Springer Handbook of Geographic Information*. Berlin: Springer: 175–194.

Toronto and Region Conservation Authority (TRCA). 2011. Wetland Vegetation Monitoring Protocol Terrestrial Long-term Fixed Plot Monitoring Program-Regional Watershed Monitoring and Reporting. 1-16.

Tuxen, K. A., L. M. Schile, M. Kelly, and S. W. Siegel. 2008. Vegetation colonization in a restoring tidal marsh: a remote sensing approach. *Restoration Ecology* 16 (2): 313-323.

United States Geological Survey (USGS). 2015. NDVI, the foundation for remote sensing phenology. http://phenology.cr.usgs.gov/ndvi_foundation.php (last accessed 12 June 2015).

USDA (United States Department of Agriculture). 2013. Four Band Digital Imagery Information Sheet. http://www.fsa.usda.gov/Internet/FSA_File/fourband_info_sheet_2015.pdf (last accessed 12 June 2015).

Verhoeven, G. 2011. Taking computer vision aloft - archaeological three-dimensional reconstructions from aerial photographs with photoScan. *Archaeological Prospection* 18 (1): 1-7.

Vittek, M., A. Brink, F. Donnay, D. Simonetti, and B. Desclée. 2014. Land cover change monitoring using Landsat MSS/TM satellite image data over west Africa between 1975 and 1990. *Remote Sensing* 6 (1): 658-676.

Wade, T.G., J.D. Wickham, M.S. Nash, A.C. Neale, K.H. Riitters, and B. K. Jones. 2003. A comparison of vector and raster GIS methods for calculating landscape metrics used in environmental assessments. *Photogrammetric Engineering & Remote Sensing* 69 (12) 1399-1405.

Watts, A. C., V. G. Ambrosia, and E. A. Hinkley. 2012. Unmanned aircraft systems in remote sensing and scientific research: classification and considerations of use. *Remote Sensing* 4: 1671-1692.

Willhauck, G. 2000. Comparison of object oriented classification techniques and standard image analysis for the use of change detection between SPOT multispectral satellite images and aerial photos. *International Society for Photogrammetry and Remote Sensing* 33: 1-8.

Whitcraft, C., B. Allen, and C. Lowe. 2013. *Huntington Beach Wetlands restoration project monitoring program: final report.* Long Beach: Rep. Long Beach: 1-94.

Wolf, P., B. DeWitt, and B. Wilkinson. 2014. *Elements of photogrammetry with application in GIS.* 4th ed. New York: McGraw Hill Education.

Woodfield, R. and K. Merkel. 2011. Huntington Beach Wetlands restoration project monitoring program. *Merkel & Associates, Inc.* 1-107.